Continuum Damage Progressive Failure Modeling for Crashworthiness and Static Analyses of Laminated Composites

Francesco Deleo

A dissertation

submitted in partial fulfillment of the

requirements for the degree of

Doctor of Philosophy

University of Washington

2019

Reading Committee:

Keith Holsapple, Chair

Marianna Maiaru’

Eli Livne

Program Authorized to Offer Degree:

William E. Boeing Department of Aeronautics and Astronautics

University of Washington

Abstract

Continuum Damage Progressive Failure Modeling for Crashworthiness and Static Analyses of Laminated Composites

Francesco Deleo

Chair of the Supervisory Committee:
Professor Keith Holsapple
William E. Boeing Department of Aeronautics and Astronautics

A new energy-based composite continuum damage model is presented for laminated composite structures. The composite laminate is modelled at the meso-scale using the finite element method, specifically: shell elements. Each composite lamina is modelled with one or four integration points, depending on if reduced or full integration elements are used. Each lamina is modelled as a 2D plane stress orthotropic material and damage is included by degrading the stiffness matrix. Element deletion is used when all integration points have failed.

The theory is developed to predict failure initiation using a modified version of the Hashin's failure criteria, and failure growth is modelled using damage variables which are developed as part of this work. The theory has been written to be used for both static failure and dynamic crush analyses. Two sets of damage variables are derived, one for static analyses and a separate one for

dynamic crush. When performing a dynamic crush analysis, the distributed damage model is utilized in order to ensure that the progressive failure crush mode correcty takes place.

The damage model is energy-based using the fracture energies of four failure directions: the fiber and matrix directions, and in each of tension and compression. Mesh-size objectivity is assured via the adoption of the Crack Band Theory. The theory is implemented into an LS-DYNA user-defined material model (UMAT) in order to take advantage of the pre-built contact algorithms needed for crush analyses and for solving the governing equations of motion.

The theory is applied to a static and crush problem, with excellent agreement between the experimental and numerical results for both cases. A tensile notched specimen is tested and simulated. Both the failure morphology and resulting load-displacement results at the constraint are found to match very well. A crush experiment carried out by the author is simulated.

In addition to matching the experimental results with a high degree of accuracy, the theory discussed herein offers significant advantages over alternative damage models present in the literature. There is no need to filter the load – displacement results using a non-physical numerical scheme, and the high impulse loads are eliminated. In addition, the theory offers a level of robustness and stability which allows it to be used with any contact type, including ‘hard’ contact, and therefore eliminates the need to calibrate the penalty-based contact algorithm’s load penetration curve with non-physical stiffnesses.

TABLE OF CONTENTS

LIST OF FIGURES

LIST OF TABLES

ACKNOWLEDGEMENTS

Doctoral research takes several years to complete and requires overcoming hardships and challenges, both personal and professional. Endeavors like these are rarely possible without the help of family, friends, mentors and/or advisers. This is especially the case for my graduate school time in which I had to face several adversities in addition to the technical challenges, which the research comprised of. Several people have been instrumental for this achievement and I would like to recognize them. My parents Carla and Antonio for their love, support and wise advices. My mentor and best friend Dr. Patrick Safarian who is a constant source of spiritual, professional and personal guidance and support. A young student could not have wished for a better mentor and friend. I consider Dr. Safarian part of my family now. My adviser Prof. Keith Holsapple has provided me with invaluable help and guidance to overcome blocks in my research and is the example I try to follow when I practice engineering and teaching. I could not have wished for a better PhD adviser. My friend and colleague Prof. Marianna Maiaru' deserves a special thank you as she was instrumental for finishing the work. Prof. Maiaru' has dedicated a lot of her time, and provided me with invaluable guidance to help me with the last push. I consider Prof. Maiaru' a close friend of mine and I look forward to working together by collaborating in further research projects.

A special thank you also goes to TerraPower LLC which has supported me in many ways to help me complete the doctoral work including providing me with a space to conduct my research while not at the university, and flexibility in work schedule.

DEDICATION

This work is dedicated to my grandfather Emilio and my aunt Carmela.

Chapter 1. INTRODUCTION

In the past few decades the use of laminated composite material systems has exponentially increased to replace metals for primary and secondary structures of weight-sensitive products across several industries: aeronautics and aerospace, automobile, energy, consumer goods and more. Composite materials offer significantly higher specific strength and stiffness values over the industry standard structural metals such as aluminum alloys, steels and titanium. In aerospace, composites were introduced in small amount in military aircrafts in the 1960s (i.e. Boron/Epoxy F4 rudders, A4 flap, F14 and F15 stabilizer and C130 control wing) and in civil aviation starting in the 1970s (707 fore flap). Aided by government funded projects (i.e. NASA/Boeing Advanced Technology Composite Aircraft Structures: ATCAS), the use of composites in generation aviation has increased very rapidly in the past decades. The latest generation of single-aisle and wide-body general aviation aircraft include the greatest percentage of composite materials in their structures to date as exemplified by the Boeing 787 and Airbus A350 families of airplanes. The automobile industry has experienced a similar rapid increase in the use of composites, starting from racing cars (Formula 1), then being introduced to supercars (i.e. Lamborghini Aventador), and currently being used in less expensive everyday vehicles such as the BMW i3, which uses an all composite frame.

In addition to offering designers the advantage of higher elastic material properties and allowables, composites can possess the capability for higher specific energy absorption (SEA) property than metals, as demonstrated by the author's Master Thesis (Deleo, 2011). The T700/2510 composite material system was found to have higher SEA then aluminum and steel when a corrugated test specimen was used. However, the SEA of composites depends on the

material lay-up and cross-sectional shape. If not properly designed, a composite structure can also offer very poor energy absorption characteristics, significantly lower than those of typical structural metals.

Several features are still preventing an even further widespread adoption of composites. One key aspect is the high cost, which is being addressed via the implementation of out-of-autoclave manufacturing technologies. Another important problem is the absence of a fully reliable and robust failure theory which is demonstrated by the three World Wide Failure Exercises discussed at length in the literature review section of this dissertation. And there is a poor understanding of the ability to dissipate energy in a crush event as compared to metals, which is partially due to the absence of specialized test methods for the characterization of the SEA.

These last two problems comport a challenge towards the certification of composite structures vehicles and certification by analysis is not permitted. The certification by test and certification by analysis supported by test evidence approaches have been used successfully to demonstrate compliance with regulatory requirements The approach known as: certification by analysis supported by test evidence is composed of a mix of testing and analysis which makes use of the Building Block Approach (BBA) (Feraboli, et al., 2010).

Several numerical approaches have been developed to model composites and model the response to static and crush problems, and therefore offer the designers tools to perform analyses to be used for certification. Several of the most prominent models are summarized in the literature review section of this dissertation.

Here is a new approach, which covers both static and crush events. It is implemented as an LS-DYNA user defined material model. It produces excellent agreement in both load-displacement results and failure morphology with experimentalresults. This theory offers

significant improvements over previous theories by eliminating the the need to filter the results with non-physical filtering algorithms, by eliminating the erroneous impulse loading which have the potential to create large shock waves through the structure and by eliminating the need of calibrating the penalty-based contact algorithms' load penetration curves.

Chapter 2. LITERATURE REVIEW

2.1 COMPOSITES FAILURE THEORY

As discussed above, the use of advanced composite materials has reached virtually every engineering field and the market predictions show an exponential increase of the industry demand in the foreseeable future (Claunch, 2015). This is happening despite the fact that composite materials suffer from a lack of a robust and comprehensive failure theory, unlike other structural materials such as metals. The use of advanced composite materials has been slowed because of the lack of robust and comprehensive failure models, although their development has been the focus of research for decades. Several books have been written on composite failure theories. This Section offers a quick summary of the state of the research on composite failure prediction.

First of all, failure is a matter of purpose. 'First ply failure' is defined as the conditions under which the weakest lamina loses its strength under the action of an external loading condition. This can occur to a single lamina or several. It can occur to all laminae simultaneously if the laminate is unidirectional. Depending on the laminate stacking sequence, when first ply failure occurs the laminate is usually still able to carry some loads, because the remaining laminae are still undamaged. If the state of loading is further increased, laminae progressively fail; when the last lamina fails the laminate is said to have undergone ultimate failure.

Failure criteria can be characterized depending on the level at which they are applied (Gibson, 2016) Failure theories which operate at the constituents' level, predicting failure from the onset of rupture of a single fiber, matrix, and their interaction are called micromechanics theories.
Theories which operate at the lamina level are said to be lamina-based. These theories treat the lamina as the laminate building block, as an anisotropic but homogenous material. The fiber reinforced matrix is considered as homogenous rather than heterogenous, and the stresses and

strains acting of the constituents is not considered. These theories can be applied in an iterative fashion from the first ply failure condition until ultimate failure. These operations are the basis of various composites damage models, which are discussed in Section 2.2. This is the level of the failure criteria selected for this dissertation.

To circumnavigate the uncertainties and unreliability of current failure theory, several industries have adopted an empirical, laminate-based failure approach relying solely on experimental data. A large number of laminates of different stacking sequences are tested and empirical equations are derived for strength as a function of the percentage of laminae in the principle fibers directions. A failure function is obtained via interpolation of the experimental results. This purely experimental approach has several limitations, including dependency on the material system. If the fiber type, resin system, or even the manufacturing method is altered, the results will not be longer applicable. This method also prevents the use of the failure equation towards predicting the strength of laminate which has fiber orientations which do not coincide with the ones tested. This method requires a very large number of tests and a large investment. The large cost is one of the principles factors which are preventing smaller companies from utilizing composites for their design.

Failure criteria can also be characterized based on the approach they undertake. A theory is said to be non-interactive if the various failure modes are considered separate. Two examples of very famous and utilized non-interactive failure theories are the maximum stress and maximum strain failure criteria. Stress or strain allowable values for each direction along the lamina's material's axes (1-2), discussed in Section 3.1 and shown in Figure 3.1-2, are obtained either experimentally via material characterization or using a rule of mixture for lamina strengths. Then,

given the lamina loading conditions, the stresses or strains are resolved from the loading axes to the material's axes and each component is compared with the allowable value.

Alternatively, a failure theory is said to be interactive if it consists in one or more equations made out of the stress or strain components and therefore failure in one direction is affected by the stress or strain states in that direction as well as others. Few very popular interactive failure theories are: the Tsai-Hill (Tsai, 1968), Hoffman (Hoffman, 1967), and Tsai-Wu criteria (Tsai, et al., 1971)- (Gol'denblat, et al., 1966).

A failure theory is said to be physics-based if each specific failure mode is represented by a unique equation that describes it. Typically, physics-based theories differentiate between fiber and matrix failure or between brittle and ductile failure. Hashin's three-dimensional failure theory, derived in Section 2.1.1, which is utilized in this dissertation, is both an example of an interactive and physics-based theory.

Lastly, damage mechanics failure theories mathematically describe the often-gradual sequence of failure which lead to ultimate failure. A damage mechanics theory can use one or more of the above-mentioned failure theories in a progressive fashion. Damage mechanics theories are discussed in Section 2.2.

Because of the large number of completely different failure theories developed for composite materials, several early studies have been performed towards comparing predictions from the various failure criteria (Chamis, 1969), (Sandhu, 1972) and (Soni, 1983). The most comprehensive study performed to date is the World Wide Failure Exercise (WWFE) (Kaddour, et al., 2017) which was developed with the goal of establishing the level of maturity of the most prominent failure theories, assessing and closing the gap between theoreticians and design practitioners, and stimulate researchers towards making improvements to the theories. To date, three WWFEs have

been completed. The format of each WWFE is the same. During Part A the most promising theories are selected and the originators are contacted to take part in the exercise. Each participant is asked to predict failure, as blind predictions, for a number of loading conditions and laminate descriptions. Each participant writes a journal paper explaining the theory and showing the results. In Part B of the exercise the experimental evidence for each test case is made available to the public and the participants. The participants are allowed to make revisions to the theory and refine their predictions.

Coordination of the first WWFE (WWFE-I) started in 1992 (Kaddour, et al., 2014). Part A officially started in 1996 and the exercise ended in 2004 with the publication of a reference book discussing failure criteria for composites in a two dimensional state of stress (Hinton, et al., 2004). The exercise consisted of 14 test cases. Nineteen theoretical approaches to predict failure and deformations of polymeric matrix composites (PMC) were compared. Various different approaches were undertaken from the participants: micro-mechanics, lamina based, interactive, and non-interactive theories were proposed. Several successful conclusions were drawn from WWFE-I; and the exercise can be deemed to be truly groundbreaking, considering the efforts on the participants and organizers. However, the exercise highlighted the weaknesses of the various theories. While most theories were found to be adequate in predicting the response of a lamina, the ability to model both first-ply and ultimate failure of laminates for all theories was inadequate. No theory was deemed to be robust and 50% accuracy was the best achieved.

One of the aspects which were not investigated in WWFE-I was the maturity of failure theories to predict the behavior of composites being subject to triaxial stresses. To answer this question a second WWFE (WWFE-II) (Hinton, et al., 2012) started after WWFE-I and ended in 2013. The results were published in a special issue of the Journal of Composite Materials

(Kaddour, et al., 2012) - (Kaddour, et al., 2013). Twelve participants either proposed or utilized existing theories to predict the material behavior in twelve test cases undergoing triaxial loading. Similar results as for WWFE-I were obtained in terms of the theory's maturity level. However, in several cases a few theories performed well, providing correlation within ±10% in terms of strength of multi-angle laminates (Kaddour, et al., 2013). Among the most promising theories was Hashin's (Hashin, 1980) although Hashin did not agree to take part to the exercise. Because of the popularity of his theory another researcher, Kress, applied Hashin's theory and participated to the exercise.

Because of those promising results, Hashin's failure theory is chosen to predict failure at the lamina level in this dissertation. A summary of derivation is offered in Section 2.1.1 and the Equations in Section 4.1. Hashin's criteria are modified in this work to include the effect of accumulated damage. The damage variables derived in Sections 4.2.3-4.2.4, respectively for static and crushing loading conditions, are added to the equations.

An unanswered aspect in both WWFE-I and -II was the maturity of current failure theories to modeling subcritical damage: the damage/matrix crack development, delamination initiation until ultimate fracture. To address this, a third and to-date final exercise was started: WWFE-III. Twelve participants took place to the exercise which consisted of thirteen test cases. As presented in (Kaddour, et al., 2013) there is a large disagreement between the various theories and the experimental evidence. Differences as high as 340% are obtained for a single-isolated lamina. Prediction results for a uniaxial tension loading on a quasi-isotropic laminate differ among models by a factor of almost 8. A conclusion is that the state of current theories is still not adequate to be used by designers and practitioners.

2.1.1 *Hashin failure theory*

While the methodology discussed in this theory can accommodate different failure initiation criteria, it is currently formulated using failure initiation according to Hashin's failure criteria (Hashin, 1980), as mentioed in Section 2.1 above and summarized in Section 4.1. In order to model the effect of the accumulated damage in the various directions they are extended in this work to include the damage variables derived in Sections 4.2.3 and 4.2.4. Because of the importance of the failure initiation criteria on the results, the derivation of Hashin's failure criteria is summarized below. A more comprehensive derivation can be found in (Hashin, 1980) and (Matzenmiller, et al., 1991).

Hashin's three-dimensional failure theory was proposed to predict failure for a transversely isotropic material and failure is predicted when the following second-order polynomial is satisfied:

$$A_1 I_1 + B_1 I_1^2 + A_2 I_2 + B_2 I_2^2 + C_{12} I_1 I_2 + A_3 I_3 + A_4 I_4 = 1 \tag{2.1}$$

The A's, B's and C's are constants discussed next in this section and the I's are the stress invariants for a transversely isotropic material defined as:

$$\begin{aligned} I_1 &= \sigma_{11} \\ I_2 &= \sigma_{11} + \sigma_{33} \\ I_3 &= \sigma_{23}^2 - \sigma_{22}\sigma_{33} \\ I_4 &= \sigma_{12}^2 + \sigma_{13}^2 \\ I_5 &= 2\sigma_{12}\sigma_{23}\sigma_{13} - \sigma_{22}\sigma_{13}^2 - \sigma_{33}\sigma_{12}^2 \end{aligned} \tag{2.2}$$

The subscripts indicate the material axes, as discussed in Section 3.1 and shown in Figure 3.1-2. The 3-axis is perpendicular to both the 1- and 2- axes. The fifth stress invariant is not

included in the failure criterion of Equation 2.1. The constants A_3 and A_4 can be solved for if only pure transverse or axial shear stress is present, the result is

$$A_3 = \frac{1}{\tau_T^2}$$

$$A_4 = \frac{1}{\tau_A^2} \tag{2.3}$$

where τ_T and τ_A are, respectively, the transverse and axial shear strengths of the lamina. At this point the assumption formulated by Hashin is that matrix fracture occurs in the plane tangential to the fibers by the combined effect of normal and shear stresses. Therefore, σ_{23} and σ_{11} do not contribute to matrix fracture and stress invariant I_1 has no influence. On the other hand, Hashin assumed that fracture for the fibers occurs perpendicular to the fibers. Therefore, σ_{22}, σ_{23}, and σ_{33} do not contribute to fiber fracture and stress invariants I_2 and I_3 have no influence.

From these assumptions, Equation 2.1 can be applied for matrix and fiber fracture to obtain:

Matrix mode:

$$A_m(\sigma_{22} + \sigma_{33}) + B_m(\sigma_{22} + \sigma_{33})^2 + \frac{1}{\tau_T^2}(\sigma_{23} - \sigma_{22}\sigma_{33}) + \frac{1}{\tau_A^2}(\sigma_{12}^2 + \sigma_{13}^2) = 1 \tag{2.4}$$

Fiber mode:

$$A_f\sigma_{11} + B_f\sigma_{11}^2 + \frac{1}{\tau_A^2}(\sigma_{12}^2 + \sigma_{13}^2) = 1 \tag{2.5}$$

Where ‘m’ and ‘f’ denote respectively the matrix and fiber modes. Equations 2.4 and 2.5 are further divided for the tensile and compressive directions. Therefore the constant A_m, B_m, A_f and B_f are further divided into A^+_m, B^+_m, A^+_f, B^+_f, A^-_m, B^-_m, A^-_f, and B^-_f, where the ‘+’ and ‘-‘ denote the loading directions: ‘+’: tension, ‘-‘: compression. These constants are derived performing simple uniaxial tension and compression tests and therefore relating them to the material strengths. The resulting Equations are shown in Section 4.1: Equations 4.28 – 4.31.

It should be mentioned that the order of the failure criterion polynomial of Equation 2.1 was not chosen by Hashin on physical reasoning but simply on curve fitting considerations. As discussed in Section 2.2, Hashin's failure criteria are utilized by many composites damage models and mentioned in the Composites Material Handbook (Composite Materials Handbook-17, 2012) because of the rather ease of implementation and good reliability of the theory with respect to experimental evidence, as mentioned in Section 2.1 as a result of the WWFEs.

2.2 COMPOSITE DAMAGE MECHANICS

Several composite failure theories have been developed to predict the onset of failure in composite laminates, as discussed in Section 2.1. Various techniques which make use of one or more failure theories have been formulated for the simulation or prediction of both failure initiation and propagation into composite laminates. Many of these techniques were implemented within the finite element framework and some have been made available in commercially available software packages. For instance, the well-known Tsai-Wu (Tsai, et al., 1971) and Hoffman (Hoffman, 1967) failure theories have been implemented in the ANSYS and ABAQUS codes. In these cases, when failure is predicted to occur, the element is considered failed and if element deletion is activated it is entirely removed from the mesh.

Later, more advanced modeling techniques were developed to model the damage progressively: those are referred to as Progressive Damage Models (PDM). In PDMs, the progressive damage causes stiffness degradation at the location of damage. Therefore, when failure is predicted to initiate in a finite element, the element does not lose all its load carrying capability at once, but the stiffness matrix is degraded proportionally to the level of accumulated damage. In most PDMs, it is assumed that different damage modes develop simultaneously, and they can

interact and hence influence one another. Therefore, composites PDMs can be categorized within the more general field of continuum damage mechanics.

Several PDMs have been proposed in the literature as summarized by (Curiel Sosa, 2011), including the well-known thermodynamically consistent model first developed by Kachanov (Kachanov, 1958) and then revised by Lemaitre (Lemaitre, 1992). Chaboche expanded on the work by Kachanov and developed a continuum damage mechanics theory which treats the damage as macroscopically homogenous, and can model both the nucleation and propagation of damage by modifying the stress-strain behavior (Cheboche, 1981). Matzenmiller et al proposed a constitutive model for anisotropic damage of a fiber reinforced lamina (Matzenmiller, et al., 1995). A constitutive model was developed which model the lamina as a homogenized continuum and, with the use of internal damage variables which degrade the stiffness matrix, damage is simulated. As is done with work presented in this dissertation, the authors distinguish between the fiber and matrix, tensile and compressive directions and apply the Hashin's failure theory. Maimi et al. proposed a continuum damage model for laminated composites and implemented into the ABAQUS finite element code via user defined material model UMAT (Maimi 2007, Parts I and II). The four failure modes: along the the fiber and matrix, tensile and compressive directions are considered separate and each has its own scalar damage variable. The LaRC04 failure criteria are used to predict the various lamina-level failure mechanisms. Barbero et al proposed a constitutive model for elastic damage for polymeric matrix composites (PMC) laminates. This continuum damage mechanics model is based on a damage surface which reduces to the Tsai-Wu failure theory in stress-space (Barbero, et al., 2002). Lapczyk el al (Lapczyk, et al., 2007) presented a progressive damage model for fiber-reinforced composites which uses Hashin's failure theory and combines it with an energy-based damage progression model. The author solved mesh sensitivity

issues using the Crack Band method, which is discussed in Section 2.2.3. Hufenbach et al introduced a plane-stress damage mechanics model for textile-reinforced composites via damage variables which degrade the material stiffness matrix. The authors modelled textile composites by assuming they are made out of unidirectional layers (Hufenbach, et al., 2004). Cuntze et al. proposed the Failure Mode Concept (FMC) -based set of criteria for multidirectional laminates. The work is performed with the goal of predicting initial failure of unidirectional (UD) laminae and treating the non-linear progressive failure of laminates undergoing a general three-dimensional state of stress (Cuntze, et al., 2004). The authors state that the model for the evolution of the stiffness degradation is more important than the initial failure criteria themselves. This is the same conclusion as the work by Barbero et al. (Barbero, et al., 2002) in which a model for damage behavior of a laminate is developed by assembling the non-linear stiffness degradation effect of each lamina.

2.2.1 *Composites fracture energy*

The fracture energy, also referred to as fracture toughness, is equal to the external energy supply needed to create and fully break a unit surface area of material. The fracture energy can be expressed in several related forms as shown in Figure 2.2-1, where linear softening is adopted for simplicity. In (a) the stress, σ, versus opening displacement, δ, is plotted and the resulting area under the curve is commonly referred to as the specific fracture energy, G_F. The crack opening displacement starts when failure initiates, after the stress reaches the strength value of σ_{ult}. The crack opening displacement is the distance between the two faces of a crack. G_F is also referred to as the cohesive fracture energy as it is utilized in cohesive crack models and calculated as shown in Equation 2.6. In part (b) of Figure 2.2-1 an idealized stress-strain, σ-ε, curve is shown.

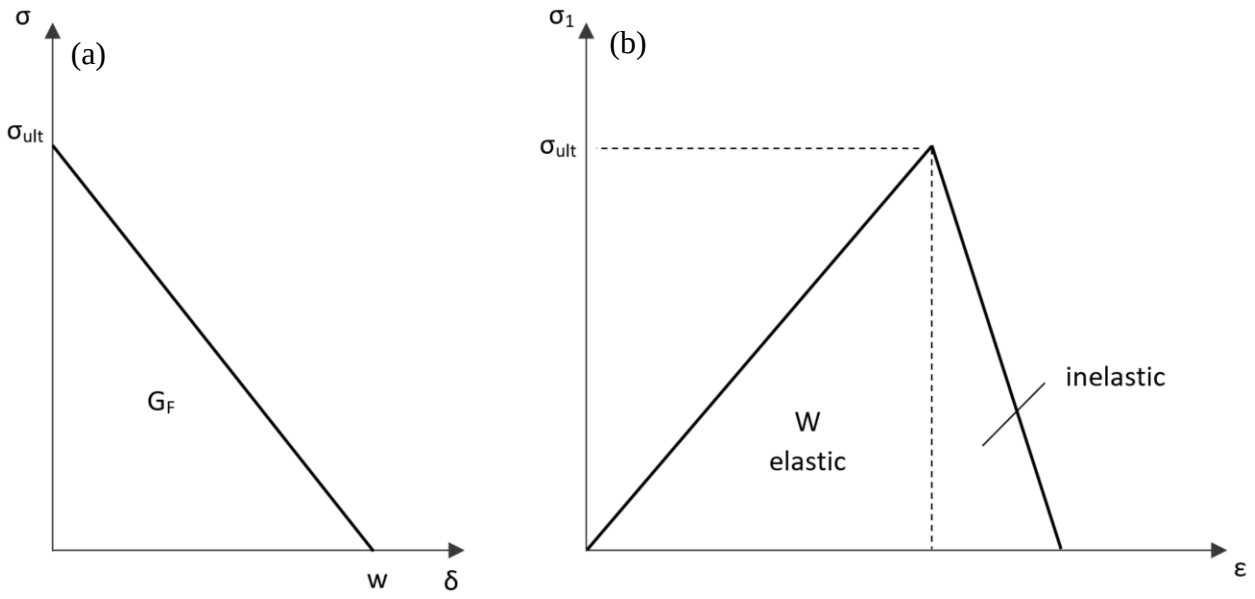

Figure 2.2-1. (a) Stress-opening displacement curve, (b) stress-strain curve.

The curve is elastic until the stress reaches the strength value of σ_{ult}, after that the curve is inelastic until full fracture. The area under the elastic region is commonly referred to as the strain energy density, W, which is the strain energy per unit of initial (undeformed) volume. The area under the inelastic part of the curve is related to the fracture energy density, γ_F, which is shown in Figure 2.2-9 and calculated using Equation 2.7. G_F and γ_F are related as shown in Equation 2.10 and discussed later in Section 2.2.3.

$$G_F = \int_o^w \sigma \, dw \tag{2.6}$$

$$\gamma_F = \int_o^\infty \sigma \, d\varepsilon^f \tag{2.7}$$

For laminated composites, due to the orthotropic nature of the composing lamina, more than one fracture energy exist. Fracture toughness testing standards for composites are still in development and there does not exist consensus of opinion within the composites community. As

explained in Section 4.2.2, in this work four lamina level fracture toughness values are utilized, one per lamina material and loading direction:

G_{1T} – Fracture energy, (1)-axis, tensile direction.

G_{1C} – Fracture energy, (1)-axis, compressive direction.

G_{2T} – Fracture energy, (2)-axis, tensile direction.

G_{2C} – Fracture energy, (2)-axis, compressive direction.

In (Dickson, et al., 1985), the fracture toughness (presented as the critical stress intensity factor in Mode I, K_{IC}) for CF/PEEK (Polyether ether ketone) was measured using a center notched specimen and a $[0/90]_{3s}$ layup specimen. The center notched specimen is show in Figure 2.2-2.

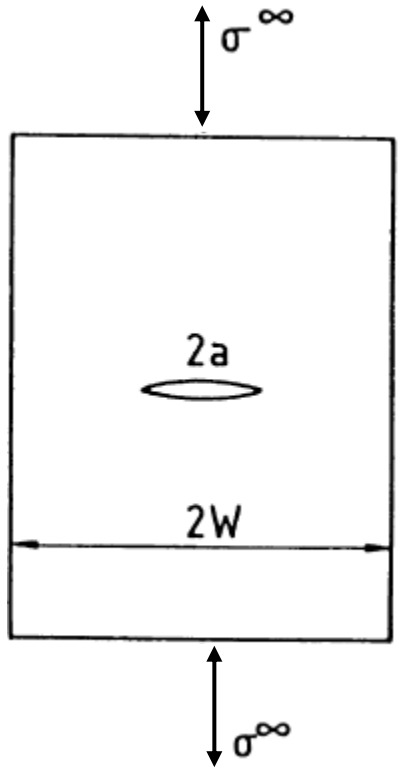

Figure 2.2-2. Center notched specimen for fracture toughness measurement of composites from (Soutis, et al., 2000). Same specimen used in (Dickson, et al., 1985).

The specimens were tested in mode I, which is tensile, and the individual contributions or [0] and [90] plies were not identified. The measured values were therefore a combination of G_{1T} and G_{2T}. In (Jose, et al., 2011), a compact tension (CT) specimen type was used to measure the intralaminar fracture toughness of laminates with $[0/90]_{15}$ stacking sequence. Intralaminar fracture implies fiber failure. The constituents sub-laminates $[0]_{30}$ and $[90]_{30}$ were also tested effectively measuring G_{1T} and G_{2T}. Thirty plies were used in order to achieve the desired thickness. The CT specimen type mimics one of the specimens used to measure fracture toughness in metals: ASTM E399 (American Society for Testing Materials, 2017).

In (Moore, et al., 1991) independent fracture toughness tests on CF/PEEK from eight laboratories were assembled. $[0]_{40}$ specimens were tested using three different specimen geometries, as shown in Figure 2.2-3.

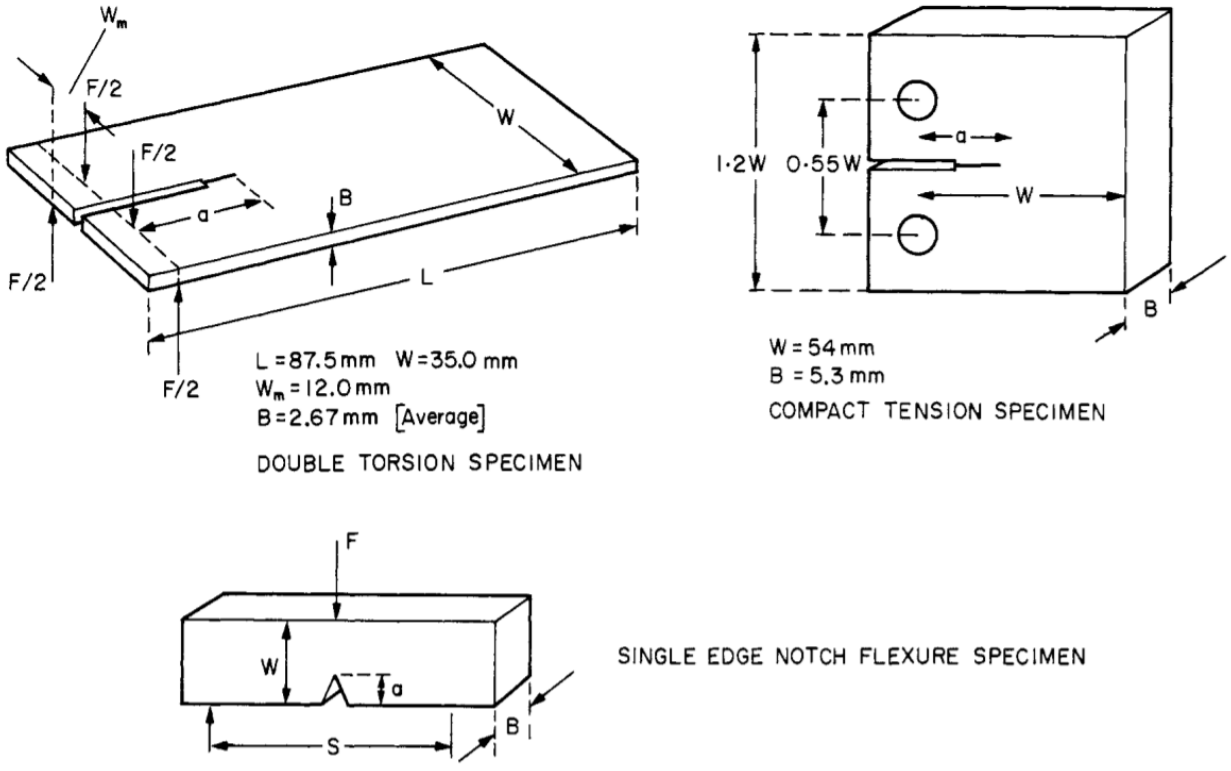

Figure 2.2-3. Fracture mechanics specimens from (Moore, et al., 1991).

The three specimen configurations investigated were the double torsion, compact tension and single edge notch flexure specimens. This study effectively focused on G_{1T} measurements.

In (Soutis, et al., 2000) the compressive fracture toughness of a $[0/90_2/0]_{3s}$ laminate was measured using a center notched specimen, as shown in Figure 2.2-1. The study focused on compressive fracture toughness and failure mode for composites, which is explained to take place via microbuckling. In (Ratcliffe, et al., 2004) and (Wade, 2014) a compact compression (CC) specimen was proposed in order to calculate the compressive fracture toughness for composite sandwich panels. The specimen is shown in Figure 2.2-4. The most complete measurements of unidirectional composites fracture toughness were presented in (Pinho, 2005) where CT and CC specimens were adopted to measure G_{1T} and G_{1C} respectively.

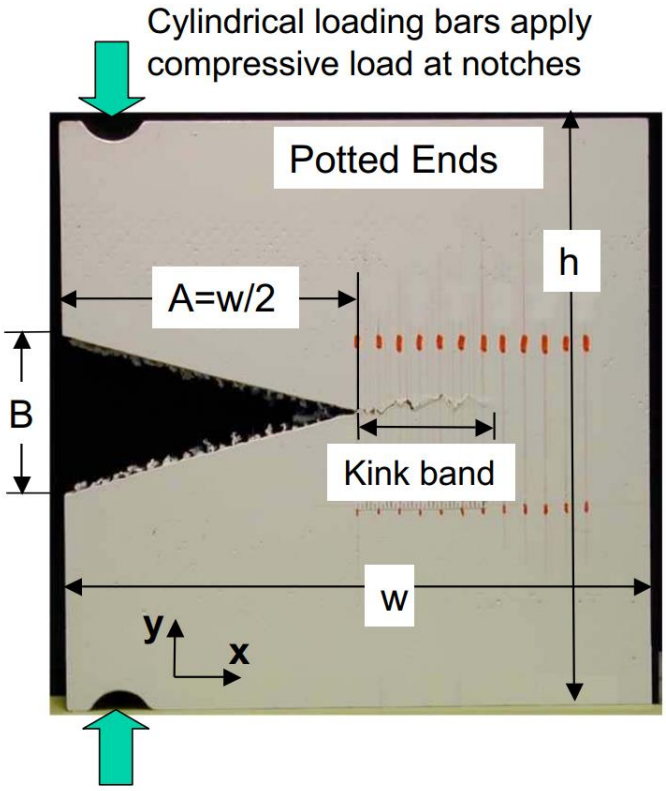

Figure 2.2-4. CC specimen used in (Ratcliffe, et al., 2004) and (Wade, 2014) to measure compressive fracture toughness for composite sandwich panels.

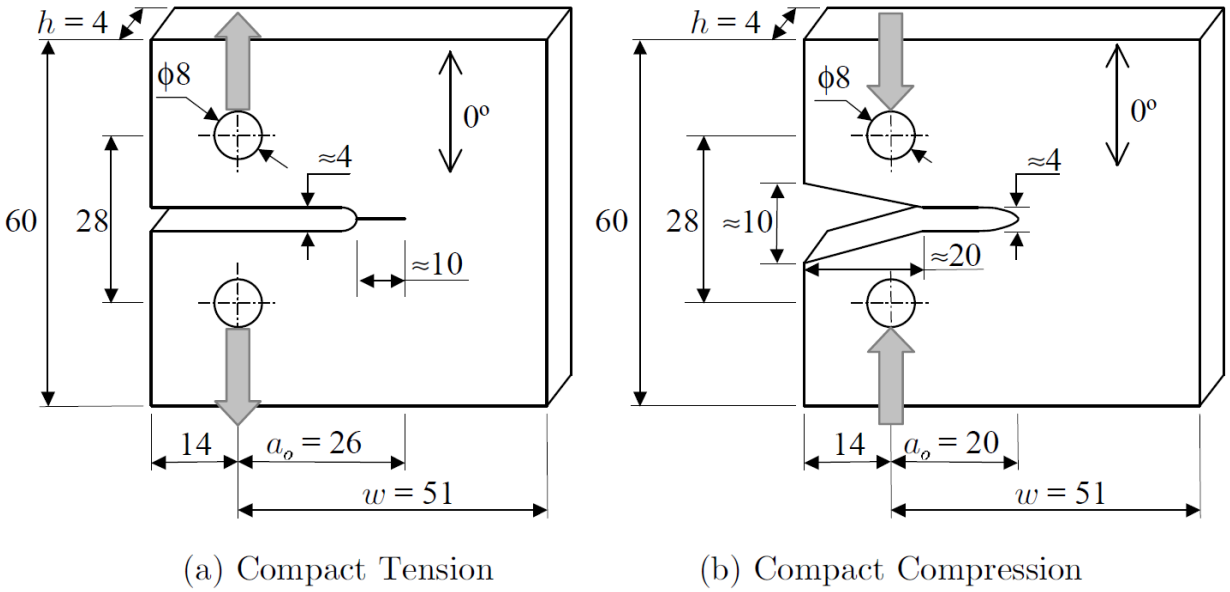

Figure 2.2-5. Fracture toughness test specimens with dimensions in [mm] for (a) tensile and (b) compressive directions along the 1-direction. From (Pinho, 2005).

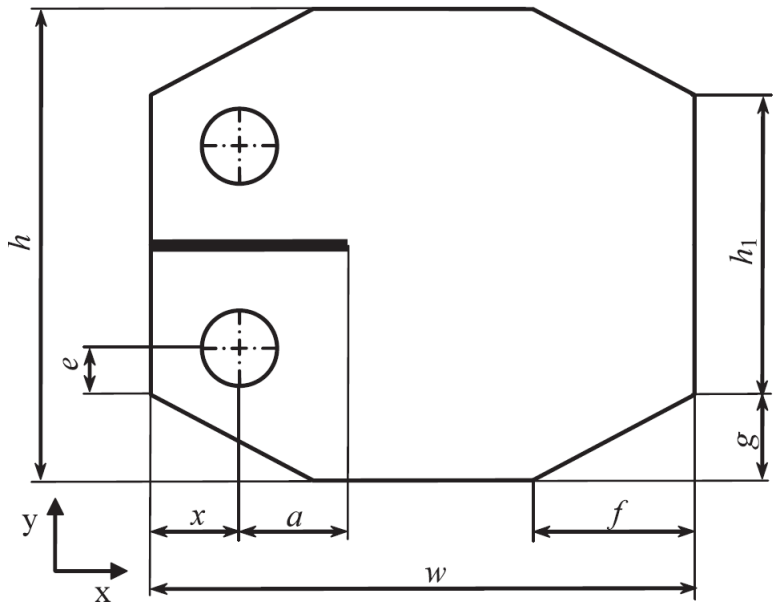

Figure 2.2-6. Doubly-tapered compact tension (2TCT) specimen geometry from (Blanco, et al., 2014).

The specimens are shown in Figure 2.2-5. The CT specimen was further investigated in (Blanco, et al., 2014) for woven composite laminates. Different geometries were investigated. The so-called

doubly-tapered compact tension (2TCT) was selected as the most appropriate geometry and it is shown in Figure 2.2-6.

A review of the most utilized techniques in the literature to measure the translaminar fracture toughness of composites is presented in (Laffan, et al., 2012). The work concluded that the CT and the extended compact tension (ECT) geometries were found to be suitable to measure the tensile fracture toughness G_{1T}, while a robust method for characterization of compressive fracture toughness has not been obtained yet. In (Bazant, 1999) the compressive failure mode of composites was investigated and proposed to occur by propagation of a kink band with fiber microbuckling. The energy dissipated in a kink band in compression in the 1-direction was given expressed as:

$$G_{1C} = \frac{w}{s} G_6 \tag{2.8}$$

Where w is the kink band thickness, s is the distance between two matrix cracks and G_6 is the mode II fracture toughness which can be measured using the four-point end notched flexure (4-ENF) test specimen as discussed in (Miami, 2006) and (Pinho, 2005). In (Miami, 2016) it is proposed that G_{2T} is measured using the Double Cantilever Beam (DCB) test according to ASTM-D5528 (American Society for Testing Materials, 2013). For G_{1T} it is suggested to follow the recommendation from (Pinho, 2005) which uses the CT test specimen. G_{1C} is recommended to be obtained using Equation 2.8 above, or alternatively using the method from (Pinho, 2005) which uses the CC test specimen. An Equation for G_{2C} was given as:

$$G_{2C} = \frac{G_6}{\cos\alpha_0} + \alpha t \mu Y_C \cos\alpha_0 \approx \frac{G_6}{\cos\alpha_0} + \alpha t \eta^T Y_C \cos\alpha_0$$

$$\eta^T = -\frac{1}{\tan(2\alpha_0)} \tag{2.9}$$

where $\alpha_0 \approx 53 \pm 3^0$ is the fracture angle which is the angle between the fracture plane and the loading direction, t is the lamina thickness, α is an adjustment parameter which varies from 0 (for a unidirectional laminate) to 1 (in a strongly confined lamina), μ is the friction term between the crack faces, and Y_C is the compressive strength of the lamina in the 2-direction.

Another interesting study to be mentionde is that of (Lisle, et al., 2015) in which infrared thermography was employed in order to follow the development of failure during an indentation test and to evaluate the compressive fracture toughness in the fiber direction.

2.2.2 *Strain localization and mesh sensitivity in Composites Damage Models*

The evolution of damage in composites Continuum Damage Mechanics (CDM) models, as discussed in Section 2.2, typically entails a post-peak gradual decline of stress at increasing strain. This material behavior, also known as strain softening, is also the case for the work presented in this dissertation, as shown in Figure 4.2-2 and Figure 4.2-3.

The strain softening material behavior utilized in this work is believed to be more representative than some progressive failure analysis methods in which once failure is detected, the relevant elastic properties are reduced to zero, as discussed in Section 2.2.

However, the adoption of strain softening material behavior leads to certain theoretical difficulties knows as localization instabilities and mesh sensitivity of the finite element results (Bazant, et al., 1998).

It is generally accepted that these numerical difficulties can be overcome by supplementing the material models with mathematical conditions aimed at preventing localization of damage into small regions of the mesh. The localization of damage into arbitrarily small regions is referred to as strain localization.

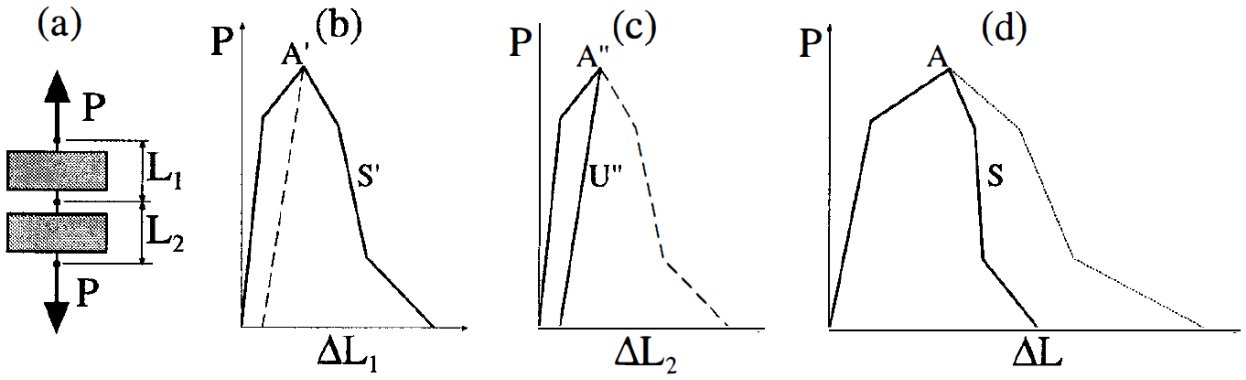

Figure 2.2-7. (a) model of two strain softening elements in series, (b) load-displacement curve for each element, (c) load-displacement curve with unloaded after reaching peak load, (d) resulting load-displacement curve for the model. From (Bazant, et al., 1998).

Strain localization is best explained in (Bazant, et al., 1998) and is summarized in this Section. Consider two elements modelled in series and subjected to tensile loading as shown in Figure 2.2-7 (a). Each element is assigned the same softening material behavior shown in (b). When the two elements are modelled in series, the resulting load – displacement curve for the system is shown in the solid line of (d). The dotted unloading line of (d) is obtained by algebraically summing the softening regions of the two elements, which one could expect to be the resulting behavior. The actual behavior, as shown, is a smaller softening region: lesser total displacement and lesser area under the curve. In the context of stress and strain, the model predicts less total mechanical energy. The dotted softening line of (d) would occur if both elements would experience softening simultaneously. In reality, due to numerical uncertainty, the two elements cannot be perfectly equal, and one would be slightly weaker.

The difference could be as small as the numerical precision of the solver and machine being utilized. An explanation based on thermodynamics is also offered in (Bazant, et al., 1998) which does not rely on the imperfection assumption.

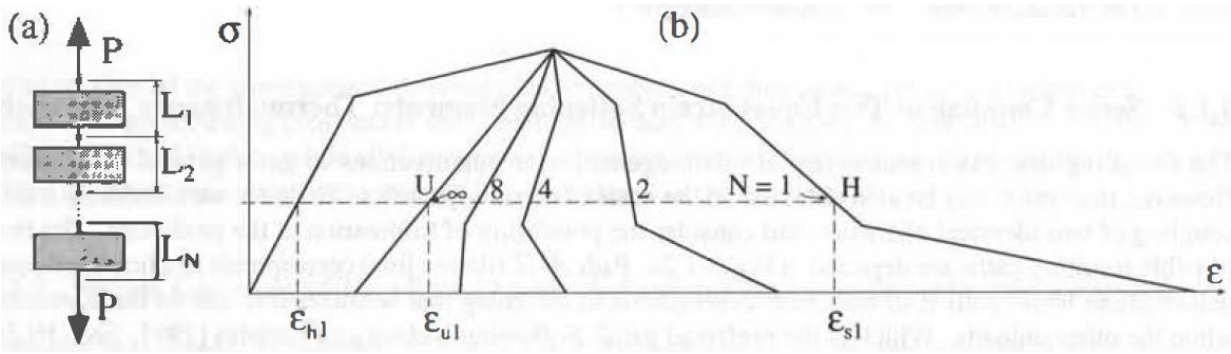

Figure 2.2-8. (a) model of N-number of elements with same softening behavior, (b) resulting load – displacement curve as N increases. From (Bazant, et al., 1998).

Continuing with the imperfection approach, when the model reaches the peak load, marked as point A in Figure 2.2-7, the weaker element would reach the softening region of the load – displacement curve a fraction of the unit of time earlier than the other element, which is still in the elastic region. As the load now decreases, the weaker element is experiencing strain localization, while the second is unloading.

As shown in Figure 2.2-8, in a model with a series of N-number of equal softening elements, because only one element, the weakest, will go through strain softening, while the rest: N-1 number of elements will unload, the resulting load – displacement (or stress – strain) curve for the model changes as a function of how many elements are utilized. The larger the number of elements and the smallest the resulting total mechanical energy: strain energy in this case.

The same concept can be extended to the size of the mesh. If a fixed geometry is meshed with a larger number of smaller elements, rather than fewer larger elements, the resulting strain energy diminishes. This objectivity of the results is a spurious numerical phenomenon and if not corrected invalidates the robustness of a CDM model, as it is the case for the LS-DYNA default material models (Livermore Software Technology Corporation, 2014) and the proposed CDM model in (Wade, 2014) among others. Without the correction of strain localization induced mesh sensitivity,

the resulting models are both physically incorrect and numerically ill-posed. This phenomenon is found to occur when modeling damage in composite material, but also found outside the realm of composites, as for instance when shear bands form in metals.

As previously mentioned, few mathematical conditions have been developed to overcome the spurious mesh sensitivity problem of CDM models. These conditions are referred to as localization limiters. A simple and very effective localization limiter is the Crack Band theory (Bazant, et al., 1983). Some composites CDM models which use the Crack Bend theory localization limiter are: (Maimi, et al., 2007), (Pinho, et al., 2006), (Lapczyk, et al., 2007), and (Xu, et al., 2016). The Crack Band Theory is utilized in the work presented in this dissertation and is summarized in the Section 2.2.3.

Another approach towards preventing strain localization is the use of a nonlocal material model. A nonlocal model is implemented differently than a classical local continuum damage model, in which the stress at a point depends solely on the strain at the same point. In a nonlocal damage model, the stress at a point is also dependent on the strain at neighboring points. This effectively serves as an averaging mechanism which prevents one region from localizing next to a region which is unloading. Some continuum damage models which use nonlocal approach are: (Bazant, et al., 1987), (Tvergaard, et al., 1995) and (Garikipati, et al., 2000). Significant work has been done by the author of this dissertation towards implementing a nonlocal damage model formulation, as discussed in Section 9.2 and it not included in the main body of work, as it requires further validation and verification. The non-localization of the formulation is only applied to the damage variables and not the stress directly. At each integration point of each elements, shown in Figure 3.3-1, local values of the damage variables are calculated, as explained in Sections 4.2.3 and 4.2.4, respectively for static and crushing loading conditions. The first step for the nonlocal

formulation is to calculate an equivalent through the thickness damage value for each damage variable and direction: (1) and (2) material coordinates, and tensile and compressive loading direction. There are four equivalent though-the-thickness sets of damage variables for a fully integrated element, and a single one for a reduced integration element. At this point, the though-the-thickness damage values are non-localized using a Gaussian's distribution function, evaluated at the Gaussian's points. Preliminary analyses have shown promising results, more details are provided in Section 9.2.

It is worth mentioning that a third localization limiter, in addition to utilizing a smeared formulation (Crack Band Theory), and a nonlocal implementation, has been successfully demonstrated to work, and consist in the use of viscosity (Van Der Meer, et al., 2009).

2.2.3 *Crack Band Theory*

The Crack Bend theory localization limiter intervenes directly in the strain softening constitutive relation by adding a length scale, h_c. h_c is the width of the crack band, and it is treated as a material property. As it will be explained below, when incorporating the Crack Band Theory within the FE framework, the strain softening behavior of the material is adjusted according to the chosen element size. This is done in order to yield macroscopically consistent results which are mesh size objective.

It is not possible to measure h_c from fracture tests as for brittle materials, such as composites, this value is very small. For instance, for concrete h_c was approximated in (Bazant, et al., 1998) and (Bazant, et al., 1983) as being: $h_c = 3d_a$ where d_a is the maximum aggregate size for the concrete material. In (Bazant, et al., 1998) it is discussed that utilizing a small value for $h_c = h^{(e)}$, where $h^{(e)}$ is the element mesh size as long as it is sufficiently small, can be used without a noticeable effect.

In (Bazant, et al., 1998) it is demonstrated that the fracture energy G_F, the total work required to break a specimen W_F, and the fracture energy density γ_F, all discussed in Section 2.2.1, are related as expressed in Equation 2.8 below:

$$G_F = \frac{W_F}{A} = h_C \gamma_F \tag{2.10}$$

Where A is the cross-sectional area. The characteristic element size, l_{ch}, is calculated as following:

$$l_{ch} = \frac{E\, G_F}{{X_T}^2} = h_C \frac{E\, \gamma_F}{{X_T}^2} \tag{2.11}$$

Where E is the Young's elastic modulus and X_T is the tensile strength of the lamina, in the case of laminated composites when using the meso-scale modelling approach.

For finite element sizes larger than h_c, the following adjustments are to be made in order to ensure objectivity of the results. The fundamental aspect of the Crack Band Theory is to ensure that the fracture energy is preserved for varying mesh sizes. In order to do so, the approximation proposed in (Bazant, et al., 1983) is to uniformly distribute the fracturing strain over the element, which comports the rescaling of the softening region of the stress-strain relation. The following equation ensures that the fracture energy is preserved by keeping the product of the element size, $h^{(e)}$, and the element fracture energy density, γ_f, constant, using Equation (2.10):

$$h_C \gamma_F = h^{(e)} \gamma_F^{(e)}$$

$$\gamma_F^{(e)} = \frac{h_C}{h^{(e)}} \gamma_F \tag{2.12}$$

Another effective manner to express the Crack Band Theory is by scaling the softening part of the stress strain curve, as expressed by the fracturing strain as shown in Figure 2.2-9 (a) and (b), as shown in the following Equation.

$$\varepsilon^{f^{(e)}} = \frac{h_C}{h^{(e)}} \varepsilon^f \tag{2.13}$$

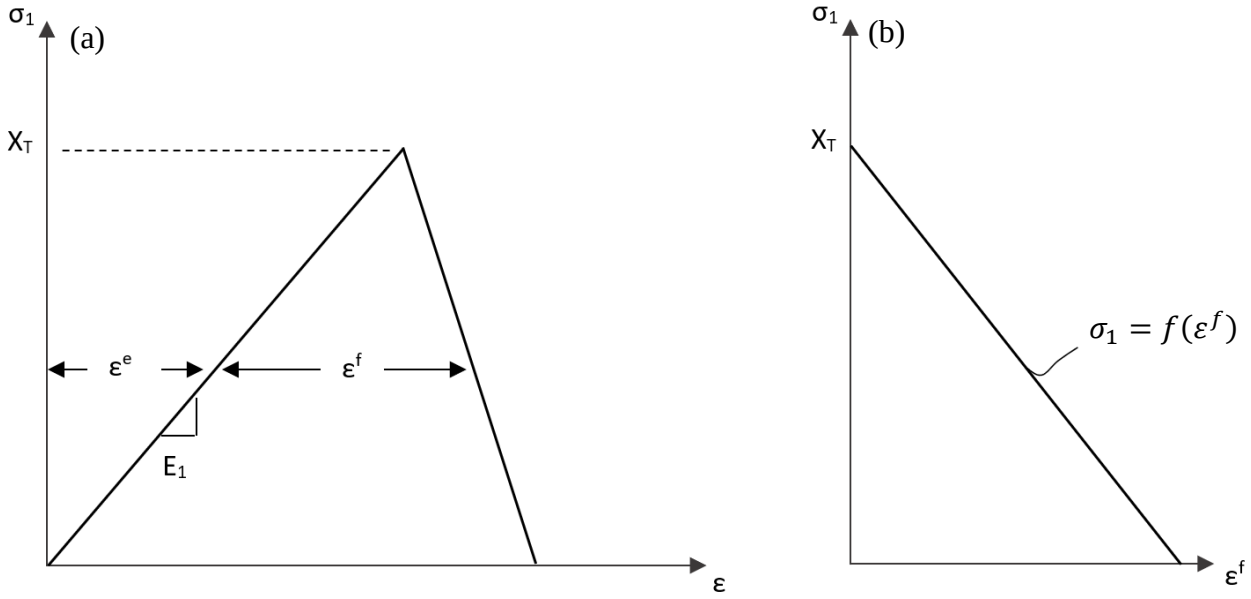

Figure 2.2-9. (a) Elastic-softening stress strain curve. (b) Stress-fracturing strain curve.

Therefore, the key point of using the Crack Band Theory is that the stress strain curve depends on the element size. As illustrated by Figure 2.2-10, if larger elements are utilized, the softening region of the stress-strain curve is reduced. The opposite applies if a smaller than hc element is adopted. There are however limits of applicability for the theory. In particular, if the chosen element size is too large, snapback could result as shown in Figure 2.2-10 (d).

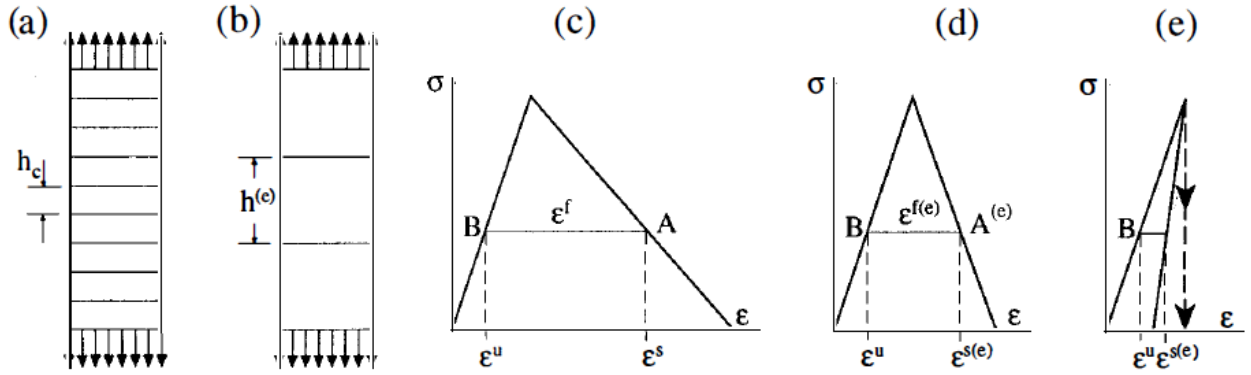

Figure 2.2-10. Bar discretized with finite elements of (a) characteristic size h_c, (b) arbitrary size $h^{(e)}$. (c) Stress-strain curve with linear softening for a physical band of size h_c. (d) Corresponding curve for an element size $h^{(e)}$ in which $\overline{BA} = \overline{BA}\ \frac{h_c}{h^{(e)}}$. (e) Stress-strain curve for an element too large in size, leading to snapback. From (Bazant, et al., 1998).

Figure 2.2-9 shows a stress-strain curve with linear elastic followed by strain softening behavior on the left, and the stress versus fracturing strain, ε_f, on the right. The tensile lamina 1-direction from 4.2.1 is used as example.

As mentioned previously, the Crack Band theory has been used in a large number of engineering computations which involves many different brittle or quasi-brittle materials. A comprehensive study was done to evaluate this technique for possible sources of errors for various finite element modeling strategies (Jirásek, et al., 2012). The finite element formulation, numerical integration scheme, stress uni-, bi- and triaxiality, and estimation of the crack band width were investigated. Among the findings from the study, it was concluded that when using full- versus reduced integration, some numerical solutions were seen to localize into sub-element domains, which is unfavorable. It was also discovered that the effective width of a crack band depends on the element orientation and shape. The conclusions from (Jirásek, et al., 2012) were considered when choosing the finite element implementation used in the work of this dissertation.
The Crack Band theory is implemented in this dissertation in a simplified manner as discussed and demonstrated in Section 4.3.

2.3 CRASHWORTHINESS AND ENERGY ABSORPTION OF COMPOSITE MATERIALS

Crashworthiness defines the ability of a vehicle or a craft, or one of its components, to endure a crash event. A structure is defined crashworthy when the damage to the payload and structure resulting from the crash is minimal, or otherwise acceptable. The overall objective of designing for crashworthiness is to eliminate damage, injuries and fatalities at relatively low energy level impacts and to reduce them as much as possible for relatively higher-level impacts (Composite Materials Handbook-17, 2012). The certification agencies and regulators define the criteria for

crashworthiness for each industry. The four necessary conditions for survivability during a crash event are:

- Maintaining sufficient occupant space
- Providing adequate occupant restraint
- Employing energy-absorbing devices
- Allowing for a safe post-crash egress from the craft

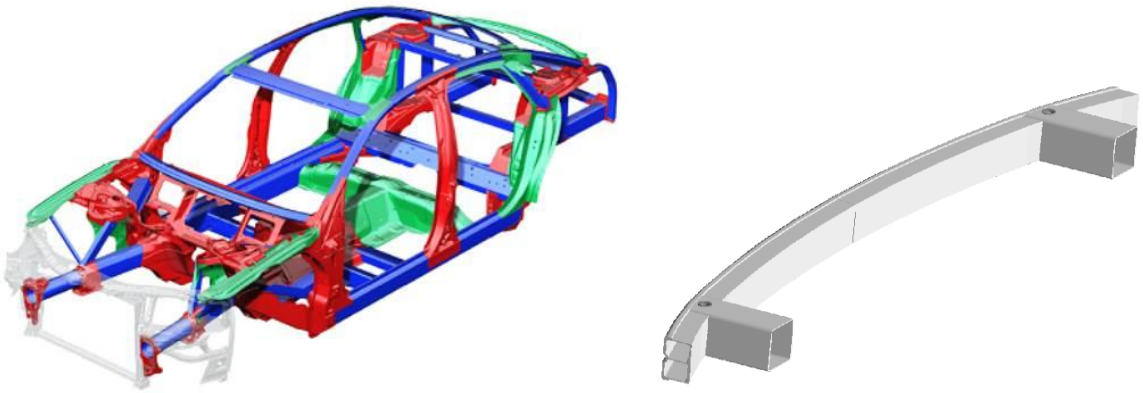

Figure 2.3-1. Bumper-rail automotive assembly for energy absorption in the event of a frontal crash from (Deleo, et al., 2011).

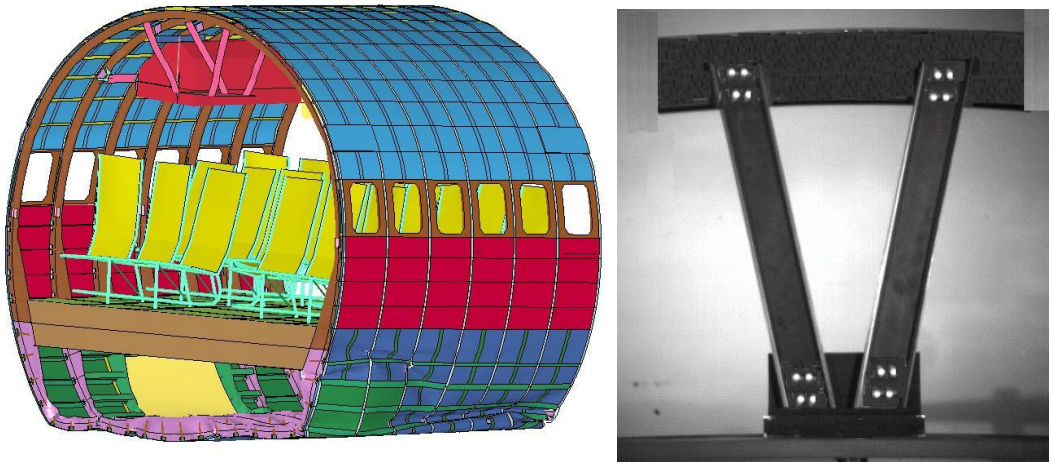

Figure 2.3-2. Stanchion-floor beam aircraft assembly for energy absorption in the event of a belly landing from (Deleo, et al., 2011).

The importance of crashworthiness in virtually every sector of transportation has been recognized and it replaces the previous philosophy of the "stronger, the better" (Carruthers, et al., 1998). Safe dissipation of kinetic energy is ensured through the controlled collapse of the energy-absorbing devices, which is fundamental to make sure that the seriousness of injuries to the occupant and damage to the payload is limited. An example of energy-absorbing devices currently employed in the automotive and commercial aircraft industries are shows, respectively, in Figure 2.3-1 and Figure 2.3-2. Typical automotive designs absorbe energy during frontal crashes via longerons, which are intended to crush via axial compression. Airplanes are certified in the US to be able to withstand a hard landing and satisfy the four forementioned criteria for crashworthiness in the event of a hard landing. Composite airplanes employ stanchions which are dedicated energy absorbing members located underneight the aircraft floor.

The ability for a material / structure to dissipate energy during crush is quantified via the specific energy absorption (SEA), which is a measure of energy absorbed per unit mass. As shown in Figure 2.3-3, the SEA for a structure of length L, undergoing a crushing force F, and being crushed a distance δ is calculated using the following Equation:

$$SEA = \frac{E}{\rho\, A\, \delta} = \frac{\int_0^L F\, dx}{\rho\, A\, \delta} \tag{2.14}$$

Where E is the total energy absorbed, ρ is the material density, and A is the cross-sectional area.

It has been proved that, if properly designed, composite members can provide normalized energy absorption capabilities which are superior to those of metals, therefore making them an attractive choice of material for energy-absorbing structural devices (Carruthers, et al., 1998).

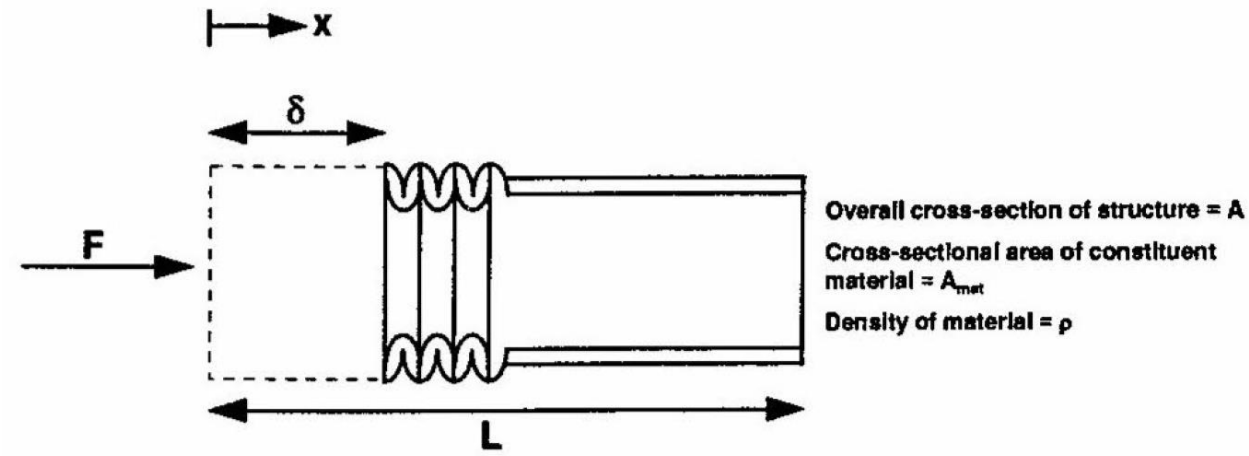

Figure 2.3-3. Representation of a crushed structure from (Carruthers, et al., 1998).

Composites tubes are found to exhibit one of three compressive failure mechanisms during crushing, as described in (Hull, 1991), these are:

- Euler (global) buckling
- Progressive folding
- Progressive crushing

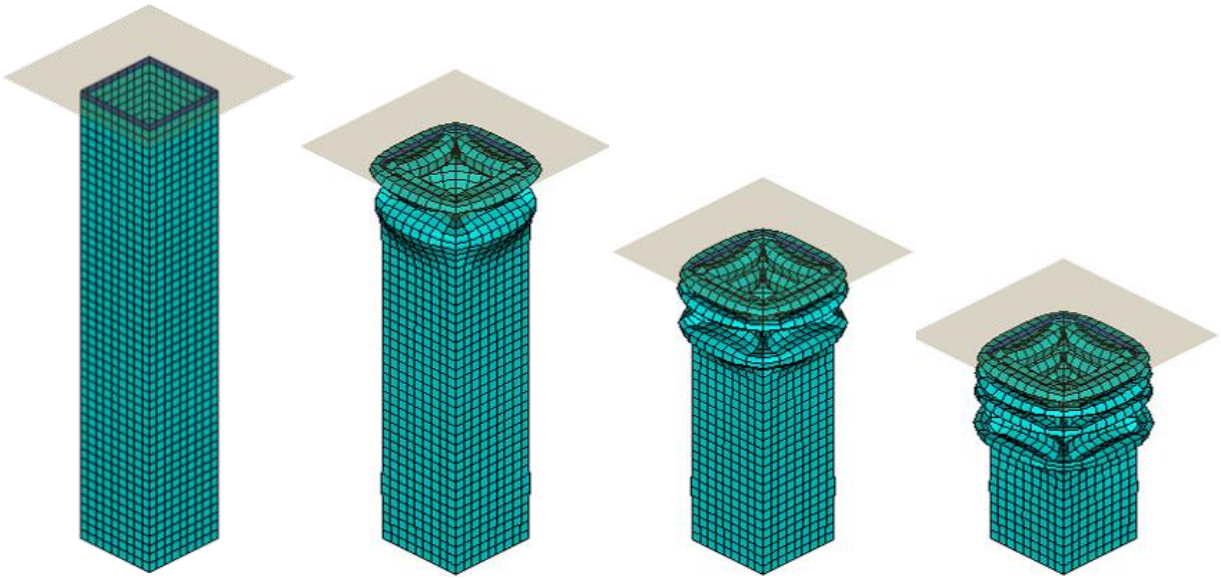

Figure 2.3-4. Progressive folding crushing mode of a simulation of a 6063-T52 aluminum tube, simulating the test shown in (El-Hage, et al., 2010)

The same three possible failure modes are encountered by the author of this dissertations during his Master research for any geometry, in addition to the tubular shape: corrugates plates, and corners. Global buckling results is the lowest amount of energy absorbed as only a small percentage of the material experiences failure and the load carrying capability of the structure is suddenly reduced after the critical buckling load is reached.

Typically, global buckling results when thin long structures undergo compressive loading. Composite structures are found to exhibit this failure mode if the lay-up is made 'too hard': highly 0º dominated.

Progressive folding is the typical crushing mode of ductile metals, composite systems with ductile fibers, such as aramid, and composites layup which are 'very soft': 90º-dominated. Progressive folding consists in the formation of successive local buckles which resemble the shape of a concertina. An example of a typical progressive folding crush mode is shown in Figure 2.3-4. The Figure shows the FE results of the crush analysis of an aluminum tube whose test results are published in (El-Hage, et al., 2010). Progressive folding a more energy absorptive mode than global buckling as the damage occurs at various location along the length of the strucutre via plastic deformation for metals and local failure for composites. However, the most energy absorptive crushing mode is the progressive crushing, which is brittle in nature.

Progressive crushing has the potential of being the most efficient crushing energy mode. Progressive crushing is a mix of a couple brittle failure modes occuring simultaneously: splaying and fragmentation. Flat segments of material tend to exhibit the splaying crushing mode, shown in Figure 2.3-5.

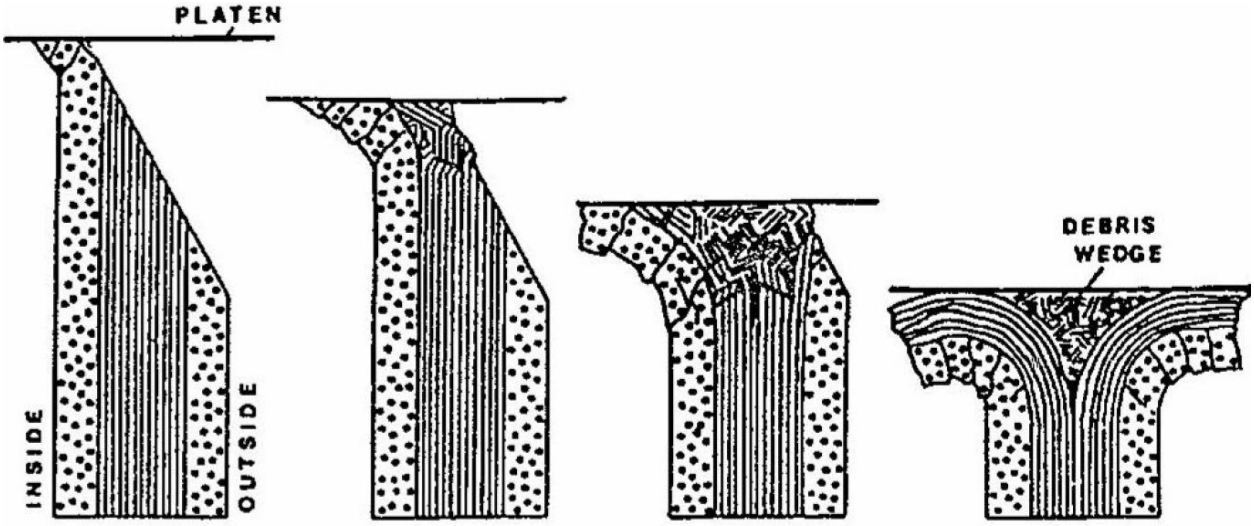

Figure 2.3-5. Schematic representation of the formation of a splaying/lamina bending mode crush zone. From (Carruthers, et al., 1998) and (Hull, 1991).

Splaying / lamina bending is not an efficient energy absorption mode. Typical CFRP geometries in which splaying is the principal crushing mode have SEA values lower than that of metals, in which progressive folding is the crushing mode.

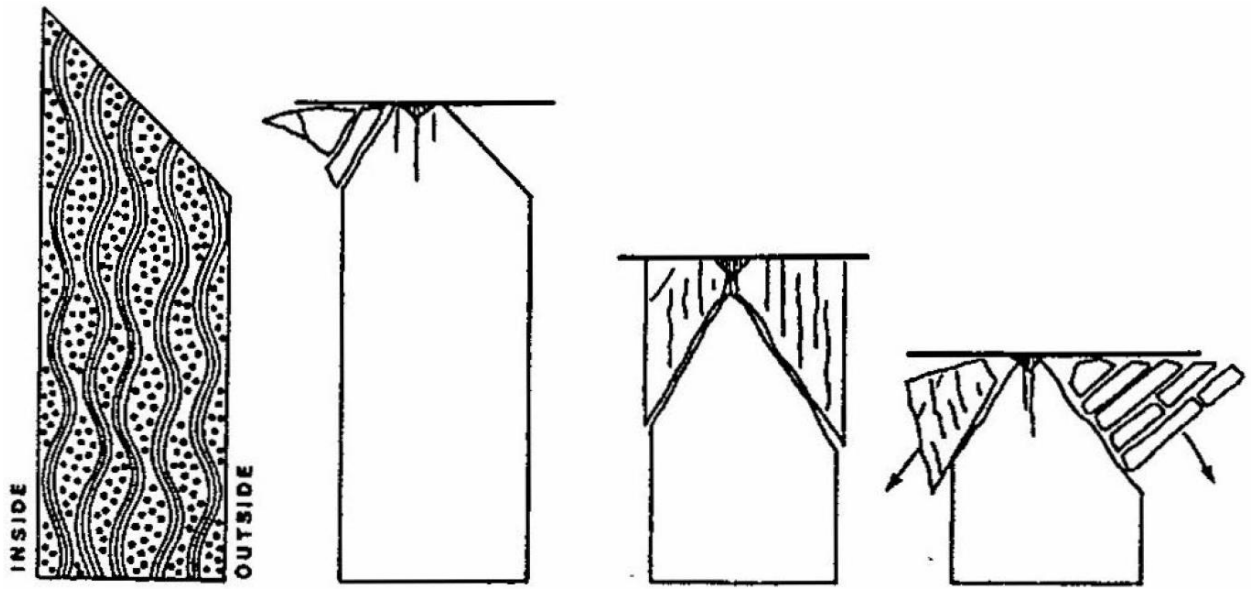

Figure 2.3-6. Schematic representation of the formation of the fragmentation/transverse shearing mode crush zone from (Carruthers, et al., 1998) and (Hull, 1991).

Curved segments of material tend to exhibit the fragmentation failure mode, shown in Figure 2.3-6, in which the material is broken down in small pieces and the crush front is characterized by a large number of small cracks. As explained in (Deleo, 2011), curved shapes offer an additional restraint in the out-of-plane direction which tend to prevent splaying and prefer the fragmentation crush mode. Due to the vast damage enforced on the material, fragmentation produces very high values of SEA. Typical CFRP composite geometries in which fragmentation is the principal crushing mode have SEA values higher than those of typical aerospace grade structural metals.

2.3.1 *Composite Damage Model for crashworthiness*

Several numerical approaches have been proposed to simulate a composite structure undergoing crushing. One of the earliest models was proposed in (Farley, et al., 1992) for the prediction of energy absorption of composite tubes, via the finite element method. In (Hamada, et al., 1997), a finite-elements based progressive crushing analysis method is developed for predicting the mean crush load of filament wound glass fiber / epoxy and wowen glass fiber / epoxy composites tubes, in which splaying is the primary failure mode. The model is very geometry dependent and consists in the modelling of the lamina bending and crack. A linear FEM analysis is carried out using plane strain elements and the crack is modelled with double nodes at the crack line, as shown in Figure 2.3-7.

In (Tabiei, et al., 2001) a micromechanics based material model for crashworthiness is proposed for laminated composites. The method utilizes shell elements. A failure criterion called: micro-failure criterion (MFC) is developed at the constituent level. The method is implemented into the DYNA3D commercially available code (which was later renamed LS-DYNA).

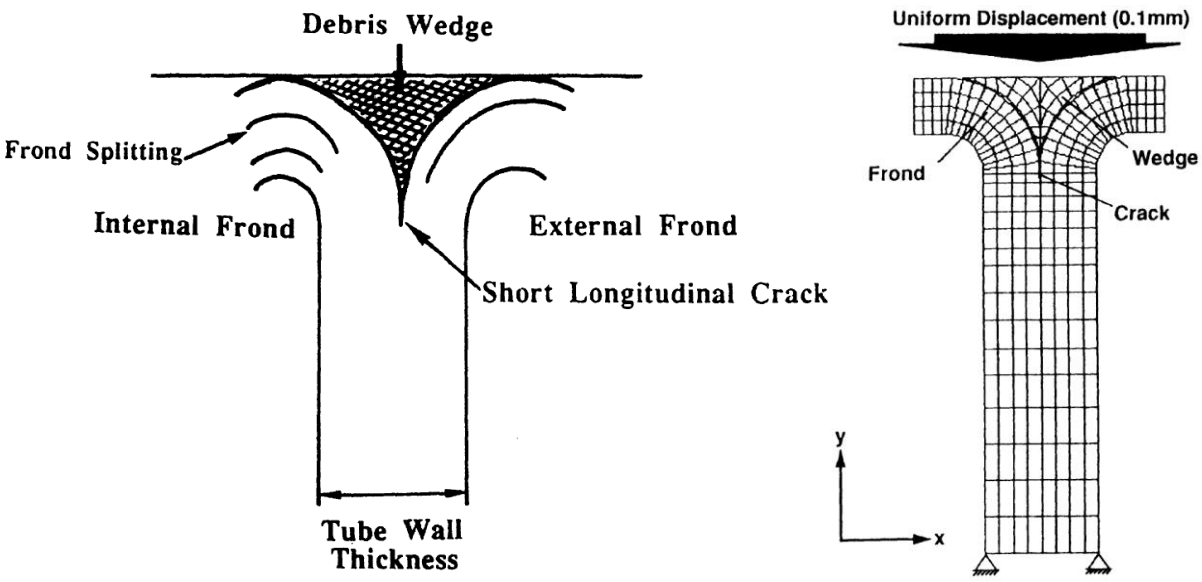

Figure 2.3-7. Left: Schematic diagram of crush zone. Right: Initial FEM mesh of a splaying mode crush zone. From (Hamada, et al., 1997).

In (Fleming, 2001) the Virtual Crack Closure Technique (VCCT) is applied to model the splaying delaminations occuring during a crash by physically modeling the two sublaminates held together by spring elements. In (Morthorst, et al., 2004) a model is proposed for the crushing of fabric composite structures. Both shell and solid finite elements are utilized to model respectively the plies and the intralaminar resin. The Hashin's failure theory described in Section 2.1.1 is employed. In (Sokolinsky, et al., 2011) a methodology for simulating the crushing process of the same corrugated specimen discussed in Chapter 7 is offered. The commercially available solver ABAQUS/Explicit is utilized, the fabric plies are physically modelled and so is the interaction among them via contact interactions. Currently this approach is overly computationally expensive for larger applications. Another model which offers promising results is proposed in (Shi, 2016), in which the laminate is modelled via a shell-beam element approach, as shown in Figure 2.3-8. The modelling approach offers the flexibility and reduced computational cost of 2D shell elements and stability of 3D elements.

A modelling approach which derives from (Deleo, 2011) and LS-DYNA built in model: MAT54 is offered in (Wade, 2014). The modelling technique is computationally efficient but suffers from the problems discussed in Section 7.3, namely the need to filter the results using a non-physical filter scheme, high impulse loading on the structure and the need to calibrate the contact algorithm by using a penalty-based method, not being energy based and not being mesh objective.

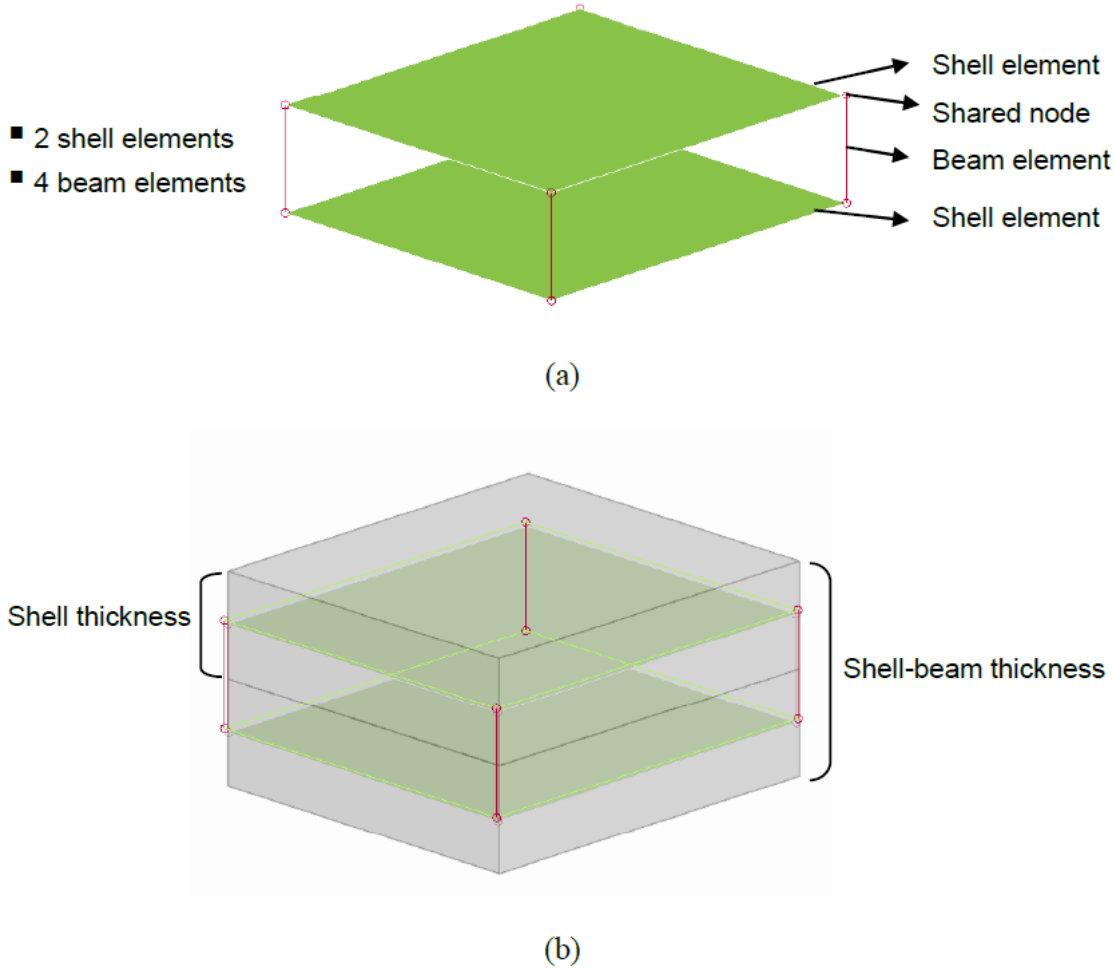

Figure 2.3-8. Schematic of the proposed shell-beam element from (Shi, 2016).

Chapter 3. THEORETICAL BACKGROUND

This Chapter discusses in detail the fundamentals which the theory of this dissertation is built on. The Equations presented in this Chapter will be referenced throughout this dissertation. Section 3.1 offers a review of the mechanics of composites, both at the lamina and laminate level. Section 3.2 introduces the finite element equations and the governing equation. Section 3.3 discusses the finite elements framework and how direct integration is used to solve the governing equation and an introduction to contact algorithms.

3.1 MECHANICS OF LAMINATED COMPOSITES

As discussed in Chapter 1, the theory presented in this dissertation has been formulated to describe the failure behavior of composites laminates build with a stacking sequence of unidirectional tape. The building block of laminated composites is the lamina. A lamina is a sheet of fiber reinforced matrix, which is also called a 'ply'. The material form used to manufacture the specimens tested as part of this dissertation is the prepreg. A prepreg is a roll of pre-impregnated fiber with a specific fiber and matrix volume ratio. Figure 3.1-1 shows the prepreg roll from which laminae were obtained to build the experimental specimens discussed in Sections 6.1 and 7.1 on the left, and a single lamina on the right.

Prepregs are commerically available in a variety of forms: with both thermoset and thermoplastic polymeric resins, unidirectional or weaved fibers. The material system shown in Figure 3.1-1 is a unidirectional Toray T700 carbon fiber embedded in 2510 thermoset polymeric resin. This is the material system used for the experiements of Chapter 6, while in Chapter 7 the unidirectional Toray T800 carbon fiber embedded in 3900-2 thermoset toughned polymeric resin is used. Additional information on the material systems used will be given in Sections 6.1 and 7.1.

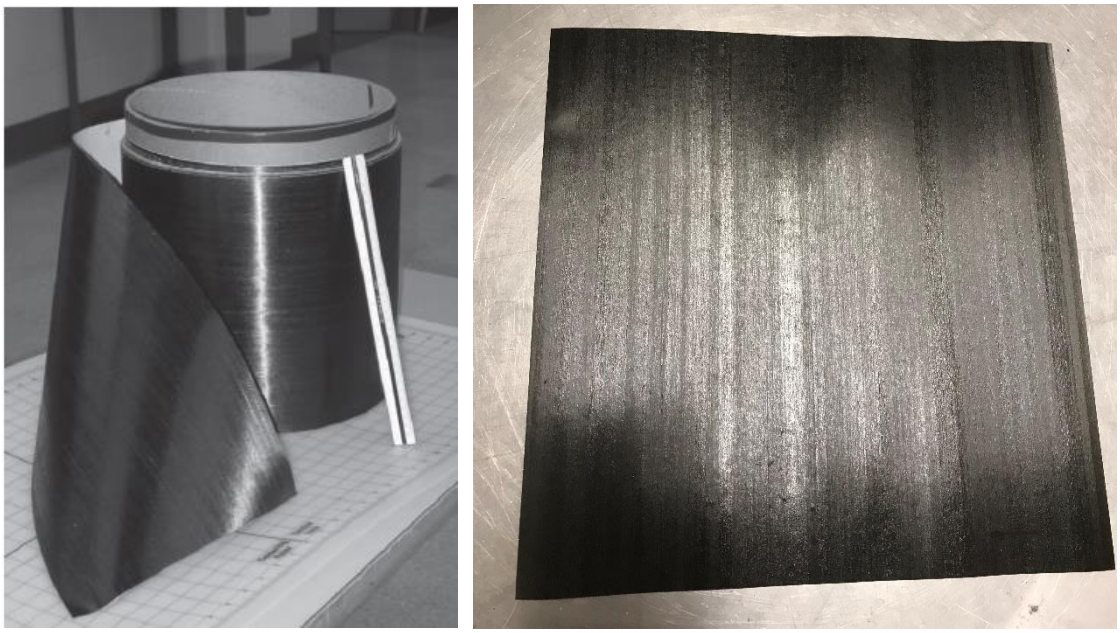

Figure 3.1-1. Prepreg rolls from which laminae were obtained for the experimental coupons (left), a single lamina (right).

Laminae can be cut-out from prepreg rolls and, depending on the direction of the cut, different lamina fiber angles can be obtained. Composite laminates are formed from several unidirectional laminae by stacking them together until the desired laminate thickness is obtained. More detailed information on general composites manufacturing can be found in (Lin, 2015), (Tuttle, 2013) and (Campbell, 2004).

The mechanics of a lamina from a macro-scale perspective is represented with the 2-D plane stress orthotropic constitutive equations shown below (Jones, 1999):

$$\begin{Bmatrix} \sigma_1 \\ \sigma_2 \\ \tau_{12} \end{Bmatrix} = [Q] \cdot \begin{Bmatrix} \varepsilon_1 - \alpha_1 \Delta T - \beta_1 \Delta M \\ \varepsilon_2 - \alpha_2 \Delta T - \beta_2 \Delta M \\ \gamma_{12} \end{Bmatrix} \tag{3.15}$$

Where [Q] is the 2-D plane stress reduced stiffness matrix, which is derived from the 3-D full stiffness matrix by making the plane stress simplifying assumptions which out-of-plane stress

components are zero, while out-of-plane strain components are not. [Q] is computed as described in Equation 3.16.

$$[Q] = \begin{bmatrix} Q_{11} & Q_{12} & Q_{16} \\ Q_{12} & Q_{22} & 0 \\ 0 & 0 & Q_{26} \end{bmatrix} = \begin{bmatrix} \frac{E_1}{1-\nu_{12}\nu_{21}} & \frac{\nu_{12}E_2}{1-\nu_{12}\nu_{21}} & 0 \\ \frac{\nu_{12}E_2}{1-\nu_{12}\nu_{21}} & \frac{E_2}{1-\nu_{12}\nu_{21}} & 0 \\ 0 & 0 & G_{12} \end{bmatrix} \tag{3.16}$$

Where the (1) and (2) subscripts denote the axes: (1) is the fiber direction, and (2) is the matrix direction (2), which is perpendicular to the fiber direction. The (1-2) axes are called the material's axes for a lamina and are shown graphically in Figure 3.1-2. σ's and ε's are the normal stress and strain components, and τ and γ are the shear stress and shear strain components as illustrated in Figure 3.1-3. E_1 and E_2 are the elastic modulus in (1) and (2) directions respectively, and G_{12} is and the in-plane shear modulus of elasticity. The Poisson's ratios ν_{12} and ν_{21} are defined as:

$$\upsilon_{12} = \frac{-\varepsilon_2}{\varepsilon_1}$$

$$\upsilon_{21} = \frac{-\varepsilon_1}{\varepsilon_2} = \upsilon_{12}\frac{E_2}{E_1} \tag{3.17}$$

α's and β's of Equation 3.15 are the coefficient of thermal and moisture expansion respectively. ΔT is the temperature change defined as: stress-free temperature minus operational temperature and is a negative number. The stress-free temperature is very close to the curing temperature. and ΔM is the change in moisture content from curing to operational conditions.

When the material's axes do not coincide with a set of chosen global axes, but are rotated in the plane, the 2-D plane stress lamina stiffness matrix needs to be transformed. The coordinate transofrmation is illustrated in Figure 3.1-4 with positive angle θ between the two coordinate sets: the (1-2) and (x-y) sets of axes. The transformation of the lamina stiffness matrix is done according to the Equations 3.18 and 3.19.

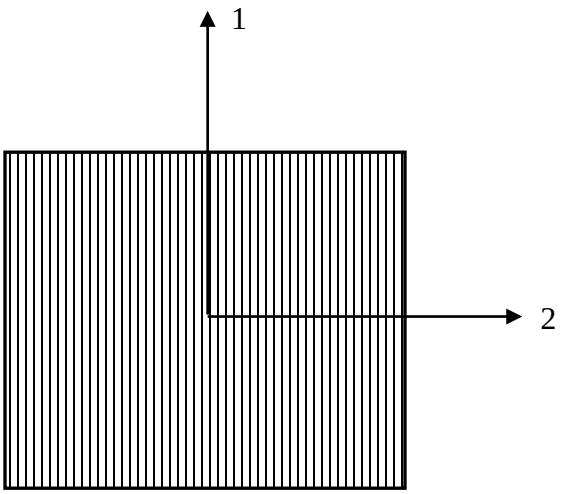

Figure 3.1-2. Material's axes (1-2) for a unidirectional tape composite lamina.

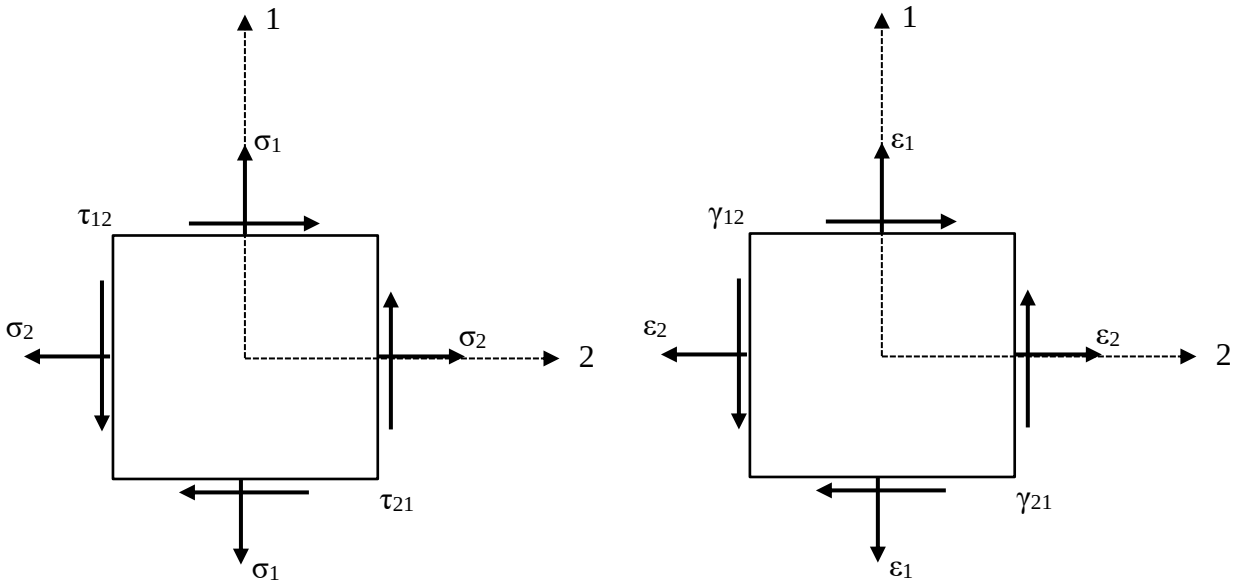

Figure 3.1-3. Stresses (left) and strains (right) 2-D components along (1-2) material axes.

$$[\overline{Q}] = \begin{bmatrix} \overline{Q}_{11} & \overline{Q}_{12} & \overline{Q}_{16} \\ \overline{Q}_{12} & \overline{Q}_{22} & \overline{Q}_{26} \\ \overline{Q}_{16} & \overline{Q}_{26} & \overline{Q}_{66} \end{bmatrix} \tag{3.18}$$

$$\overline{Q}_{11} = Q_{11}(\cos\theta)^4 + 2(Q_{12} + 2Q_{66})(\sin\theta)^2(\cos\theta)^2 + Q_{22}(\sin\theta)^4$$

$$\overline{Q}_{12} = (Q_{11} + Q_{22} - 4Q_{66})(\sin\theta)^2(\cos\theta)^2 + Q_{12}[(\sin\theta)^4 + (\cos\theta)^4]$$

$$\overline{Q}_{22} = Q_{11}(\sin\theta)^4 + 2(Q_{12} + 2Q_{66})(\sin\theta)^2(\cos\theta)^2 + Q_{22}(\cos\theta)^4$$

$$\overline{Q}_{16} = (Q_{11} - Q_{12} - 2Q_{66})\sin\theta\,(\cos\theta)^3 + (Q_{12} - Q_{22} + 2Q_{66})(\sin\theta)^3\cos\theta$$

$$\overline{Q}_{26} = (Q_{11} - Q_{12} - 2Q_{66})(\sin\theta)^3\cos\theta + (Q_{12} - Q_{22} + 2Q_{66})\sin\theta\,(\cos\theta)^3$$

$$\overline{Q}_{66} = (Q_{11} + Q_{22} - 2Q_{12} - 2Q_{66})(\sin\theta)^2(\cos\theta)^2 + Q_{66}(\sin\theta)^4(\cos\theta)^4 \qquad (3.19)$$

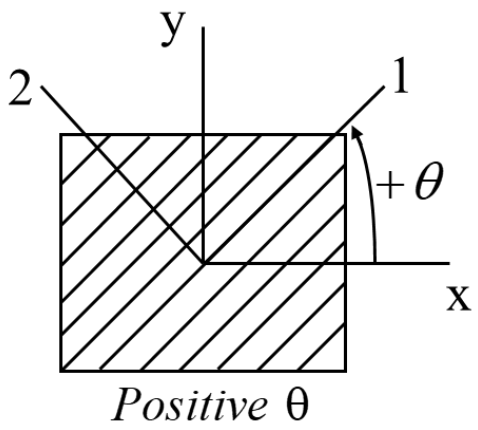

Figure 3.1-4. Lamina's material's (1-2) and global (x-y) axes with positive angle θ between the two sets.

The mechanics of a laminate is described by the Classical Lamination Theory (CLT). CLT offers a mathematical relation between laminate in-plane forces and moments and the resulting laminate's in-plane strains and curvatures, and vice-versa. The relations, which can be think of as the laminate stiffness or compliance, is obtained by combining the contributions of each composing lamina of the laminate. Any of the following references offer the derivation and additional explanation on the CLT: (Jones, 1999), (Kollar, et al., 2003), (Lin, 2015) and (Tuttle, 2013). The CLT relation in the form of stiffness, which relate forces and moments to strains and

curvatures by the famous [ABD] matrix is shown in Equation 3.20. The inverse form can be easily computed and the relating matrix is called the [abd].

$$\begin{Bmatrix} N_x \\ N_y \\ N_{xy} \\ M_x \\ M_y \\ M_{xy} \end{Bmatrix} = \begin{bmatrix} A_{11} & A_{12} & A_{16} & B_{11} & B_{12} & B_{16} \\ A_{12} & A_{22} & A_{26} & B_{12} & B_{22} & B_{26} \\ A_{16} & A_{26} & A_{66} & B_{16} & B_{26} & B_{66} \\ B_{11} & B_{12} & B_{16} & D_{11} & D_{12} & D_{16} \\ B_{12} & B_{22} & B_{26} & D_{12} & D_{22} & D_{26} \\ B_{16} & B_{26} & B_{66} & D_{16} & D_{26} & D_{66} \end{bmatrix} \begin{Bmatrix} \varepsilon_x^{\circ} \\ \varepsilon_y^{\circ} \\ \gamma_{xy}^{\circ} \\ \kappa_x \\ \kappa_y \\ \kappa_{xy} \end{Bmatrix} \tag{3.20}$$

Where A_{ij}, B_{ij} and D_{ij} are the extensional, coupling and bending stiffness components respectively, which are obtained by combining components of each lamina's 2-D plane stress stiffness matrix as described in Equation 3.21. ε^0's are the in-plane strain components and κ's are the curvatures.

$$A_{ij} = \int_{-t/2}^{t/2} \left(\overline{Q}_{ij}\right)_k dz = \sum_{k=1}^{N} \left(\overline{Q}_{ij}\right)_k \left(z_k - z_{k-1}\right)$$

$$B_{ij} = \int_{-t/2}^{t/2} \left(\overline{Q}_{ij}\right)_k z dz = \frac{1}{2} \sum_{k=1}^{N} \left(\overline{Q}_{ij}\right)_k \left(z_k^2 - z_{k-1}^2\right)$$

$$D_{ij} = \int_{-t/2}^{t/2} \left(\overline{Q}_{ij}\right)_k z^2 dz = \frac{1}{3} \sum_{k=1}^{N} \left(\overline{Q}_{ij}\right)_k \left(z_k^3 - z_{k-1}^3\right) \tag{3.21}$$

Where k is the lamina index in the laminate stacking sequence and z is the lamina's distance from the neutral axis. Once the laminate strains and curvature are obtained, the stresses on each lamina can be calculated using the following equation:

$$\{\sigma\}_k = \left[\overline{Q}\right]_k (\{\varepsilon^0\} + z\{\kappa\}) \tag{3.22}$$

$\{\varepsilon^0\}$is the vector of in-plane strains shown by Equation 3.22 along the global axes (x-y). $\{\kappa\}$ is the vector of laminate curvatures along the (x-y) axes as shown in Equation 3.24. $\{\varepsilon^0\}$ and $\{\kappa\}$ are

calculated by CLT as a result of loading condition using the inverse of Equation 3.20. $[\overline{Q}]$ is given in Equations 3.18 and 3.19 for each lamina's angle with respect to the (x-y) axes.

$$\{\varepsilon^0\} = \begin{Bmatrix} \varepsilon_x^0 \\ \varepsilon_y^0 \\ \gamma_{xy}^0 \end{Bmatrix} \tag{3.23}$$

$$\{\kappa\} = \begin{Bmatrix} \kappa_x \\ \kappa_y \\ \kappa_{xy} \end{Bmatrix} \tag{3.24}$$

3.2 GOVERNING EQUATIONS FOR FAILURE ANALYSIS OF COMPOSITES

The Finite Element Method (FEM) is a computer-aided mathematical technique used to obtain an approximate numerical solution to the abstract equations of motion which predict the physical behavior of a system undergoing an external influence. The modern development of the FEM for the field of structural engineering started in the 1940s. Hrennikoff (Hrennikoff, 1941) and McHenry (McHenry, 1943) used one dimensional elements (rods and beams) to calculate stresses in continuous solids, while Courant (Courant, 1943) used piecewise polynomial interpolation over triangular sub-regions to investigate torsion and was the first author to refer to these functions as *shape functions*. In 1950s the FEM equations started to be expressed in matrix form, taking advantage of the advances in high-speed digital computing. Due to research efforts between the department of Aeronautics and Astronautics at the University of Washington (UWAA) and Structural Dynamics Unit at the Boeing Airplane Company, Turner, Clough, Martin and Topp published the revolutionary paper which presented a method for calculating stiffness influence coefficients of complex shell-type structures (Turner, et al., 1956). In the paper the authors first applied the FEM, using the Direct Stiffness Method, to solve a complete aerospace structural problems. The authors included in their paper that: "Considerable extension of the material

presented in the paper is possible". This was the case and, in the decades to follow, the FEM was applied to structural, fluid flow, heat conduction, electro-magnetism, linear and nonlinear, static and dynamic problems. It is safe to state that FEM is now popular for virtually all aspects on engineering, which is partly due to the astonishing advances in computational power.

The theory of this dissertation has been developed to fit within the FEM framework. Because the theory discussed in this dissertation treats failure initiation and propagation of composite structure due to static and dynamic events, the structural dynamic FEM framework is adopted. A structural dynamic analysis is performed when the variation of displacements with time are so rapid that inertia effects are not to be ignored. Unlike for the static formulation, for structural dynamic analyses the structural accelerations and velocities, respectively the second and first derivatives of displacement, are included in the governing equations. Accelerations and velocities are respectively used to account for inertia and damping effects. The governing equations to be solved are listed in the following system:

$$\overrightarrow{F(t)} = [K]\vec{d} + [C]\dot{\vec{d}} + [M]\ddot{\vec{d}} \tag{3.25}$$

Where [K], [C], and [M] are respectively the global stiffness, damping (viscous) and mass matrices, which are obtained by assembling all element equations within a model. The case where damping is not considered is explained in detail in (Logan, 2017). The more general case is described in (Bathe, 1976).

3.3 NUMERICAL IMPLEMENTATIONS WITHIN FINITE ELEMENTS FRAMEWORK

As mentioned in Chapter 2, the finite element method has been vastly used to analyze composite structures and several examples exist in the literature. Cases which require a great level

of details approach the problem from the constituent level and model the fibers and surrounding matrix and their interaction. This approach operates at the *micro-level*.

Another approach, which uses the lamina as the building block operates at the *meso-scale* level, and it is the approach adopted in this methodology. The lamina is considered as a homogenous equivalent orthotropic material, which is comprised of fibers, matrix and interface. Two advantages of this approach are evident. First, the materials' uncertainties are included in the empirical characterization of the material in the unidirectional form; second, the method has a reduced computational cost which is more suitable to immediate application in industry.

At the meso-scale level, composites are either modelled with shell or 3-D elements. 3-D elements are required when the shell simplification is not adequate. Examples of this include woven fabrics or thick laminates (side-to-thickness ratio less than 10). Another example is the detail study of free-edge effects which cannot be captured by a shell element. Because composite structures are usually thin, especially for aerospace and automotive applications, local effects such as the free-edge effect, can be calculated by hand or with dedicated local numerical models. In that case the shell element is the most suitable element type and it chosen to be utilized in the method of this dissertation.

For completeness of the introduction to FEM modeling of composites, composites finite element analyses can also be approached from a *macro-scale* level. In this case the whole laminate is analyzed as a homogenous equivalent unit, which uses the apparent material properties obtained from the application of CLT. Essentially, the stacking sequence and lamina properties are used in the CLT to calculate apparent (or equivalent) properties which are then assigned to the elements as a homogenous material. This approach cannot be used for a fracture mechanics analysis, but it

finds its usefulness when the only required output are displacements, buckling loads and modes, or vibrational frequencies and modes.

The meso-scale approach using shell finite elements is utilized in this dissertation and therefore the lamina is chosen as the building block. During the analysis, calculations are computed at both the lamina and laminate level. The shell element stiffness matrix, [k] can be calculated using the following Equation, which can be derived using the Principle of Minimum Potential Energy (PMPE) (Zienkiewicz, et al., 2013):

$$[k] = \iint [B]^T [D][B] dxdy \tag{3.26}$$

Where [B] is the gradient matrix, which is calculated by taking partial derivates of the element shape functions, and [D] is the material matrix, also sometimes referred to as stiffness matrix but not to confused with [k] itself. The equations for shape functions and gradient matrix for shell elements are too cumbersome to be included in this dissertation and the reader is referred to (Zienkiewicz, et al., 2013). In addition, the composite fracture mechanics theory discussed in this dissertation has been successfully been applied by the author using a variety of element types, which include plates and several types of shells, which have different shape functions. Equation 3.26 is general and can be used with any 2-D element type.

[D] is composed of material properties. For instance, [D] for a 1-D rod is simply the material's elastic modulus 'E'. [D] can include any anisotropic properties. For laminated composites analyzed at the meso-scale level, [D] is composed of the [ABD] matrices as described in Equation 3.21.

As part of the finite element method framework, all elements stiffness matrices are combined into the single global stiffness matrix [K] according to the degrees of freedom the elements share.

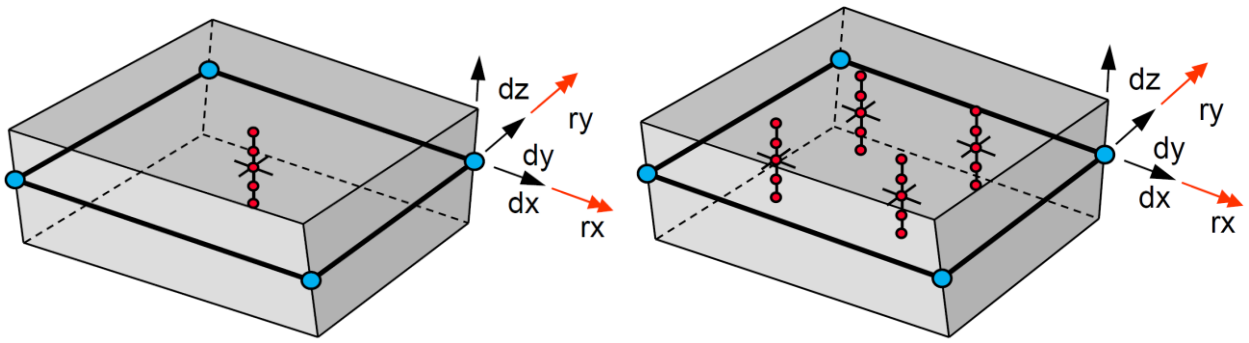

Figure 3.3-1. Four-noded shell element for a five-laminae stacking sequence with reduced (left) and full integration (right).

The local element stiffness matrix [k] is a square, singular matrix of size: number of degrees of freedom of the element by number of degrees of freedom of the element; while the global stiffness matrix [K] is a square, singular matrix of size: number of degrees of freedom of the whole model by number of degrees of freedom of the whole model. [K] is then used in Equation 3.25.

Equation 3.26 is computed by numerical integration, using Gaussian Quadrature. For laminated composites, the shell elements' integration points through the thickness are located at each lamina location. For instance, a four-noded shell element which is assigned a five-laminae stacking sequence has either five or twenty integration points, depending if it is reduced or fully integrated.

3.3.1 *Explicit direct integration scheme*

The governing equations of Equation 3.25 are solved by time discretization using numerical integration in time: direct integration. The integration technique is defined as 'direct' because Equation 3.25 is solved in a step-by-step fashion directly, therefore without prior transformation into a different form. With direct integration the nodal displacements are solved for at each time increment. The nodal velocities and acceleration are then obtained from the nodal displacements. Direct integration methods are classified into *implicit* and *explicit*. Examples of implicit methods are the Newmark-Beta (Newmark, 1959), the Wilson-Theta (Bathe, 1976) and Houbolt (Houbolt,

1950) methods. An example of an explicit method is the well-known and vastly utilized Central Difference method.

Implicit and explicit numerical integration schemes have several fundamental differences. Nonlinear implicit schemes, in order to obtain a solution at each timestep, require a series of trial solutions known are iterations. The iterations are performed until equilibrium is established within a pre-determined tolerance. In an explicit analysis no iterations are required as the nodal accelerations are solved directly. When employing an explicit integration procedure the size of the timestep needs to be less than a critical value, which is dictated by the Courant-Friedrichs-Levy (CFL) condition (Courant, et al., 1967). Satisfying the CFL is necessary for convergence. Because Equation 3.25 is dynamic, which include inertia and damping effects, stress waves through the material result as a consequence of loading conditions. At each timestep nodal displacements are calculated. The critical aspect is to ensure that the code calculates the displacements of the next node before the wave from the previous node calculation can impact it. More generally, the CFL conditions dictates that the time increment for the solution be smaller than the time the stress wave takes to travel through the mesh. Given that the stress waves travel in the material at the speed of sound, the timestep requirement in a plane media (2D-continuum) is given by the following Equation:

$$\Delta t_c = \frac{L}{\sqrt{\frac{E}{(1-\nu^2)\rho}}} \tag{3.27}$$

Where E is the maximum modulus of elasticity for the case of an orthotropic material, such as the one discussed in this dissertation, ρ is the material density, ν is the minimum Poisson's ratio, and L is the minimum element edge length.

While a MATLAB solver has been written as part of this work to offer some code-to-code validation for simplified problems, and increase confidence in the solution, the theory presented in this dissertation has been implemented into the commercially available solver called LS-DYNA as discussed in Chapter 5. LS-DYNA, as utilized in this work, solves Equation 3.25 using an explicit scheme.

3.3.2 *Contact algorithms within the finite elements framework*

As discussed in Chapter 5, one of the main reason the theory discussed in Chapter 4 is implemented into LS-DYNA is to take advantage of the already implemented contact algorithms. The contact phenomenon is intrinsically non-linear in nature and can be classified in three main categories, normal, tangential, and thermal (Konter, 2000), (King, et al., 2013). When a region of a body is found to be in contact with another body, the contact condition is divided in normal and tangential directions at any contact point within the contact region. Tangential contact can be sub-categorized in two: frictionless (sliding) or with friction. In a frictionless contact problem no constraints are added to the tangential displacement near the contact surface. As a result, the nodes are free to move along the surface. This tangential displacement results from the deformation or large displacements of the bodies or from rigid body motions. If accounting for friction is required by the analysis goal, a friction model needs to be included. In addition, thermal contact phenomena refer to the change in boundary conditions, i.e. thermal conductance, as bodies come into physical conduct. If bodies are in contact, heat transfer will take place between the bodies. If they are not in contact, heat transfer is only due to radiation. Thermal conductance is similar to the friction coefficient, in that is a function of many factors, such as surface roughness, contact pressure, temperature difference and material properties (Madhusadana, et al., 1986). Thermal contact

phenomena are not deemed significant for this type of analyses and are therefore not considered in the mathematical formulations.

Several Finite Element approaches exist to solve a contact problem, as discussed in (Konter, 2000), (King, et al., 2013). The methods for contact analysis generally consider contact between two or more deformable bodies and contact between deformable and rigid bodies. In all contact methodologies several methods of contact handling are categorized as:

- Node to node
- Node to surface
- Surface to surface

In the three methods above, contact is enforced at discrete points, in an average sense over a region surrounding each slave node, and between a feature edge and a surface respectively. The benefits of using a surface-to-surface approach are a reduced likelihood of large localized penetrations, reduced sensitivity of results to master and slave roles, more accurate contact stresses and a better inherent smoothing, which improved overall convergence.

There are several ways to mathematically model normal contact. The most common is the strict enforcement, also referred to as “hard”. This enforcement is achieved with the Lagrange multiplier method in LS-DYNA. The constraint equations and the Lagrange multiplier are added to the finite element system of equations. While this method is the most intuitive, the following drawbacks are possible: it can be challenging for Newton iterations to converge, overlapping constraints are problematic for equation solver, and Lagrange multipliers add to equation solver cost.

A penalty based normal contact allows a small amount of penetration and bases the normal response to the stiffness of the load versus penetration behavior. The “hard” and penalty-based normal contacts are shown graphically in Figure 3.3-2. The advantages of using a penalty based

constraint enforcement are: improved convergence rate, better equation solver performance (no Lagrange multiplier degree of freedom) and good treatment of overlapping constraints. The disadvantages are: a small amount of penetration, and the need to validate / calibrate the penalty stiffness value. The penalty stiffness value should be low enough to maximize the computational efficiency while still provide realistic contact behavior.

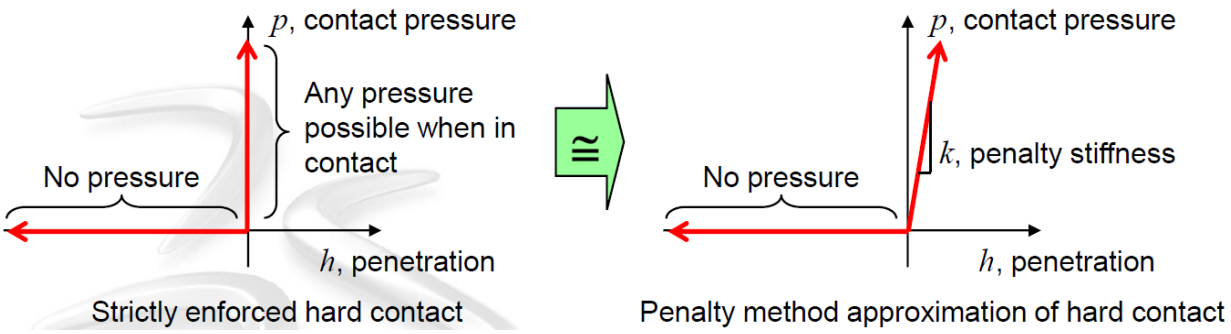

Figure 3.3-2. Hard normal contact enforcement versus penalty method, from (King, et al., 2013).

Chapter 4. COMPOSITE DAMAGE MODEL FOR CRUSH AND STATIC FAILURE

In this Chapter, the continuum damage progressive failure model developed as part of this research is introduced for both static failure and crash loading conditions. In Section 4.1, the Hashin's failure criteria, discussed in Section 2.1.1, is shown as modified as part of this work. In section 4.2 the failure propagation methodology is discussed. The proposed lamina strain softenining behavior is introduced in Section 4.2.1, the fracture energies as used in this study are summarized in Section 4.2.2, in Sections 4.2.3 and 4.2.4 the derivations of the damage variables used respectively for the static failure and crash loading models are derived. The damage variables are then used to degrade the finite element stiffness matrix to simulate damage. Damage propagation and the Distribute Damage Model (DDM) developed as part of this research are discussed in Sections 4.2.5 and 4.2.6 respectively.

The methodoly is summarized graphically in Figure 3.3-1. The method can be applied to both static and crush failure. The difference between the two loading conditions consists in the damage variables for compressive failure in the 1- and 2- directions: D_{1C} and D_{2C}. The derivation of compressive damage variables for static and crash loading are presented in Section 4.2.3 and 4.2.4 respectively.

Static loading:

$$D_{1C} = D_{1C\_STATIC}(\varepsilon_1, X_C, E_1, E_2, \nu_{12}, \nu_{21})$$

$$D_{2C} = D_{2C\_STATIC}(\varepsilon_2, Y_C, E_1, E_2, \nu_{12}, \nu_{21})$$

Crash loading:

$$D_{1C} = D_{1C\_CRASH}(\varepsilon_1, X_C, E_1, E_2, \nu_{12}, \nu_{21})$$

$$D_{2C} = D_{2C\_CRASH}(\varepsilon_2, Y_C, E_1, E_2, \nu_{12}, \nu_{21})$$

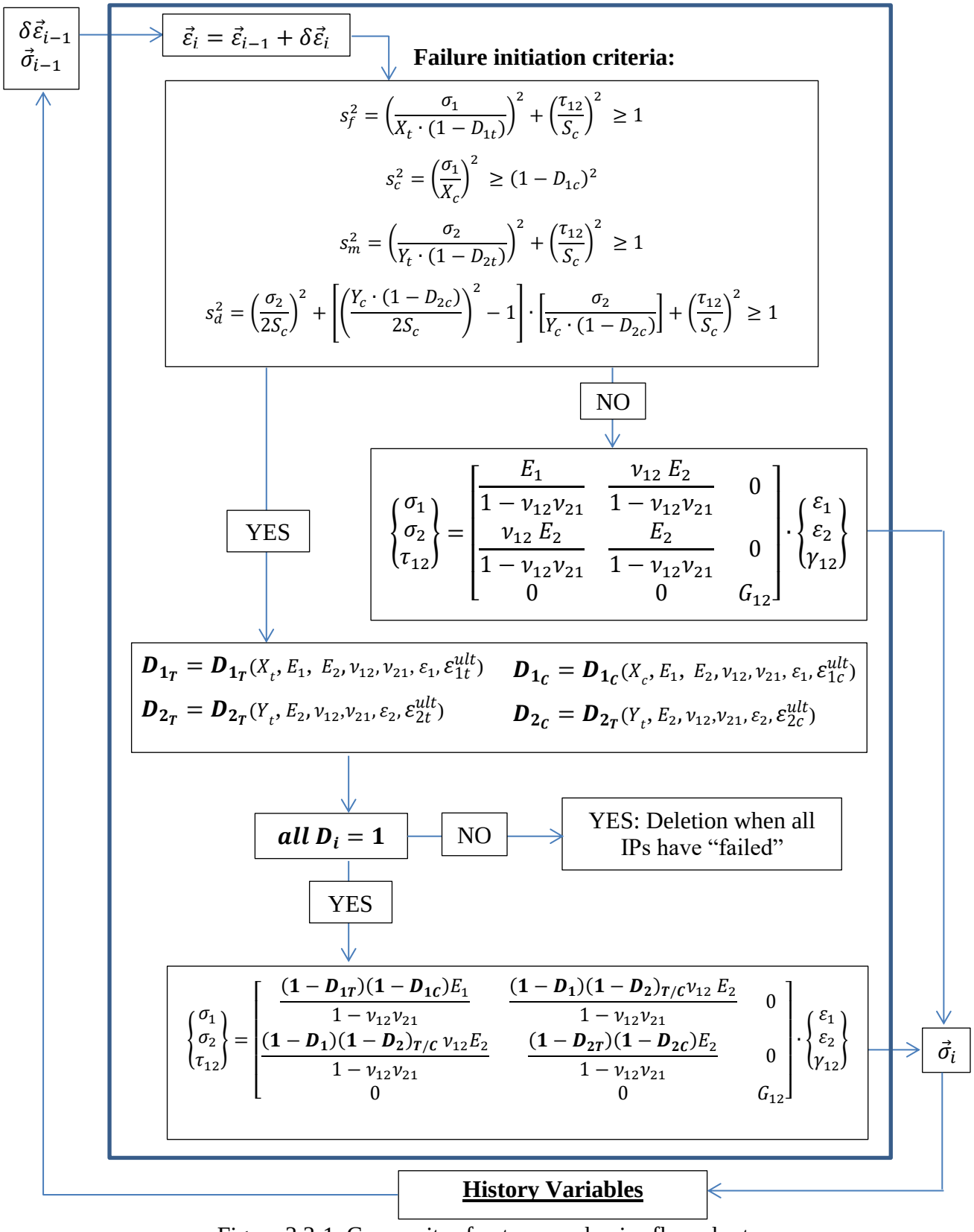

Figure 3.3-1. Composites fracture mechanics flow chart.

Where ε_1, ε_2, E_1, E_2, ν_{12} and ν_{21} are the normal strain components and elastic moduli the moduli in the 1- and 2- directions and the two in-plane Poisson's ratio for a lamina respectively, as discussed in Section 3.1. X_C and Y_C are the compressive lamina strength respectively in the 1- and 2- directions, and S_C is the shear strength. The other difference between the two loading conditions consists in the implementation of the Damage Distributing Model (DDM), which is nonlocal in nature and it applies pre-damage to a row of elements when the previous row failed .

Because of the differences discussed above, models for the two loading conditions are implemented separately in LS-DYNA as UMATs. The implementation is discussed in Chapter 5. The UMAT for crush analyses keeps track of failure: records the failed integration points. This serves two purposes: 1: it allows the implementation of the Distribute Damaging Model, and 2: allows the algorithm to identify the crashfront during the crush analysis.

This methodology is developed so that when a damage variable assumes the value of 1, the integration point in question is deemed failed. When all integration points within the element are failed, the element is removed from the mesh and deleted. This is the case for both static and crash conditions, except for the crash solution which includes a re-hardening, compacting, region in the compressive stress-strain curve, as shown in Figure 4.2-4. This solution is discussed in Section 4.2.4. This composites fracture mechanics method is designed to be applied in an iterative fashion, where each iteration is a timestep towards the solution of Equation 3.25. The flowchart procedure of Figure 3.3-1 is applied at each integration point of each element at each timestep.

At the beginning of the UMAT call, the solver provides the stresses from the end of the previous cycle and the strain increments. The strain increments are calculated by the solver outside of the UMAT using the previous stresses, boundary conditions and global to material axes transformation. The first operation into the UMAT is to update the strain tensor by summing each

component with the associated strain increment: the two in-plane normal and three out-of-plane shear strain components are updated. The strains in each lamina are always along the material's axes: (1-2).

Next, the stress failure initiation criteria checks are applied. There are four criteria enforced at the lamina level: tensile and compressive modes in the 1- and 2- directions. Currently there is not a dedicated shear failure criterion, but the shear stress and shear stress allowable have been included in the 1- and 2-direction failure criteria, except for the compressive failure criterion in the 1-direction. All failure criteria chosen for this work are stress-based. As discussed in Chapter 2, composite materials suffer from the lack of a robust, fully predictive and comprehensive failure theory. The failure criteria chosen for this work, the Hashin's theory, have been shown to provide an adequate level of predictability (Kaddour, et al., 2013), however the methodology developed for this dissertation has been written to be able to accommodate for a change in failure criteria. If a more robust failure criterion is developed in the future, the failure initiation criteria module in the UMAT can be simply updated while the rest of the methodology will remain. This offers a level of flexibility which is crucial for a lasting fracture mechanics theory into a field that is quickly evolving. If all four failure theories result in negative findings, the UMAT updates the stresses using the 2-D plane stress orthotropic constitutive relation shown in Equation 3.15 and outputs them back to the solver.

If one of more failure criterion detect failure initiation, a dedicated damage variable is calculated for each failure mode: tensile and compressive modes in the 1- and 2- directions. The damage variables are derived using a conservation of energy principle which utilizes the fracture energies. Unlike fracture mechanics theory for isotropic material, or other theories for laminated composites, this theory makes use of four distict fracture energies values, one for each failure mode: tensile

and compressive modes in the 1- and 2- directions. As shown in Figure 3.3-1, if the element is not yet to be deleted, the damage variables are then utilized to degrade the 2-D plane stress stiffness matrix according to the damage variable mode. New stresses are calculated and output to the solver.

4.1 FAILURE INITIATION CRITERIA

As discussed above, this composites damage mechanics model includes failure initiation criteria, one for each failure mode: tensile and compressive modes in the 1- and 2- directions. As discussed in Section 2.1, composite materials suffer from the lack of a robust a comprehensively reliable failure theory. As part of the methodology discussed here four failure criteria are utilized and are shown in Equations 4.28 – 4.31, for each failure mode respectively: tensile and compressive modes in the 1- and 2- directions. No dedicated mode is included for shear. The shear contribution is however included in the other failure directions, which the except of compression in the 1-direction. The shear contribution in the tensile mode in the 1- and 2- directions can be adjusted depending on the material using the parameters β_{1T} and β_{2T} respectively.

Tensile mode in 1- direction:

$$s_f^2 = \left(\frac{\sigma_1}{X_T \cdot (1 - D_{1t})}\right)^2 + \beta_{1T}\left(\frac{\tau_{12}}{S_C}\right)^2 \geq 1 \tag{4.28}$$

Compressive mode in 1- direction:

$$s_c^2 = \left(\frac{\sigma_1}{X_C}\right)^2 \geq (1 - D_{1c})^2 \tag{4.29}$$

Tensile mode in 2- direction:

$$s_m^2 = \left(\frac{\sigma_2}{Y_T \cdot (1 - D_{2t})}\right)^2 + \beta_{2T}\left(\frac{\tau_{12}}{S_C}\right)^2 \geq 1 \tag{4.30}$$

Compressive mode in 2- direction:

$$s_d^2 = \left(\frac{\sigma_2}{2S_C}\right)^2 + \left[\left(\frac{Y_C \cdot (1-D_{2C})}{2S_C}\right)^2 - 1\right] \cdot \left[\frac{\sigma_2}{Y_C \cdot (1-D_{2C})}\right] + \left(\frac{\tau_{12}}{S_C}\right)^2 \geq 1 \quad (4.31)$$

Where X_C and Y_C are the compressive lamina strength respectively in the 1- and 2- directions, and S_C is the shear strength. S_f, S_c, S_m and S_d are flags used in the FORTRAN code discussed in Chapter 5 and are utilized to detect failure in each mode. Equations 4.28 and 4.30 are modified from the Chang-Chang failure criteria (Chang, et al., 1987). Equation 4.29 is simply the maximum stress failure criterion applied in the compressive 1-direction. Equation 4.31 contains three parts: one of pure compressive stress and allowable in the 1-direction, one of pure shear stress and allowable, and a mixed one. The same Equations are also utilized in (Matzenmiller, et al., 1991). The set of failure theories, in the unmodified version therefore not including the damage variables, were first proposed in (Hashin, 1980) by Professor Hashin and are referred to as the Hashin failure theory. The derivation of Equations 4.28 – 4.31 is summarized in Section 2.1.1.

The criteria are stress based. The various damage parameters, which are proposed in this methodology: D_{1T}, D_{1C}, D_{2T} and D_{2C} are added to reduce the strength in the case of accumulated damage. This is particularly important when loading and unloading is present during the simulation, as it occurs often during a crush analysis. At re-loading, following an unloading, the material at each integration point remembers the accumulated damage and if the conditions are such, the damage will further accumulate.

4.2 FAILURE PROPAGATION CRITERIA

The failure initiation criteria implemented in this work were presented in Section 4.1. This Section discusses the how the fracture process is modelled. Section 4.2.1 discusses why a degradation law is implemented at the lamina level. The degradation law is energy based and utilizes four distinct fracture energy values, and the derivation is shown in Section 4.2.2. The

stiffness and strength degradation of failing laminas is implemented via four damage variables, one for each material principle axis: 1-2 axes, and loading direction: tension / compression. The damage variables for static loading and crashworthiness are respectively discussed in Sections 4.2.3 and 4.2.4.

4.2.1 *Strain softening behavior of composites laminas*

It is common knowledge that unidirectional fiber reinforced composites when tested in the principle material axis (1-direction), for instance in tension, exhibits typical brittle to failure behavior: nearly linear load-displacement (or stress-strain) curve until the peak stress. At the peak stress, catastrophic dynamic failure occurs. A common misconception is that the fracture occurs instantaneously and no fracture process strain softening behavior occurs; this is not the case. As discussed in Section 2.2.3 and shown from FEA results in Section 4.3, the damage is localized to an area, with theoretical width equal to h_c. During the damage process, the region of the material which is not localizing is unloading elastically, while the area which is localizing is undergoing strain softening and fracture strain (inelastic) accumulation.

A similitude exists between the fracture of advanced fiber reinforced plastics (FRPs) and other brittle and quasi-brittle materials, such as concrete. This similitude was already explored in this dissertation, specifically in Section 2.2.3 when the Crack Band Theory strain localization limiter was discussed. In fact, the Crack Band Theory was originally developed for concrete and later successfully applied to model FRPs. When modelling concrete, the simplest technique is to utilize a cohesive crack model (Bazant, et al., 1998). A cohesive crack is a way to degrade the stiffness of the material, at the location undergoing damage, such as the crack front, and therefore transfer stress from one face to the other. Using a cohesive crack model, the fracture process is therefore modeled with a softening behavior after the peak stress. This approach is referred to as the

Hillerborg's approach (Hillerborg, 1985) and was experimentally validated in the late 1960s as shown in (Hughes, et al., 1966) and (Evans, et al., 1968). A similar material behavior also exists for FRPs. As discussed in (Kaw, 2006). When a lamina fails it still contributes to the stiffness and strength of the laminate according to a pre-determined degradation law. As discussed in Section 2.2, several continuum damage models have been proposed to date for laminated composites which use different degradation laws. The failure propagation criteria developed for this dissertation is explained in the following Sections: 4.2.2 - 4.2.6 both for static loading and crashworthiness.

4.2.2 *Fracture energies densities:* $\gamma_{1T}, \gamma_{1C}, \gamma_{2T}, \gamma_{2C}$

As discussed in Section 2.2.1, the fracture energy is the composites equivalent of fracture toughness for metal. The term fracture toughness is sometimes not used because it implies the presence of cracks. Cracks, by definition, have a crack tip radius of zero, and therefore present a singularity at the crack tip. Composites do not crack, because the damage which initiates and propagated have a finite damage tip radius (Composite Materials Handbook-17, 2012). The damage propagation methodology between metals and composites is also different. Damage growth via crack propagation in metals (Schijve, 2009), while for composites generally damage grows via delaminations (Composite Materials Handbook-17, 2012). As discussed in Section 2.2.1, unlike for metals, for composites there is not an acceptable method to measure fracture toughness. Several specimen types were presented in Section 2.2.1. Developing a new reliable test standard for testing for composite fracture energies is not the scope of the current work. In the methodology presented in this dissertation, the fracture energies are input material properties.

The fracture energy for composites can be intended as the energy available to dissipate via damage. It can also be visualized as the work required to fully break a unit of volume of material. When all available energy is dissipated, damage propagates. In the context of the Finite Element

Method, as introduced in Section 3.3, when a finite element's strain energy reaches the appropriate fracture energy value (depending of direction) the element is deemed 100% failed and is physically removed from the mesh. An easier, but equivalent way to track damage is via the damage variables discussed in Sections 4.2.3 - 4.2.4. When a damage variable reaches unity, the element is deemed failed.

Because of the orthotropic and non-homogenous nature of an advanced composites lamina, a single fracture energy is not deemed sufficient for the model described in this dissertation. This work is formulated to accommodate as input the fracture energy densities, which are related to the specific fracture energies by Equation 2.10. A fracture energy density value per lamina material axis and loading direction are proposed for a total of four as described below:

γ_{1T} – Fracture energy, (1)-axis, tensile direction.

γ_{1C} – Fracture energy, (1)-axis, compressive direction.

γ_{2T} – Fracture energy, (2)-axis, tensile direction.

γ_{2C} – Fracture energy, (2)-axis, compressive direction.

Where the (1) and (2) axes are the lamina material axes described in Section 3.1. It is important not to confuse the (1) and (2) axes with fracture modes I (opening) and II (sliding) for cracks. Because of the lack of available test standards and data in the literature, for the purpose of this dissertation, values for the total work required to break a specimen, in the four directions mentioned above are utilized. The values are listed together with the other material properties.

4.2.3 *Derivation of damage variable for static loading: D_{1T}, D_{1C_STATIC}, D_{2T}, D_{2C_STATIC}*

The damage variables discussed in this Section are derived from the assumptions that strain softening is linear and ultimate failure occurs when the appropriate fracture energy is fully dissipated via elastic and plastic straining. The shape of the strain softening is chosen for numerical

simplicity and to reduce the amount of possible numerical instability associated with changes in strain softening slope during an explicit dynamic simulation, as discussed in Section 9.1.

Experimentally, when performing material characterization testing at the lamina level, it is possible to measure the strength and stiffness of the material. The ASTM standards which were followed in order to obtain the material properties for this work are the D3039 (ASTM International, 2008), D695 (ASTM International, 1996), and D7078 (ASTM International, 2005), respectively for tension, compression, and shear loading directions. Measuring the strain softening response of the lamina, and/or the strain to failure values is not possible following the aforementioned ASTM standards, and it is currently not done while characterizing a material system. In this work, the strain to failure values in the four directions considered by the failure initiation criteria of Section 4.1, are calculated, not measured, using the available elastic material properties, lamina strengths and fracture energies as shown next.

The strains to failure are derived next. The strain to failure in the tensile 1-direction for a unidirectional lamina, $dfail_{1T}$, is used to explain the derivation procedure for all four of them and is derived as discussed next.

The fracture energy in the tensile 1-direction, γ_{1T}, which is discussed in Section 4.1, is expressed in terms of the area under the stress-strain curve as shown in Figure 4.2-1 and expressed in Equation 4.32.

$$\gamma_{1T} = \frac{X_T{}^2}{2 \cdot E_1} + \frac{X_T \cdot \left(dfail_{1T} - {X_T}/{E_1} \right)}{2} \tag{4.32}$$

Where all variables are described in Sections 3.1 and 4.1. The first and second terms in Equation 4.32 are respectively the area under the elastic and softening regions of the stress-strain curve. $dfail_{1T}$ is solved from Equation 4.32 as shown in Equation 4.33.

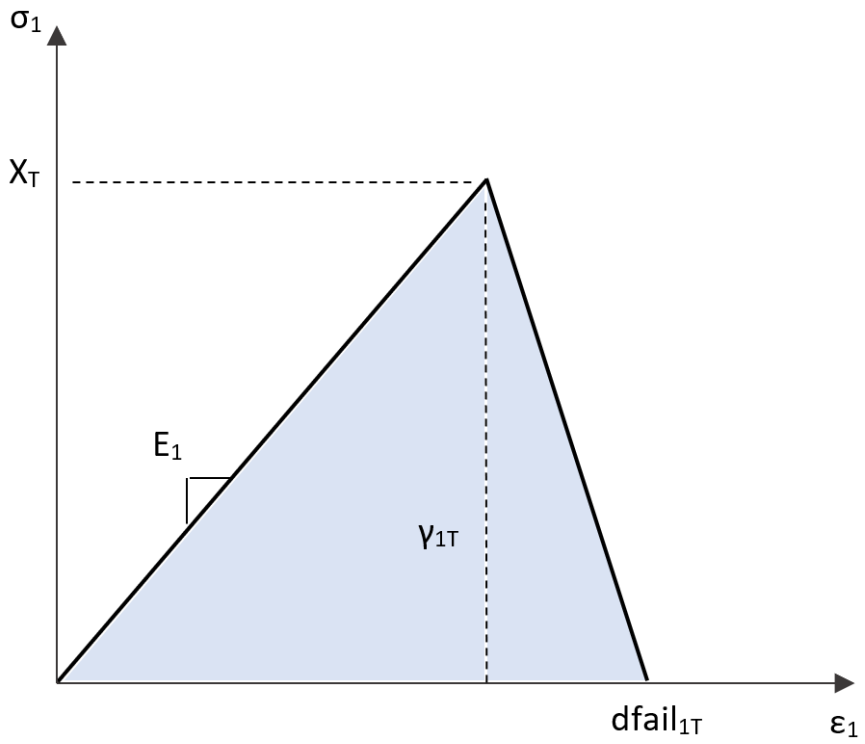

Figure 4.2-1. Stress-strain behavior of a unidirectional lamina in tension in the 1-direction.

The strains to failure in the remaining directions: the compressive 1-direction, $dfail_{1C}$, and in the tensile and compressive 2-direction: $dfail_{2T}$ and $dfail_{2C}$, are derived following the same procedure, and are shown in the Equation below:

$$dfail_{1T} = \frac{2 \cdot \gamma_{1T}}{X_T}$$

$$dfail_{1C} = \frac{2 \cdot \gamma_{1C}}{X_C}$$

$$dfail_{2T} = \frac{2 \cdot \gamma_{2T}}{Y_T}$$

$$dfail_{2C} = \frac{2 \cdot \gamma_{2C}}{Y_C} \tag{4.33}$$

The damage variables are derived next. The damage variable for the tensile 1-direction, D_{1T}, is used as example. The same procedure applies for the compressive damage variable, D_{1C_STATIC} (for static loading) also. D_{1C_CRASH} is derived in Section 4.2.4.

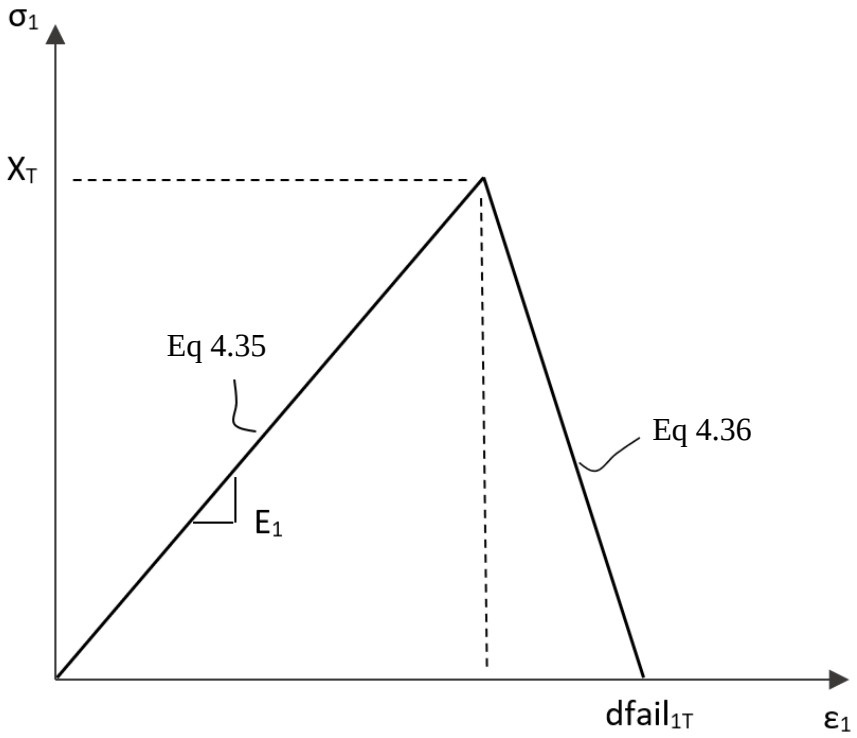

Figure 4.2-2. Tensile stress-strain curve in 1-direction showing linear elastic and strain softening region.

The stress-strain curve in the tensile 1-direction, as shown in Figure 4.2-2, is represented algebraic a piecewise linear function. Equation 4.35 governs the linear elastic region, while Equation 4.36 governs the plastic stress-softening region.The elastic region is represented by the first equation of the system in Equation 4.15, written below:

$$\sigma_1 = \frac{E_1\,\varepsilon_1}{\text{denom}} - \frac{\nu_{12}\,E_2\,\varepsilon_2}{\text{denom}}$$

$$\text{denom} = 1 - \nu_{12}\nu_{21} \tag{4.34}$$

Using the definition of Poisson's ratio of Equation 3.17, Equation 4.34 is re-written as:

$$\sigma_1 = \left(\frac{E_1}{\text{denom}} - \frac{{\nu_{12}}^2\,E_2}{\text{denom}}\right)\varepsilon_1 \tag{4.35}$$

The linear strain softening region part is governed by the following Equation, which includes the damage variable D_{1T}:

$$\sigma_1 = \left(\frac{E_1}{denom} - \frac{\nu_{12}{}^2 E_2}{denom}\right)(1 - D_{1T})\varepsilon_1 \tag{4.36}$$

The linear stress-softening region can also be represented the equation of line going through two points. The points are: P1: ($\varepsilon_1 = X_T/E_1$, $\sigma_1 = X_T$) and P2: ($\varepsilon_1 = dfail_{1T}$, $\sigma_1 = 0$).

$$\sigma_1 - X_T = m_{1T}\left(\varepsilon_1 - \frac{X_T}{E_1}\right) \tag{4.37}$$

Where m_{1T} is the slope of the stress-softening region which is expressed in the following Equation. The stress-softening slopes for the compressive 1-direction, tensile and compressive 2-direction, respectively m_{1C}, m_{2T} and m_{2C} are obtained following the same procedure and shown in the next Equation.

$$m_{1T} = -\frac{X_T}{dfail_{1T} - \frac{X_T}{E_1}}$$

$$m_{1C} = -\frac{X_C}{dfail_{1C} - \frac{X_C}{E_1}}$$

$$m_{2T} = -\frac{Y_T}{dfail_{2T} - \frac{Y_T}{E_2}}$$

$$m_{2C} = -\frac{Y_C}{dfail_{2C} - \frac{Y_C}{E_2}} \tag{4.38}$$

D_{1T} is the damage variable to quantify and keep track of damage in the tensile 1-direction. It is solved for by equating Equations 4.36 and 4.37 and it is expressed by the following Equation. In a similar fashion, the damage variable for the compressive 1-direction under static loading: D_{1C_STATIC}, is obtained:

$$D_{1T} = 1 - \frac{m_{1T}\left(\varepsilon_1 - \frac{X_T}{E_1}\right) + X_T}{\left(\frac{E_1}{denom} - \frac{\nu_{12}{}^2\, E_2}{denom}\right) \cdot \varepsilon_1}$$

$$D_{1C\_STATIC} = 1 - \frac{m_{1C}\left(\varepsilon_1 - \frac{X_C}{E_1}\right) + X_C}{\left(\frac{E_1}{denom} - \frac{\nu_{12}{}^2\, E_2}{denom}\right) \cdot \varepsilon_1} \tag{4.39}$$

The damage variable for the tensile 2-direction, D_{2T}, is used as example. The same procedure applies for the compressive damage variable, D_{2C_STATIC} (for static loading) also. D_{2C_CRASH} is derived in Section 4.2.4. The stress-strain curve in the tensile 2-direction is shown in Figure 4.2-3. The elastic region is represented by the second equation of the system in Equation 3.15, written below:

$$\sigma_2 = \frac{\nu_{12}\, E_2\, \varepsilon_1}{denom} + \frac{E_2\, \varepsilon_2}{denom} = \left(\frac{1 - \nu_{12}{}^2}{denom}\right) E_2\, \varepsilon_2 \tag{4.40}$$

The linear strain softening region part is governed by the following Equation, which includes the damage variable D_{2T}:

$$\sigma_2 = \left(\frac{1 - \nu_{12}{}^2}{denom}\right)(1 - D_{2T})\, E_2\, \varepsilon_2 \tag{4.41}$$

The linear stress-softening region can also be represented the equation of line going through two points. The points are: P1: ($\varepsilon_2 = Y_T/E_2$, $\sigma_2 = Y_T$) and P2: ($\varepsilon_2 = dfail_{2T}$, $\sigma_2 = 0$).

$$\sigma_2 - Y_T = m_{2T}\left(\varepsilon_2 - \frac{Y_T}{E_2}\right) \tag{4.42}$$

D_{2T} is the damage variable to quantify and keep track of damage in the tensile 2-direction. It is solved for by equating Equations 4.41 and 4.42 and it is expressed by the following Equation. In a similar fashion, the damage variable for the compressive 2-direction under static loading: D_{2C_STATIC}, is obtained:

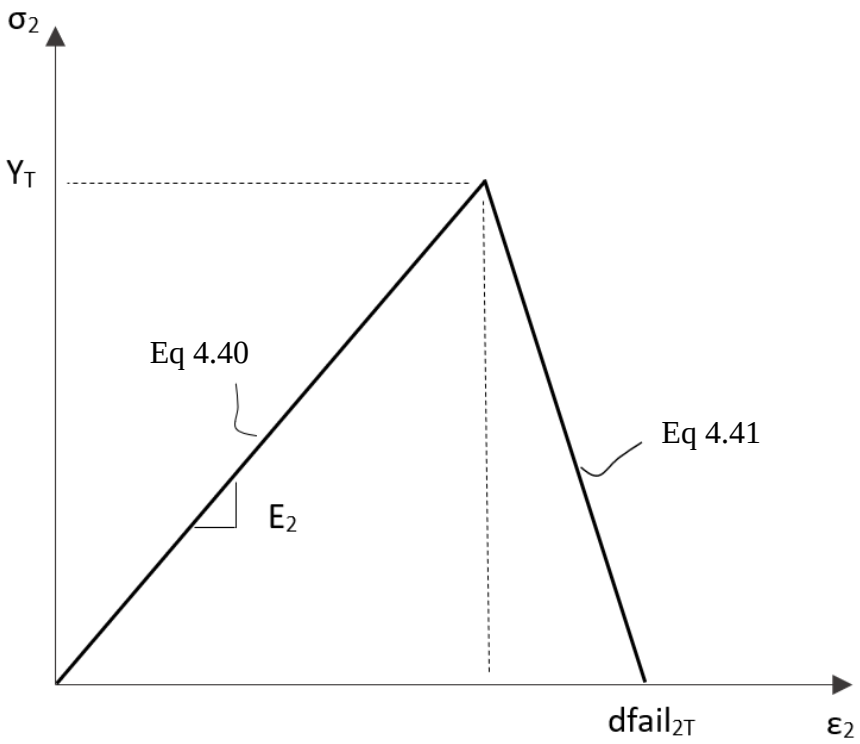

Figure 4.2-3. Tensile stress-strain curve in 2-direction showing linear elastic and strain softening region.

$$D_{2T} = 1 - \frac{m_{2T}\left(\varepsilon_2 - \frac{Y_T}{E_2}\right) + Y_T}{\left(\frac{1 - \nu_{12}{}^2}{\text{denom}}\right) \cdot \varepsilon_2}$$

$$D_{1C\_STATIC} = 1 - \frac{m_{2C}\left(\varepsilon_2 - \frac{Y_C}{E_2}\right) + Y_C}{\left(\frac{1 - \nu_{12}{}^2}{\text{denom}}\right) \cdot \varepsilon_2} \tag{4.43}$$

The damage variables serve a dual purpose: 1. they numerically quantify damage, 2. they offer a way to monitor damage evolution. The damage variables values range from 0 to 1:

Dxx = 0 ⟶ no damage at integration point

Dxx = 1 ⟶ 100% damaged at integration point

When a damage variable assumes the value of 1, the integration point is deemed failed. As discussed in Chapter 4, when all integration points within an element have failed, the element is physically removed from the mesh and deleted.

4.2.4 *Derivation of damage variables for crash loading: D_{1T}, D_{1C_crash}, D_{2T}, D_{2C_crash}*

A separate set of compressive damage variables for crash analyses is derived in this Section and it is the results of various long studies which are not documented in this work. While the tensile damage variables, D_{1T} and D_{2T}, respectively expressed in Equations 4.39 and 4.43 are unchanged for both static and crash loading conditions, the compressive damage variables are not found to work well when simulating a crushing event. The main reason is that the stress-strain curve for compression is not suitable to model the material behavior during crushing. When attempting to do so, as it is done in (Deleo, 2011), (Wade, 2014), (Feraboli, et al., 2011) and (Feraboli, et al., 2016), incorrect results are obtained as discussed in Section 2.3.1. The way that previous authors have approached the problem of modeling crushing is by artificially increasing the strength of the material (or not reducing it sufficiently, as discussed in Section 4.2.6), prematurely deleting elements, and then smoothing the resulting load-displacement curve to match the experimental results. While it can be argued that the energy is conserved, as the area under the curve is the same, with their approach, the model sees artificially high impulse loading and it is therefore not suitable for outputting stresses or to be used in large models outside dedicated coupon testing.

In this work, the compressive damage variables are derived from the idea that the unidirectional lamina material performance assumes a linear elastic – perfectly plastic behavior during progressive failure crushing. As discussed in Section 2.3, several damage modes occur

simultaneously during crushing of laminated composites. When the composites crashes in a progressive failure manner, the resulting behavior tends to hold a constant crush load.

Two solutions have been developed. After the linear elastic region and the region of perfect plasticity, the first approach assumes a re-hardening region, as shown in Figure 4.2-4. The linear elastic region is governed by Equation 4.35.

The perfectly plastic region is expressed by Equation 4.44. The re-hardening compacting region of Figure 4.2-4 is represented by Equation 3.38.

$$\sigma_1 = \left(\frac{E_1}{\text{denom}} - \frac{\nu_{12}{}^2 E_2}{\text{denom}}\right)\left(1 - D_{1C\_CRASH}\right)\varepsilon_1 = X_C \tag{4.44}$$

From which the damage variable for the 1-direction crushing direction, D_{1C_CRASH} is derived:

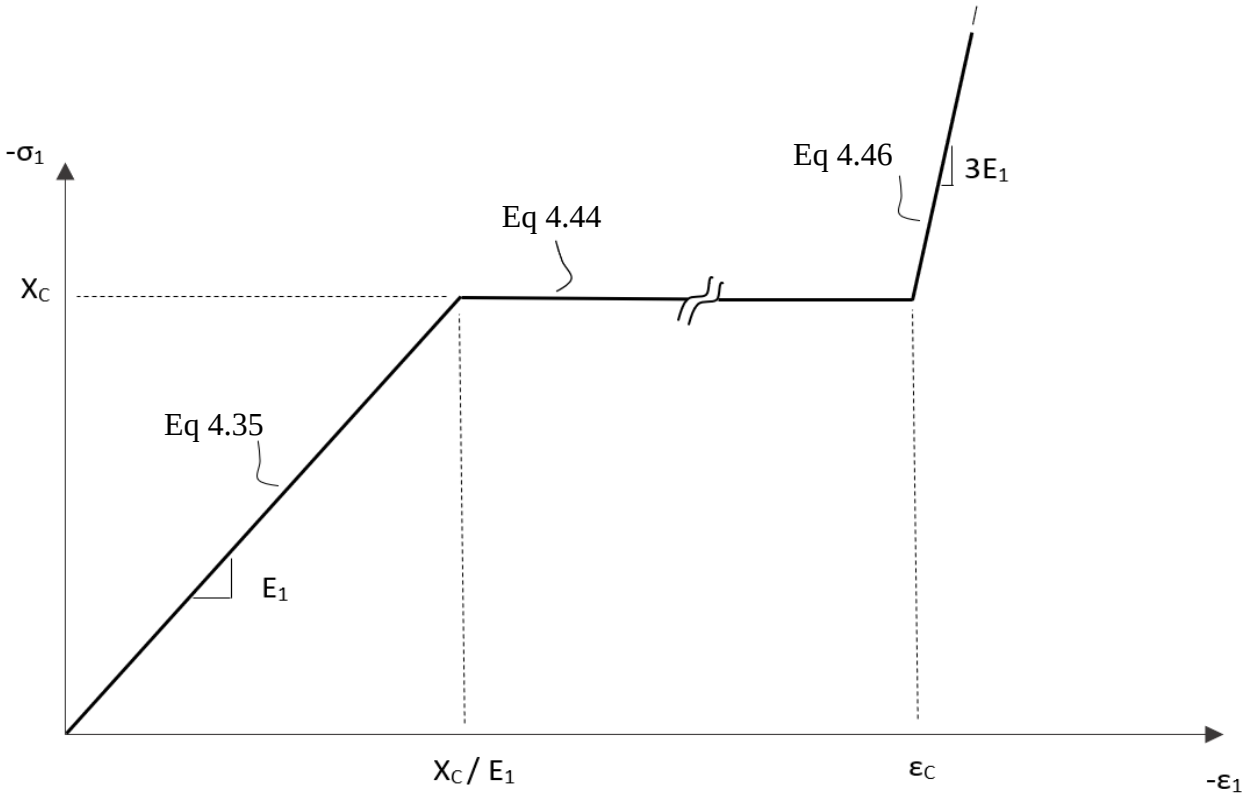

Figure 4.2-4. Stress-strain behavior of a lamina crushing in the 1-direction with the compacting region.

$$D_{1C\_CRASH} = 1 - \frac{X_C \cdot denom}{E_1\varepsilon_1 + \nu_{12}E_2\varepsilon_2} \qquad \frac{X_C}{E_1} \leq \varepsilon_1 \leq \varepsilon_C \tag{4.45}$$

The linear compacting region is represented the equation of line going through two points. The points are: P1: ($\varepsilon_1 = -\varepsilon_C$, $\sigma_1 = -X_C$) and P2: ($\varepsilon_2 = -\varepsilon_C - X_C / E_1$, $\sigma_2 = (1+3)\, X_C$).

$$\sigma_1 - X_C = 3E_1(\varepsilon_1 + \varepsilon_C) \tag{4.46}$$

D_{1C_CRASH} for the compacting region is solved for by equating Equations 4.44 and 4.46 and it is expressed by the following Equation.

$$D_{1C\_CRASH} = 1 - \frac{[X_C + 3E_1(\varepsilon_1 + \varepsilon_C)] \cdot denom}{(E_1 - \nu_{12}{}^2 E_2) \cdot \varepsilon_1} \qquad \varepsilon_1 > \varepsilon_C \tag{4.47}$$

In a similar fashion, the damage variable for the compressive 2-direction under static loading: D_{2C_STATIC}, is obtained:

$$D_{2C\_CRASH} = 1 - \frac{[Y_C + 3E_1(\varepsilon_2 + \varepsilon_C)] \cdot denom}{(1 - \nu_{12}{}^2) \cdot E_2\, \varepsilon_2} \qquad \varepsilon_1 > \varepsilon_C \tag{4.48}$$

The second approach does not include the re-hardening, compacting, region as shown in Figure 4.2-5, but instead fails the integration point when the strain reaches the pre-determined critical strain value, ε_C. As discussed in Section Chapter 4, when all integration points within an element have failed, the element is physically removed from the mesh and deleted. A discussion on how to select the strain value ε_C is included in Section 7.1.

During a crash analysis, the first row of elements is either pre-damaged or modelled with a reduced thickness. This is referred to as the trigger. It is needed both experimentally and numerically, respectively discussed in Sections 7.1 and 7.2, in order to avoid the global buckling failure mode and to insure that crashing starts in locally and then evolves in a progressive fashion. Experimentally damage always localizes at the crashfront. Numerically, damage localizes at one

row of elements. The latter naturally comports a mesh objectivity tendency of the results, as in the case of in (Deleo, 2011), (Wade, 2014), (Feraboli, et al., 2011) and (Feraboli, et al., 2016).

Mesh objectivity can be avoided by a numerical model by implementing a nonlocal continuum model for damage localization. This method has been extensively investigated by the author with some success but not included in this dissertation to reduce the scope of the work presented.

Another method developed to solve strain localization induced mesh objectivity of the results is the Crack Bend theory (Bazant, et al., 1983). The Crack Bend theory wash was originally developed for concrete but has been successfully applied for laminated composites, as discussed in Section 2.2.2. The utilization of the Crack Bend theory is discussed in Section 4.3.

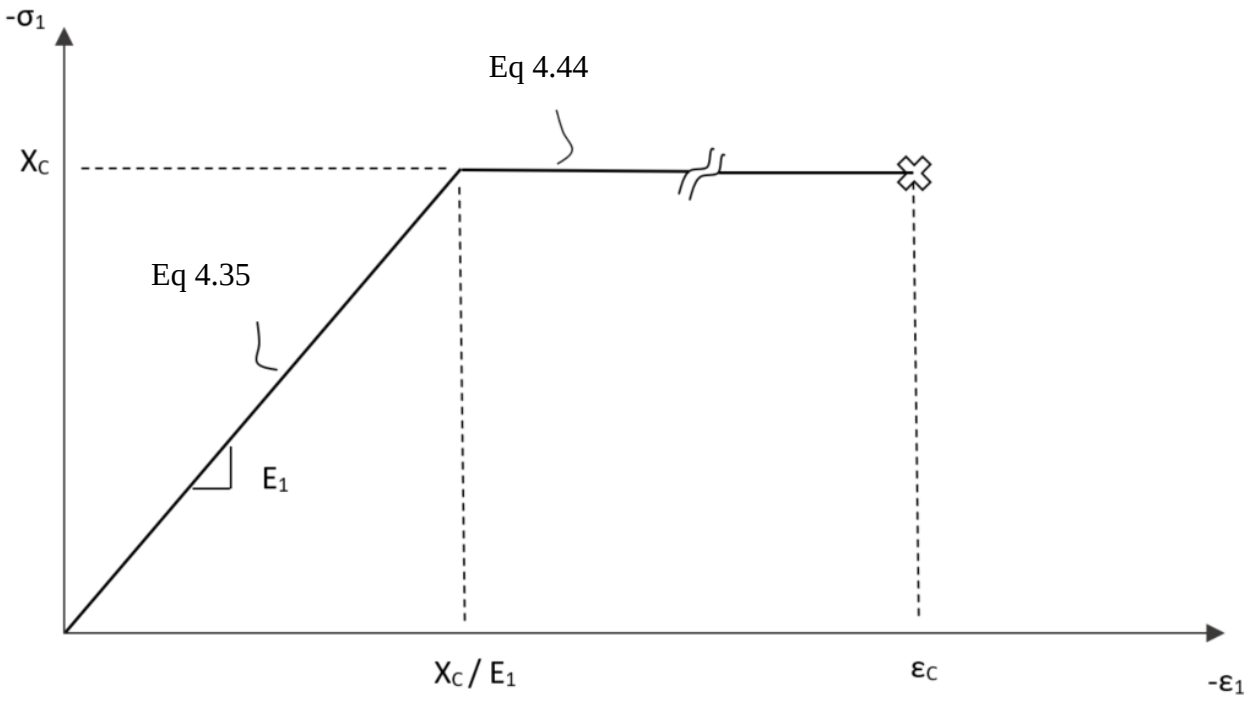

Figure 4.2-5. Stress-strain behavior of a lamina crushing in the 1-direction without the compacting region.

In the numerical method developed as part of this dissertation, after a row of elements is fully 'crushed', the next row becomes the new damage localization zone and the process is repeated until the end of the simulation. Using the first approach which includes the compacting region in the stress-strain curve as shown in Figure 4.2-4, the transition from perfectly plastic to compacting occurs at a pre-determined strain value: $\varepsilon_{C.}$ Upon reaching this value the element being crushed becomes stiffer than the rest of the part and therefore stops taking load, but still transfers the loading from the previous to the next row of elements. The compacting region stiffness is assigned an arbitrary value equal to three times the linear elastic stiffness. This value has shown to be appropriate in assuring that the element ceases to accumulate strain. Using the distributing damage model developed as part of this work and discussed in Section 4.2.6, when an element is 'deemed' fully crashed, the next element along the loading direction is pre-damaged, and therefore it starts to localize.

4.2.5 *Damage propagation in laminated composites.*

In the methodology developed in this work, the continuum damage model discussed in this Chapter is applied at each integration point of each element of the mesh. The model has been developed and implemented to work with four-node shell elements, with either reduced or full integration, as shown in Figure 3.3-1. The stresses are then integrated from each integration point within an element and the element level stresses are obtained. From the strains at the integration points the nodal displacements are calculated.

Because each integration point is treated separately, during certain loading conditions and stacking sequences, it is possible, and quite common, that failure initiates and propagates at certain integration points within an element, while other integrations points in the same element are still elastic. To illustrate this, two examples are shown in Figure 4.2-6 via two single element models

which are assigned the four plies stacking sequences of $[0/90]_s$ and $[0]_4$ respectively. Reduced integrations is utilized, therefore a total of four integrations points are utilized. In (a) the element is loaded in tension via prescribed nodal displacements, while in (b) the bending rotations are applied at the right-side nodes. The material is modelled with the material properties shown in Table 6.1-1.

The tensile model's result are shown in Figure 4.2-7. In (a) the stress-strain curves for all plies are shown. The [0] plies are stiffer and stronger than the [90] plies. As the loading progresses, the [90] plies go through failure initiation, propagation and full failure while the [0] are still elastic as shown in (a). In (b) the stress-strain curve for the [90] plies are isolated for clarity. Figure 4.2-8 shows the element-level stress-strain curve which is obtained from the ply stresses.

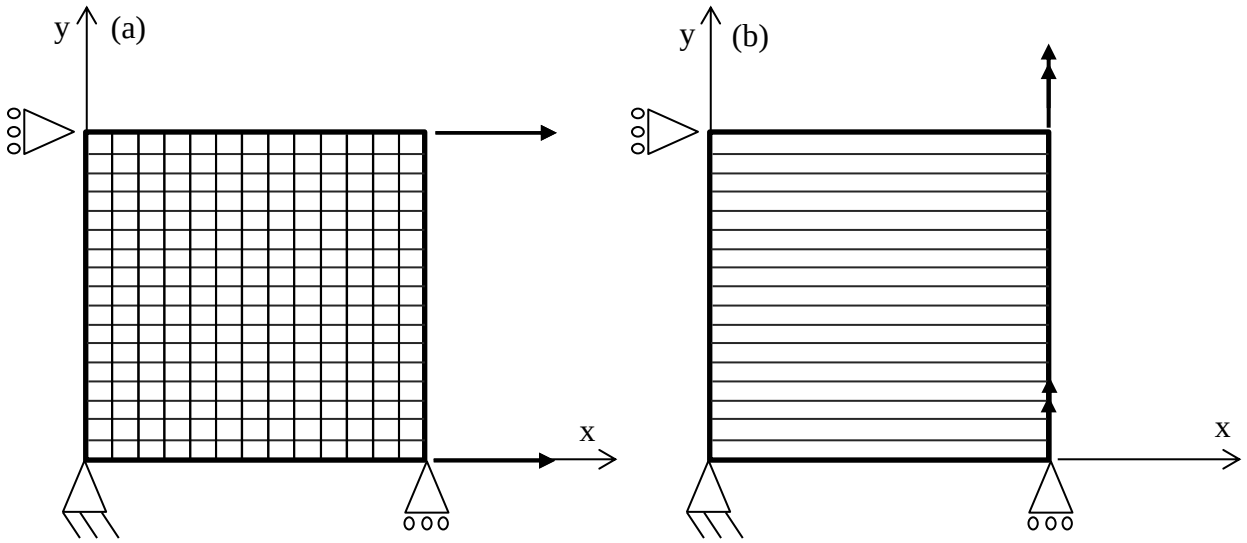

Figure 4.2-6. Single element model with assigned [0/90]s layup illustration tested in (a) tension, and (b) bending.

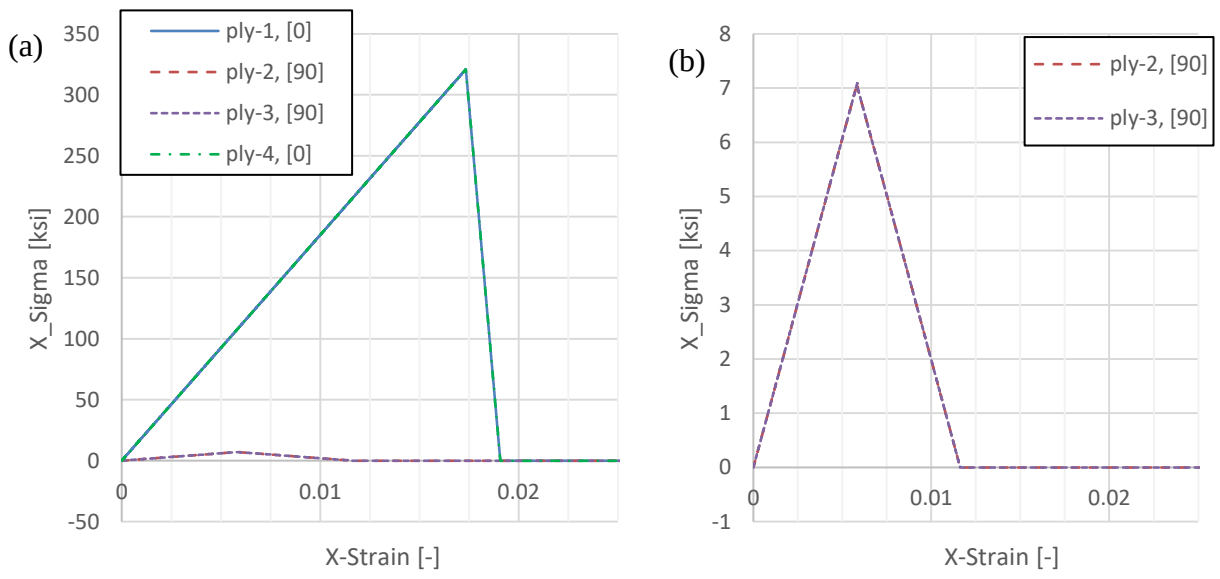

Figure 4.2-7. Single element tensile [0/90]s model stress-strain curves for (a) all four laminae, (b) only the [90] laminae.

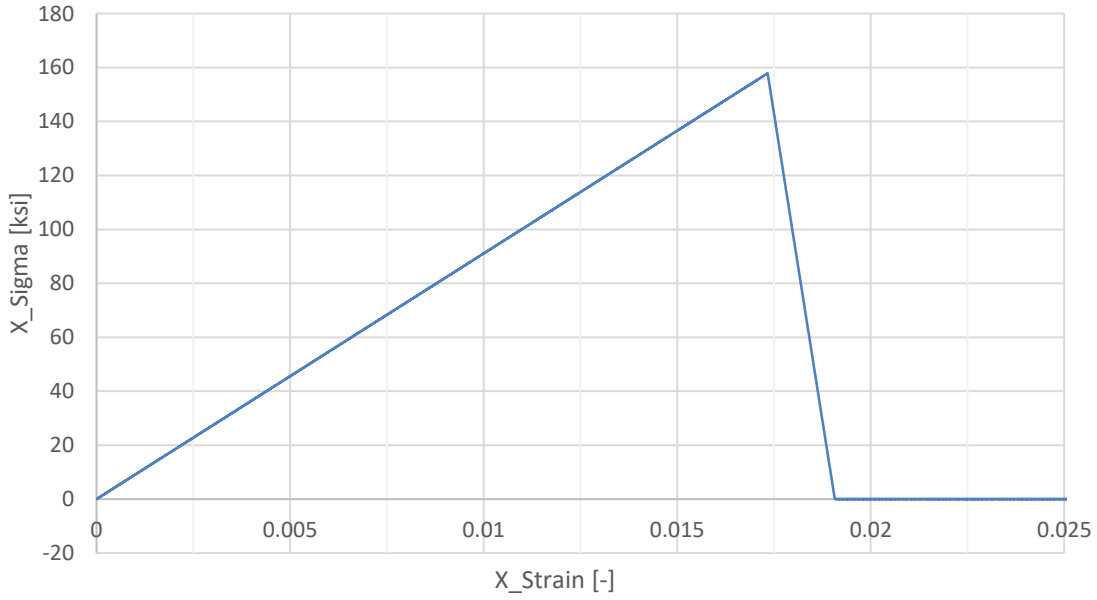

Figure 4.2-8. Single element tensile [0/90]s model element stress-strain curve.

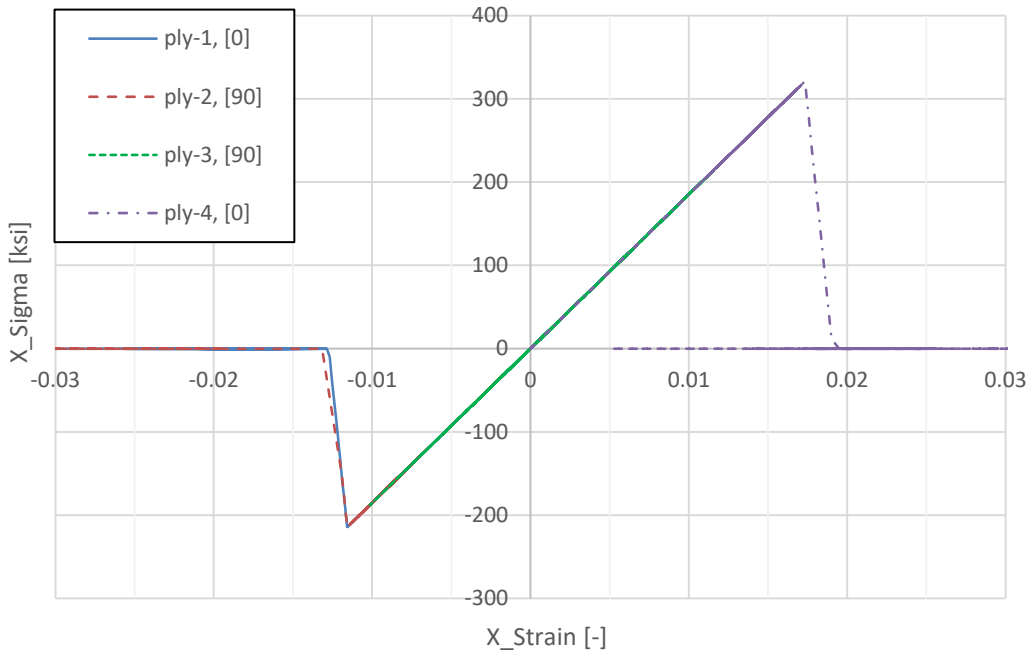

Figure 4.2-9. Single element bending [0/90]s model stress-strain curves for all four laminae.

The lamina stresses for the bending model are shown in Figure 4.2-9 and separately for each ply in Figure 4.2-10 (a) – (d). The top two plies shown in (a) and (b) are loaded in compression, while the bottom two plies shown in (c) and (c) are loaded in tension. As shown in Table 6.1-1, the lamina compressive strength is less than the tensile strength. Both compressive laminae experience failure initiation and propagation until the complete damage: $D_{1C\_STATIC} = 1.0$ as discussed in Section 4.2.3.

The lower lamina is also completely damaged, while the third ply is still elastic. If after the analysis is completed, an additional analysis step would have been added, the element retained a fourth of the strength as one ply is still elastic.

Element deletion is included in the methodology when all integration points within an element have failed: meaning that the damage variable for the respective loading direction reaches 1.0.

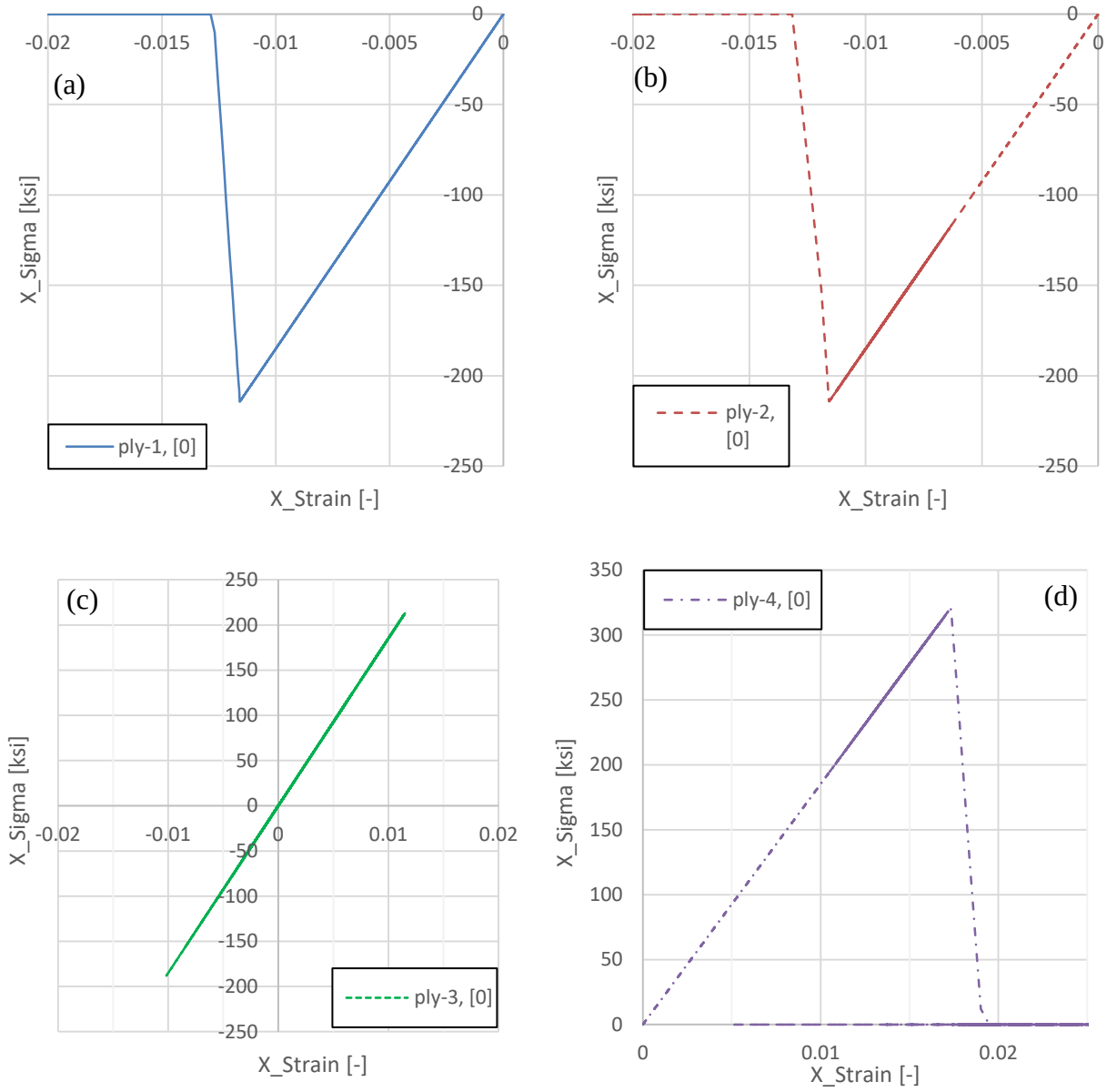

Figure 4.2-10. Stress-strain curves from the single element bending [0/90]s model for each individual ply (a) – (d).

4.2.6 *Non-local damage progression for crashworthiness using the Distribute Damage Model (DDM)*

When using the theory presented in this work to run a crash analysis, the distribute damage model (DDM) is activated. The distributing damage model is developed to overcome the shortcoming of finite element discretization and damage localization, introduced in Section 4.2.4.

The DDM functioning is shown graphically in Figure 4.2-11. As discussed previously, when modeling a continuum with a finite number of elements, damage localizes at a single elements row. This damage localization phenomenon starts with the trigger (mentioned in Section 4.2.4). The trigger effectively serves as damage starter in a localized fashion, and therefore avoiding the Euler-buckling failure mode discussed in Section 2.3.

Experimentally, while the section of material immediately adjacent to the load application point is being crushed, some damage propagates forward, effectively pre-damaging the next section of the material, which will soon become the crush front. The pre-damage occurs in two ways: via splaying and/or fragmentation, respectively shown in Figure 2.3-5 and Figure 2.3-6. As it was discovered by previous research from the author and published in (Deleo, 2011), the amount of splaying and fragmentation depends on the cross-sectional geometry, as discussed in Section 2.3. Damage in flat sections tend to propagate via splaying, while in curved sections it propagates via fragmentation. Splaying propagates deeper than fragmentation and is the primary responsible factor for pre-damage propagation.

Because of the pre-damage discussed above, when a piece of material becomes the new crashfront, it is not pristine and therefore does not possesses full initial strength. Numerically, a dedicated subroutine is needed to distribute damage from the crashfront row of elements to the next one. The distribute damage model is written to accomplish this task, as discussed in Section 5.2, via a series of FORTRAN subroutines and the utilization of supporting text files in which the functions write to and read information from as the analysis progresses.

Pre-damage is applied via strength reductions. As it will be discussed in the implementation section, when an element is found by the subroutines to need pre-damage, the strengths are reduced by a factor, redFac, which is dependent on the cross-sectional shape of the part being crushed.

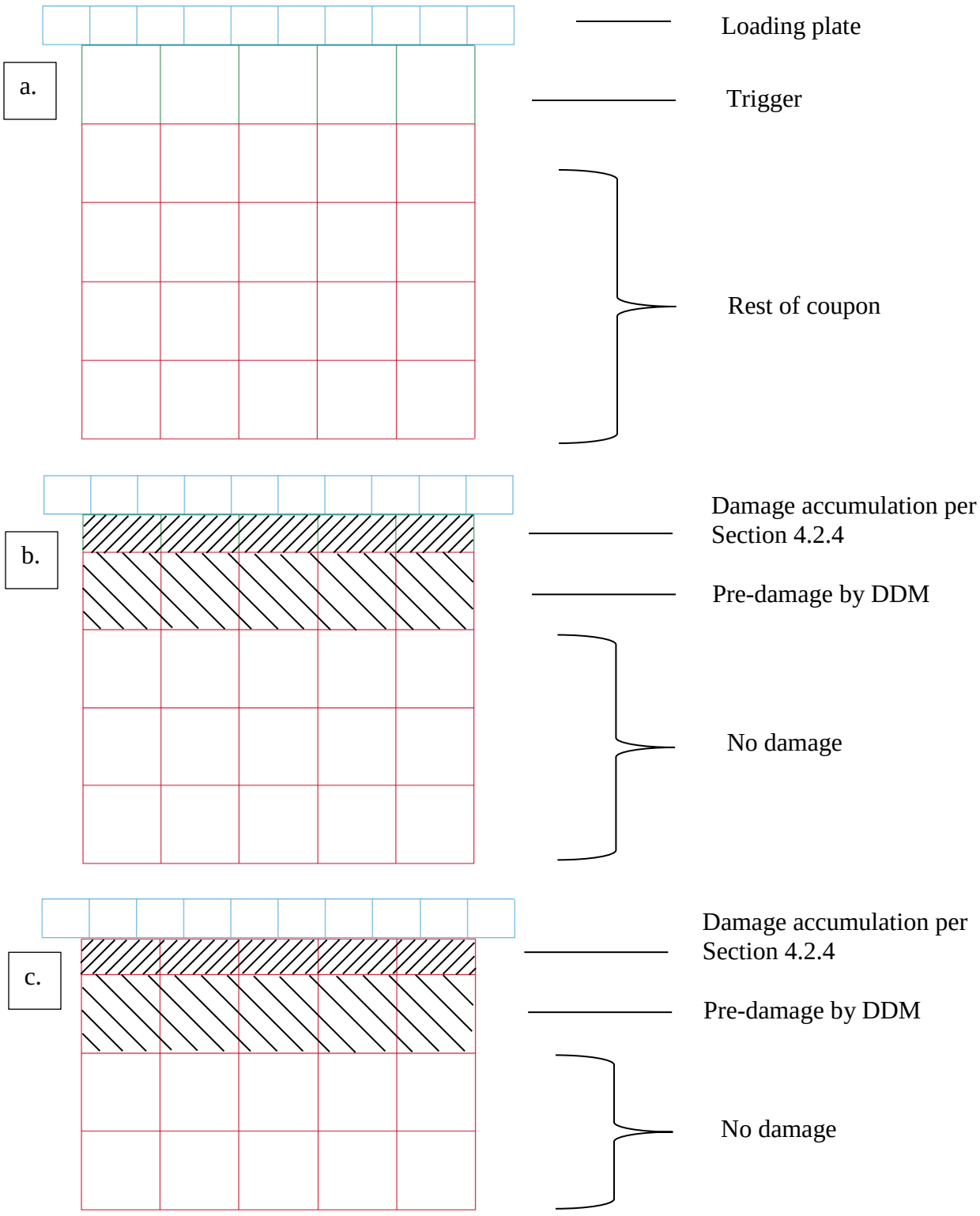

Figure 4.2-11. Representation of functioning of the DDM: a. no damage, b. trigger being crushed and DDM pre-damaging the next row, c. second row being crushed and DDM pre-damaging the third row.

Where S_C, X_T, X_C, Y_T, and Y_C are the lamina strength values discussed in Section 3.1. The strength values in the equations for failure initiation of Section 4.1, Equations 4.28 – 4.31, are updated using the reduced strength allowable values of Equation 4.49 and shown below:

$$\begin{aligned} S_{C\_red} &= S_C \cdot \text{redFac} \\ X_{T_{red}} &= X_T \cdot \text{redFac} \\ X_{C_{red}} &= X_C \cdot \text{redFac} \\ Y_{T_{red}} &= Y_T \cdot \text{redFac} \\ Y_{C\_red} &= Y_C \cdot \text{redFac} \end{aligned} \tag{4.49}$$

Tensile mode in 1- direction:

$$s_f^2 = \left(\frac{\sigma_1}{X_{T\_red}}\right)^2 + \left(\frac{\tau_{12}}{S_c}\right)^2 \geq (1 - D_{1t} - D_{1c})^2 \tag{4.50}$$

Compressive mode in 1- direction:

$$s_c^2 = \left(\frac{\sigma_1}{X_{C\_red}}\right)^2 \geq (1 - D_{1t} - D_{1c})^2 \tag{4.51}$$

Tensile mode in 2- direction:

$$s_m^2 = \left(\frac{\sigma_2}{Y_{T\_red}}\right)^2 + \left(\frac{\tau_{12}}{S_{C\_red}}\right)^2 \geq (1 - D_{2t} - D_{2c})^2 \tag{4.52}$$

Compressive mode in 2- direction:

$$s_d^2 = \left(\frac{\sigma_2}{2S_{C\_red}}\right)^2 + \left[\left(\frac{Y_{C\_red}}{2S_{C\_red}}\right)^2 - 1\right] \cdot \left[\frac{\sigma_2}{Y_{C\_red}}\right] + \left(\frac{\tau_{12}}{S_{C\_red}}\right)^2 \geq (1 - D_{2t} - D_{2c})^2 \tag{4.53}$$

4.3 MESH OBJECTIVITY

As discussed in Sections 2.2.2 and 4.2.4, spurious mesh sensitivity of the results is a direct consequence of localization instabilities, caused by strain and damage localization. The method utilized in this work to guarantee the mesh objectivity of the result is the Crack Band Theory discussed in Section 2.2.3. The Crack Band Theory is implemented in a simplified fashion. The main reason is that the width of the crack band, h_c, is not a measurable property because given the brittleness of composites it is too small to capture experimentally. Therefore, the principle that fracture energy needs to be preserved when varying the mesh size is adopted, as stated by Equation 2.12. The fracture energies, discussed in Section 4.2.2, are material properties. When modeling the material with an element of unitary size the stress-strain curve with linear softening for a physical band of size hc is obtained. When using an element of larger size, the softening region is reduced, and vice-versa. In the damage model framework developed in this work the strain to failure values: $dfailt_{1T}$, $dfail_{1C}$, $dfail_{2T}$ and $dfail_{2C}$ are utilized to control the size of the softening region for the various material directions. The strain to failure values are utilized to control the mesh objectivity of the model methodology. As shown in Equation 4.54, the element size, 'h', is included in the strain to failure calculations. The mesh size for each element is calculated using the nodal coordinates and therefore can vary from element to element within a finite element model.

$$\begin{aligned} \mathrm{dfail}_{1T} &= \frac{2 \cdot \gamma_{1T}}{X_T \cdot h} \\ \mathrm{dfail}_{1C} &= \frac{2 \cdot \gamma_{1C}}{X_C \cdot h} \\ \mathrm{dfail}_{2T} &= \frac{2 \cdot \gamma_{2T}}{Y_T \cdot h} \\ \mathrm{dfail}_{2C} &= \frac{2 \cdot \gamma_{2C}}{Y_C \cdot h} \end{aligned} \tag{4.54}$$

The modified strain to failure values are then utilized to calculate the strain softening slopes of Equation 4.38, which in turn are used to calculate the damage variables of Equations 4.39 and 4.43. The functioning mechanism of the simplified Crack Band Theory implementation are illustrated using a single element model as shown in Figure 4.3-1. A single four-noded reduced integration shell element model is created and constrained in a simply supported fashion. The material 1-direction is aligned parallel to the direction of loading for this example. Parts (a) and (b) respectively shown the tensile and compressive loading directions. The results are shown in Figure 4.3-2 and Figure 4.3-3 respectively. As the size of the element is reduced, in order to preserve the fracture energy (per Equation 2.12) , the fracture energy density is increased by elongating the strain to failure value, according to Equation 4.54.

The technique is applied to a larger multi-element model as shown in Figure 4.3-4. A unnotched tensile coupon following the ASTM testing standard D3039 (ASTM International, 2008) specimen dimensions is modelled with varying mesh sizes. The coupon is 1.5” x 12.0” in size and an applied stacking sequence of $[0]_8$. The ply thickness is 0.0065” for a total thickness of 0.052”.

The geometry, loading and boundary conditions shown in Figure 4.3-4 (a) is meshed with 0.5” x 0.5”, 0.25” x 0.25” and 0.1” x 0.1” reduced integration bi-linear shell elements for a total number of elements of respectively: 72, 288 and 1800. The resulting load versus time results for the three models are shown in Figure 4.3-5 showing no differencesand verifying the mesh objectivity of the model.

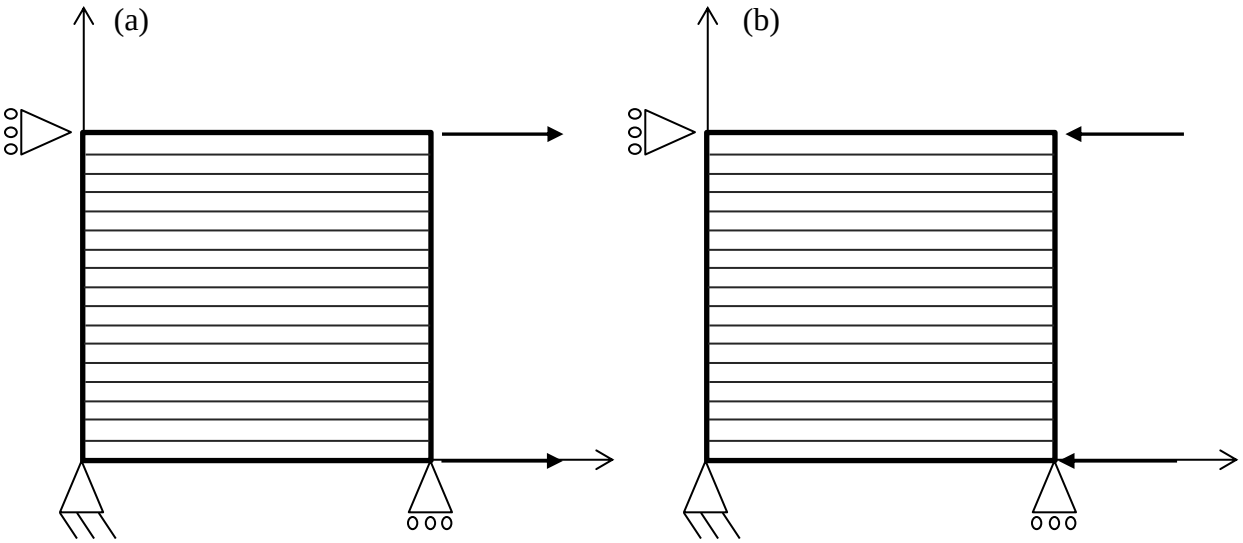

Figure 4.3-1. Single element model illustration tested along the fiber direction in (a) tension, and (b) compression.

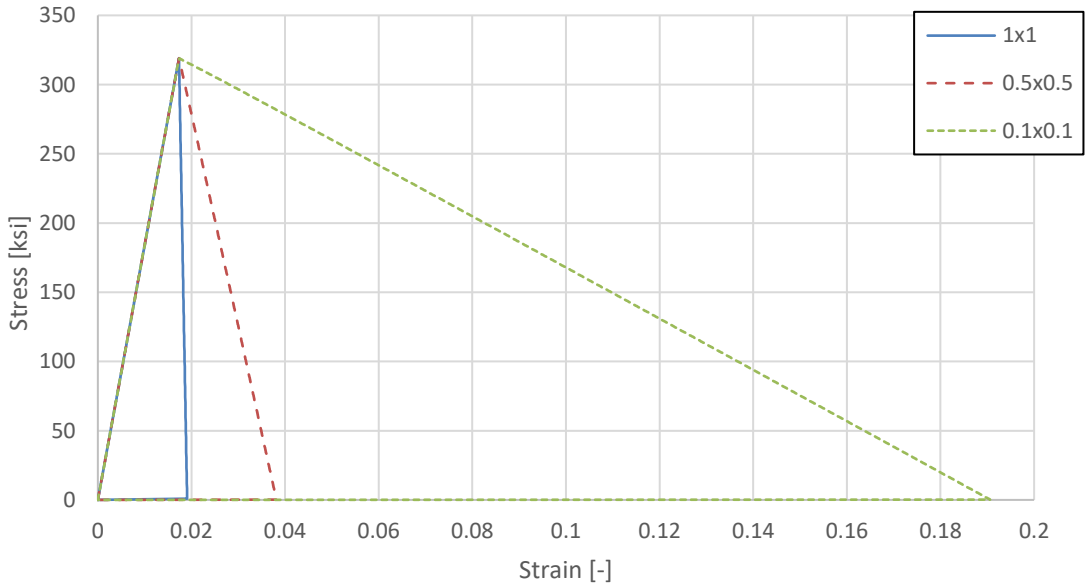

Figure 4.3-2. Single element tensile results loaded in the 1-direction for various mesh sizes.

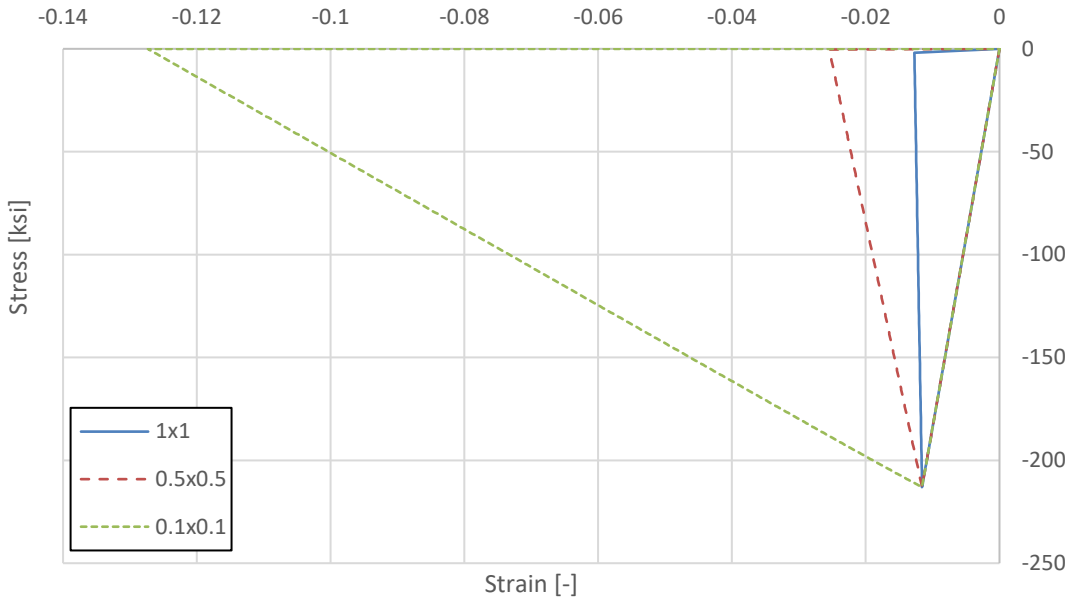

Figure 4.3-3. Single element compressive results loaded in the 1-dir for various mesh sizes.

The load is obtained by summing the reaction loads in the direction of loading. The loading speed was 80 in/s which is much faster than that specified in (ASTM International, 2008) but still guarantees quasi-static conditions. When performing an explicit dynamic simulation for a quasi-static problem, increasing the loading rate while avoiding inertial effect is a common computational cost reduction technique, as discuss in more details in Section 5.3. The failure progression for the 0.5" x 0.5" and 0.25" x 0.25" is shown respectively in Figure 4.3-6 and Figure 4.3-7. Strain localization always occurs on a single row of elements. As shown in Figure 4.3-5, even when using small elements, which result in a very long strain softening region, shown in Figure 4.3-2, the overall response exhibit typical brittle failure results.

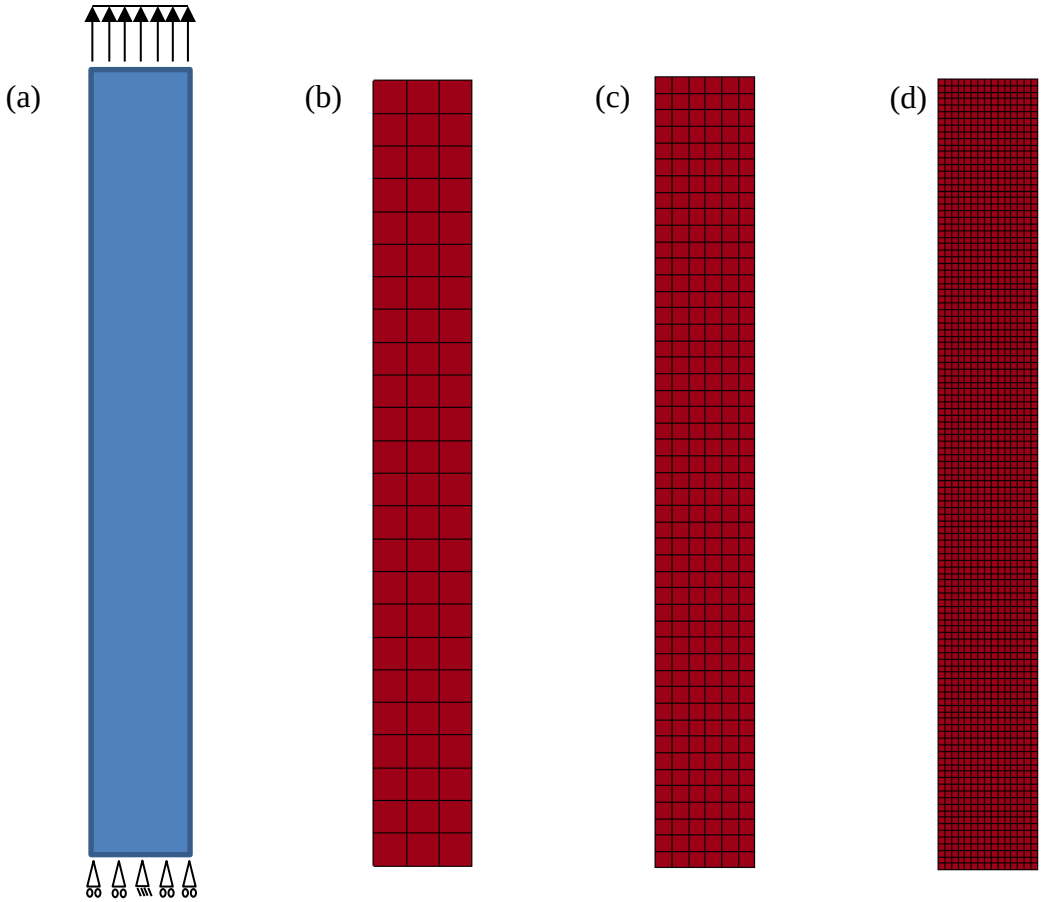

Figure 4.3-4. Unnotched tensile coupon: (a) geometry, loading and BCs, (b) – (d) FEMs meshed with shell elements of size respectively 0.5”x0.5”, 0.25”x0.25” and 0.1”x0.1”

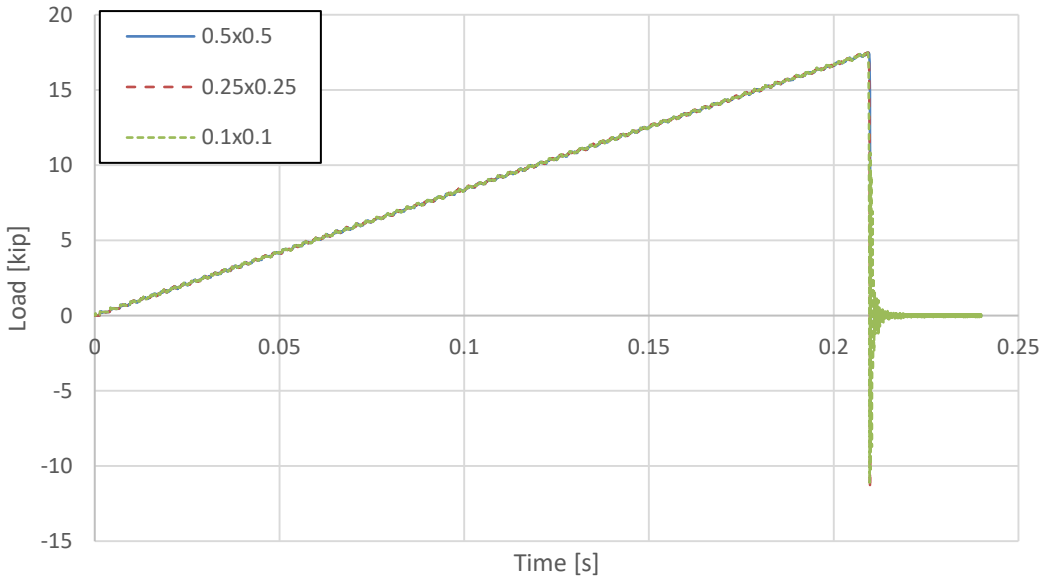

Figure 4.3-5. Load-time results for the models with varying mesh size shown in Figure 4.3-4.

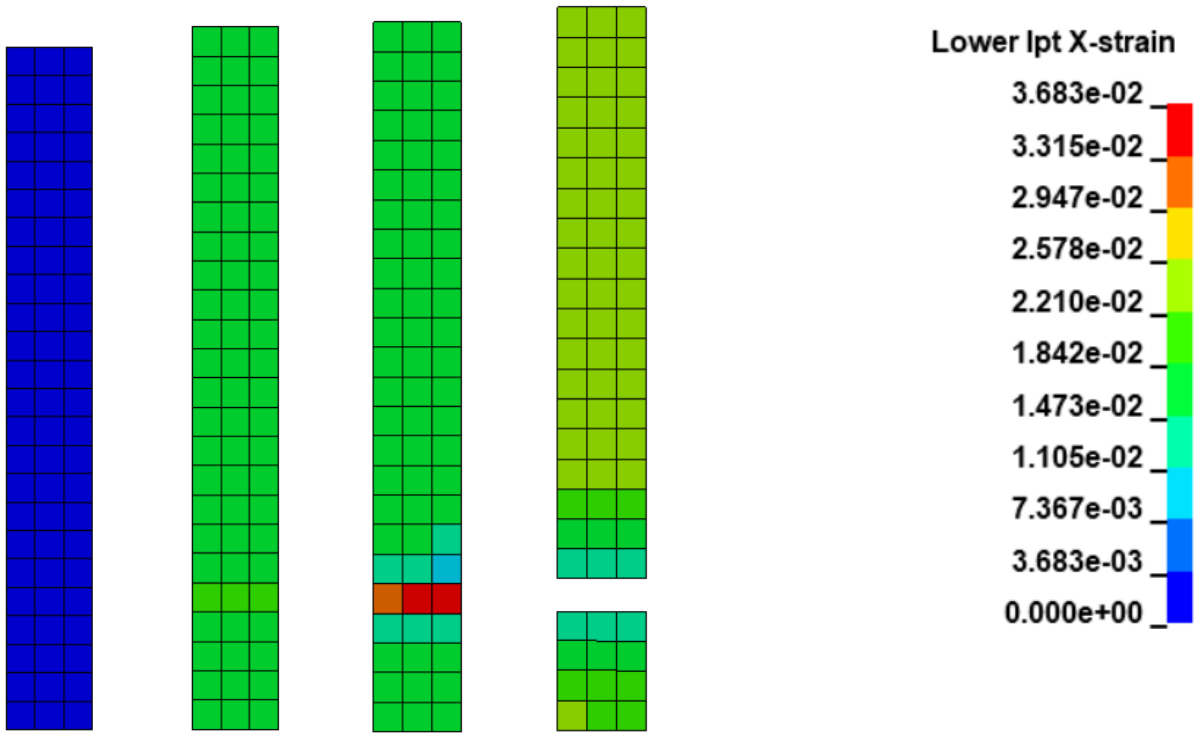

Figure 4.3-6. Strain countor plots at (a) beginning of test, (b) moment prior, and (c) during to stress localization. (d) fracture for 0.5” x 0.5” meshed model.

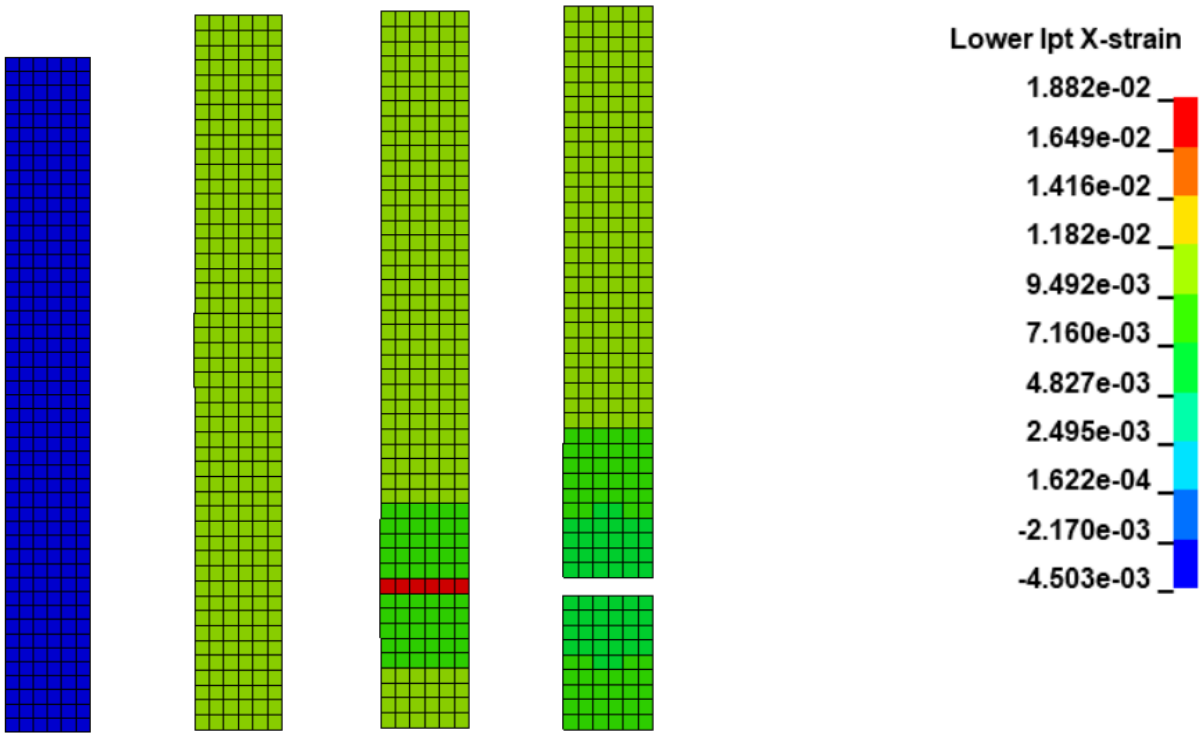

Figure 4.3-7. Strain countor plots at (a) beginning of test, (b) moment prior, and (c) during to stress localization. (d) fracture for 0.25” x 0.25” meshed model.

Finally, the results shown in Figure 4.3-2 show an undulatory trend after failure of the elements. This is due to the fully dynamic capability of the solver, discussed in Section 3.2. When the specimen breaks in half, stress waves form which quickly travel the length of each half back and forward. These waves are partially attenuated by adding damping control but cannot be eliminated. Furthermore, these stress waves are real and would be captured if highly precise instrumentation were used during a mechanical test.

4.4 LOADING AND RELOADING

During dynamic simulations which involve impacts and crashes, a robust method to deal with loading, unloading and reloading in the presence of damage is necessary. Due to stress waves, the material is constantly subjected to loading and reloading. In this methodology the damage amount at each integration point that is calculated during damage propagation is saved during unloading. When the element experiences reloading, the failure initiation criteria are lowered to account for a non-pristine state of the material and the damage continues to accumulate if the failure criteria are surpassed.

The failure initiation criteria are lowered by the addition of the respective damage variable according to the loading and material direction as listed in Equations 4.50 – 4.53.

To demonstrate the damage accumulation modeling strategy adopted in this work during loading and reloading, two examples are shown next. A single element model is used with a single lamina at [0], as shown in Figure 4.3-1.

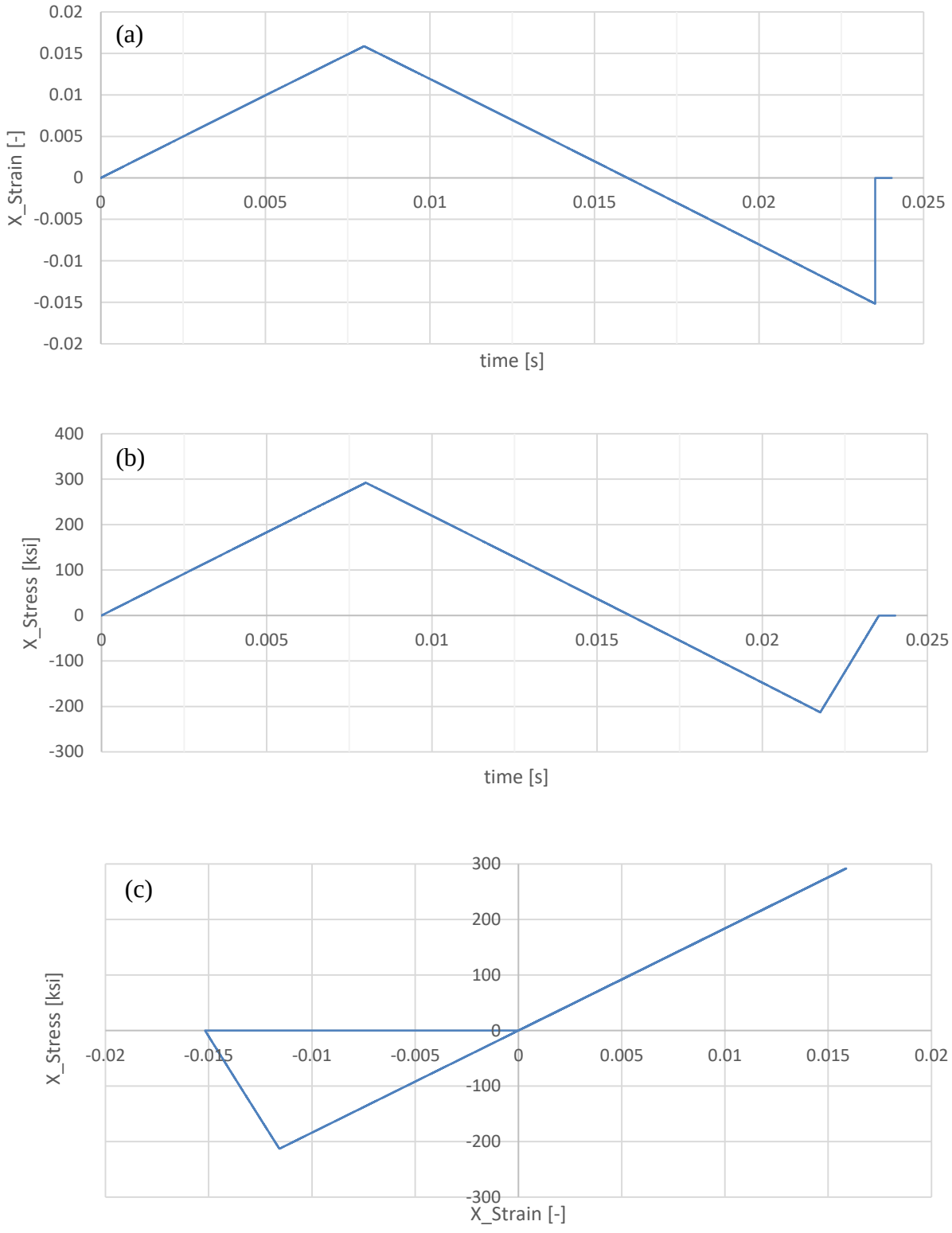

Figure 4.4-1. (a) strain versus time, (b) stress versus time, and (c) stress – strain curves for single element model with [0] layup.

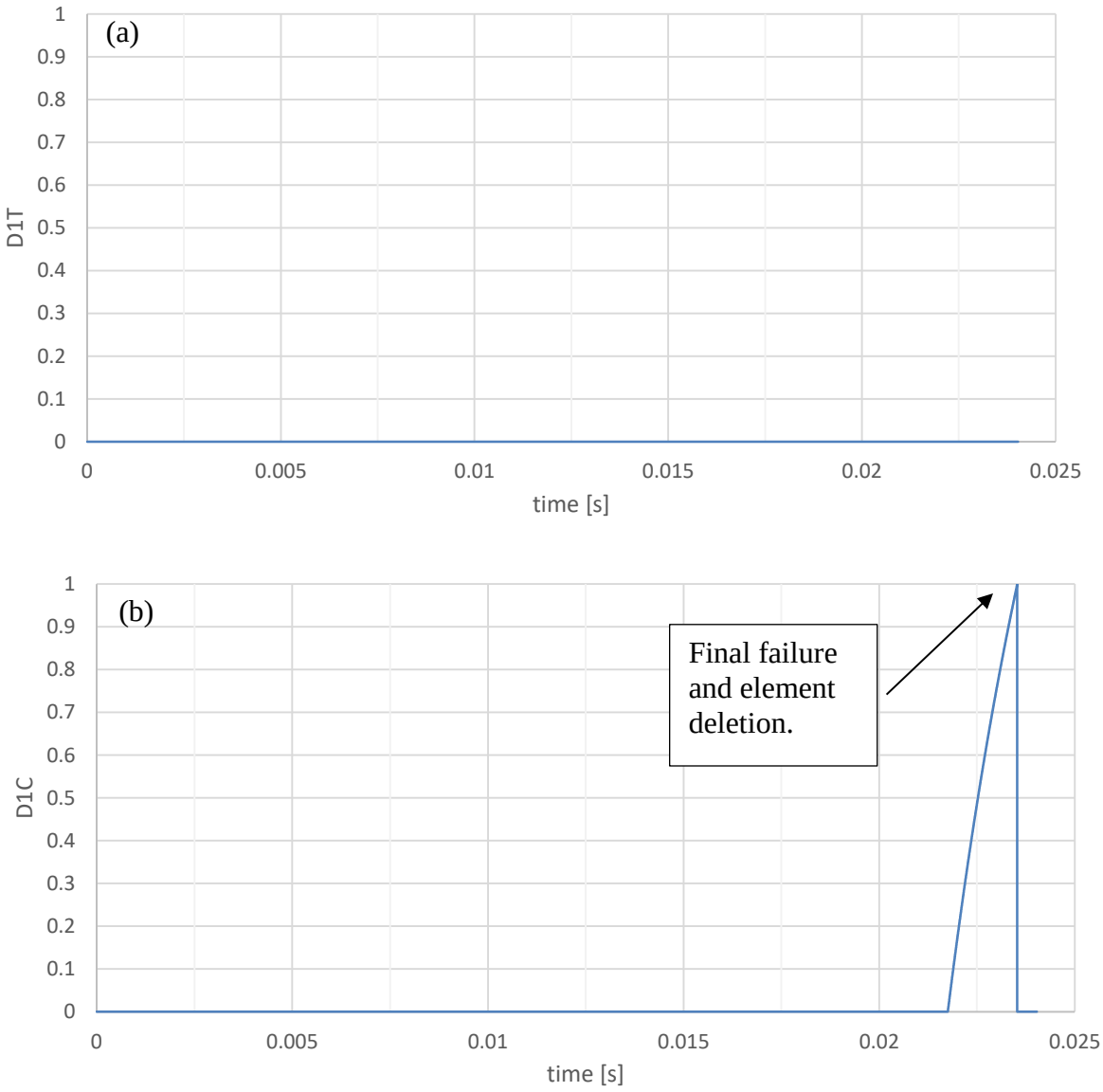

Figure 4.4-2. Damage variables as discussed in Section 4.2.3 plotted versus time. (a) tensile damage variable: D_{1T}, and (b) compressive damage variable D_{1C}.

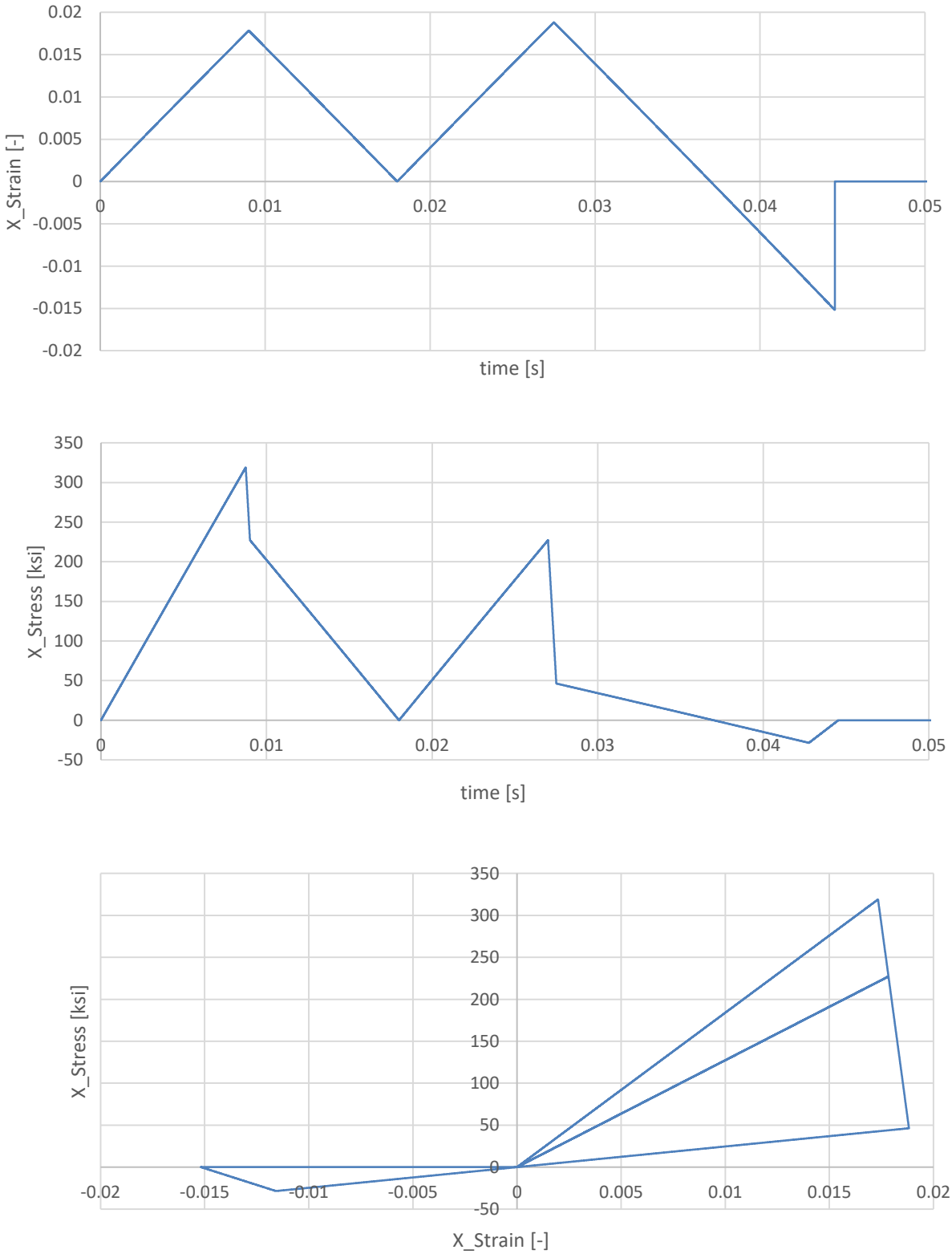

Figure 4.4-3.(a) strain versus time, (b) stress versus time, and (c) stress – strain curves for single element model with [0] layup.

As shown in Figure 4.4-1, the element is first loaded in tension until it reaches a tensile stress in the 1-direction equal to 290 ksi, then in compression until final failure and element deletion. The strain versus analysis time, stress versus time, and stress-strain curves are respectively shown in parts (a) – (c). The tensile and compressive static damage variables, discussed in Section 4.2.3, are shown respectively in Figure 4.4-2 (a) and (b).

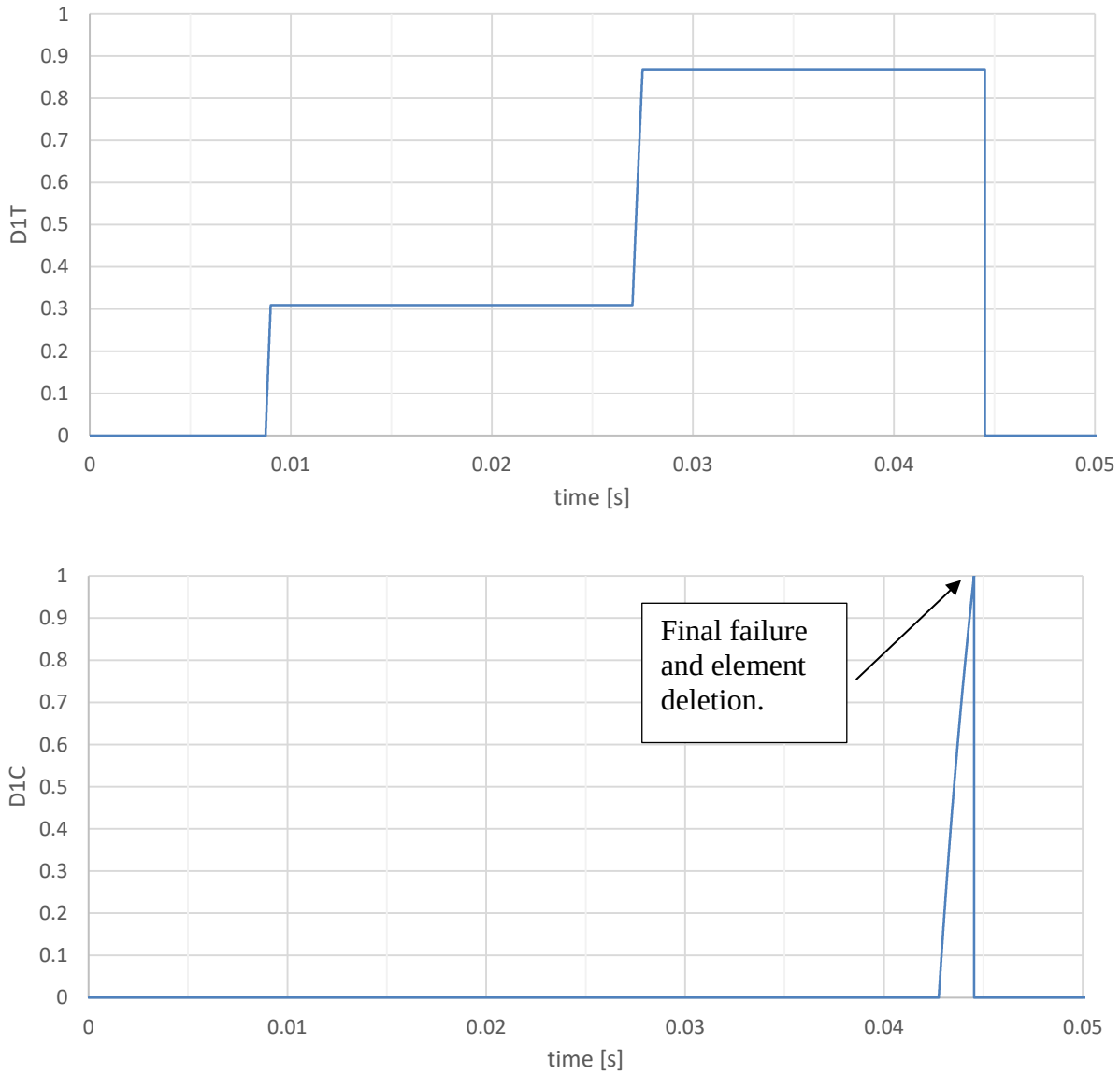

Figure 4.4-4. Damage variables as discussed in Section 4.2.3 plotted versus time. (a) tensile damage variable: D_{1T}, and (b) compressive damage variable D_{1C}.

No damage in the tensile 1-direction results from the tensile loading and D_{1T} has value of zero throughout the duration of the analysis. When the loading reverses to the compressive direction, the compressive failure initiation criterion is met and D_{1C} progressively rises from 0 to 1 as damage is being accumulated. Finally, when the work done on the element is equal to the fracture energy γ_{1C}, D_{1C} assumes the unitary value and the element is deleted.

The second example is shown in Figure 4.4-3. The element is first loaded in tension past the peak stress and until 30% damage in the tensile 1-direction: D_{1T} is accumulated. Then the element is fully unloaded and reloaded in tension again and the damage is further accumulated to 88%. The element is then first completely unloaded and then loaded in compression to failure.

The strain versus analysis time, stress versus time, and stress-strain curves are respectively shown in parts (a) – (c). The unloading and then reloading modulus of elasticity is degraded according to the amount of damage imparted in the material. Damage in tensile or compressive 1-direction occurs via fiber damage. Because of the fiber strength variability, usually expressed with a Gaussian distribution, the weaker fibers fail first and the stronger fibers will be the last ones to fail. When load is reversed, the broken fibers are assumed not to be able to take load, as would be the case of further loading in the original load direction, and therefore the modulus of elasticity is degraded accordingly. However, no plastic strain is considered, as unidirectional fiber-reinforced composites have not been shown to retain residual stresses when partly damaged and then unloaded. As seen in Figure 4.4-3 (b) and (c), the failure initiation is compression occurs earlier than it would for a pristine element, as compared with Figure 4.4-1. The tensile and compressive static damage variables, discussed in Section 4.2.3, are shown respectively in Figure 4.4-4 (a) and (b).

The same loading, unloading and reloading and damage accumulation and retention framework is implemented in the 2-direction but not shown for conciseness. While no fibers are present in the 2-direction, the accumulated damage takes place via micro-cracking which are modelled to affect the modulus of strength both in tension and compression.

4.5 CRUSH STUDIES ON REDUCED SIZE MODEL

The composite damage model presented in this Chapter is applied to a simplified crush problem, as shown in Figure 4.5-1 with the goal of exemplify the progressive crushing behavior and effect of certain modelling parameters, such as trigger and loading speed. This model was used extensively to understand the effect of element type, amount of damping, and contact algorithm, among the various analysis parameters, and for code development debugging.

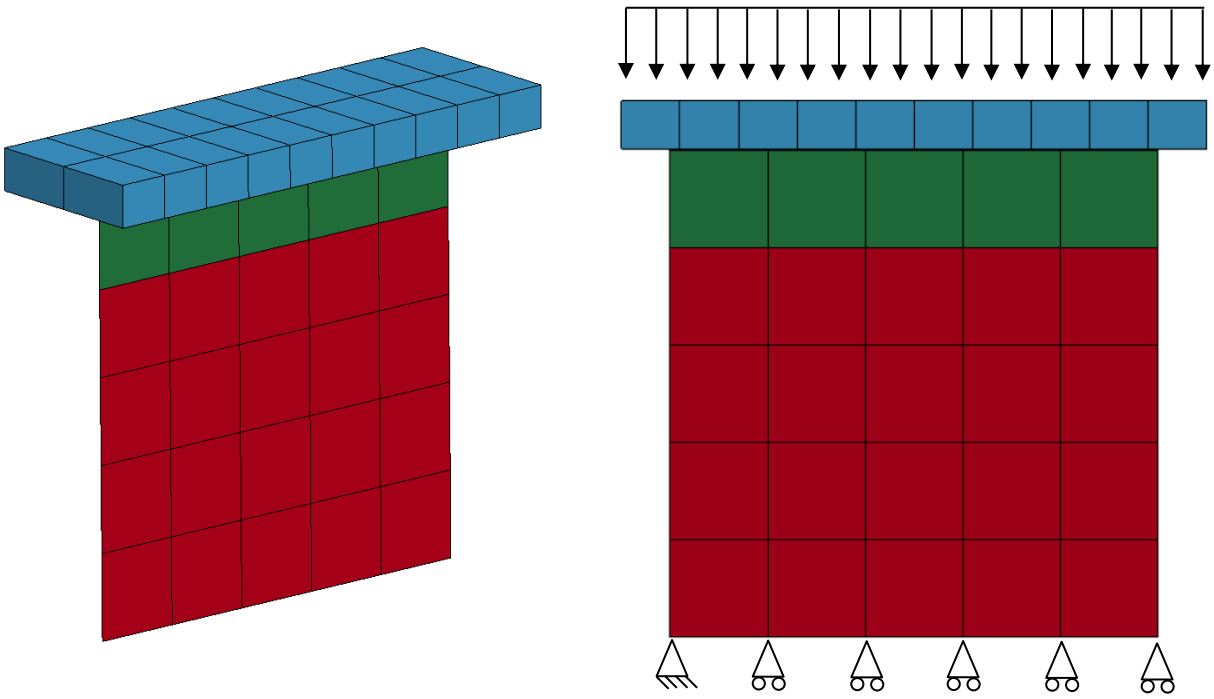

Figure 4.5-1. Simplified flat crush model for methodology demonstration, constraining and loading conditions.

The model consists of a laminate meshed with 5x5 elements of unitary size, which includes the first trigger row, and a loading plate meshed with solid rigid elements. The parts identification is shown in Figure 4.2-11 (a). The need for a trigger is discussed in Section 4.2.4. The LS-DYNA's *CONTACT_AUTOMATIC_NODES_TO_SURFACE contact algorithm is chosen. As discussed in Section 7.3, this contact algorithm uses a hard normal behavior.

The composite specimen and trigger are assigned T700/2510 material properties as listed in Section 7.2 while the loading plate is meshed with rigid elements. The composite specimen is modelled with 12 plies, with the following stacking sequence: $[0/90]_{3s}$.

To exemplify the effect that the trigger has on the crushing behavior three different layups are assigned to it. Figure 4.5-2 compares the results for the crushing of a flat plate with a $[0/90]_s$ versus $[0/90]_{2s}$ trigger. As discussed in Section 4.2.4, the trigger's primary goal is to initiate crushing. It accomplishes this function by being weaker than the rest of the material. If progressive crushing initiates correctly, the strength of the trigger affects the resulting crush load while the trigger element row is undergoing crushing. As shown in Figure 4.5-2, the 8 plies trigger has a higher initial crushing load then the 4 plies trigger. The progressive crushing morphology of the configuration with the $[0/90]_{2s}$ trigger is shown in Figure 4.5-3. When the trigger is assigned the same stacking sequence as the rest of specimen, no initial weakness is provided and the specimen fails in global buckling. This scenario is shown in Figure 4.5-4.

The effect of two loading plate speeds are shown in this Section: 150 and 15 in/s. Both speeds are quasi-static, in that the inertia effects are not experienced. As explained in Section 5.3, the loading speed is directly proportional to the computational cost. As the speed is reduced from 150 to 15 in/s the computational cost is increased tenfold.

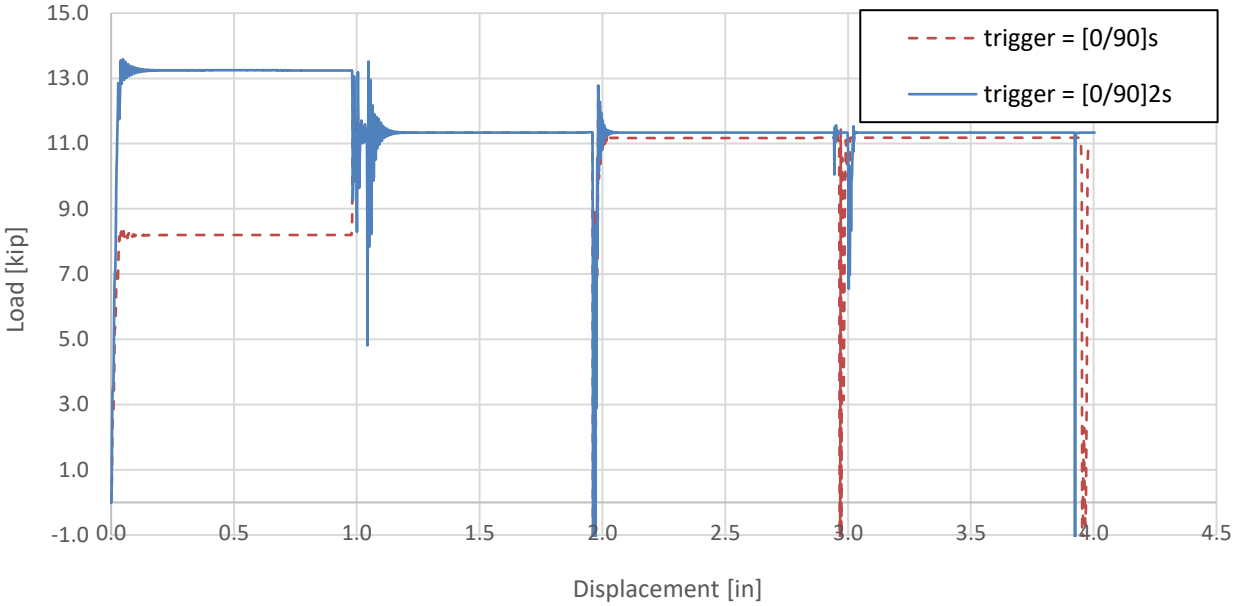

Figure 4.5-2. Load versus stroke results for crushing of plate with two different modelling strategies for the trigger. Loading speed: 150 in/s.

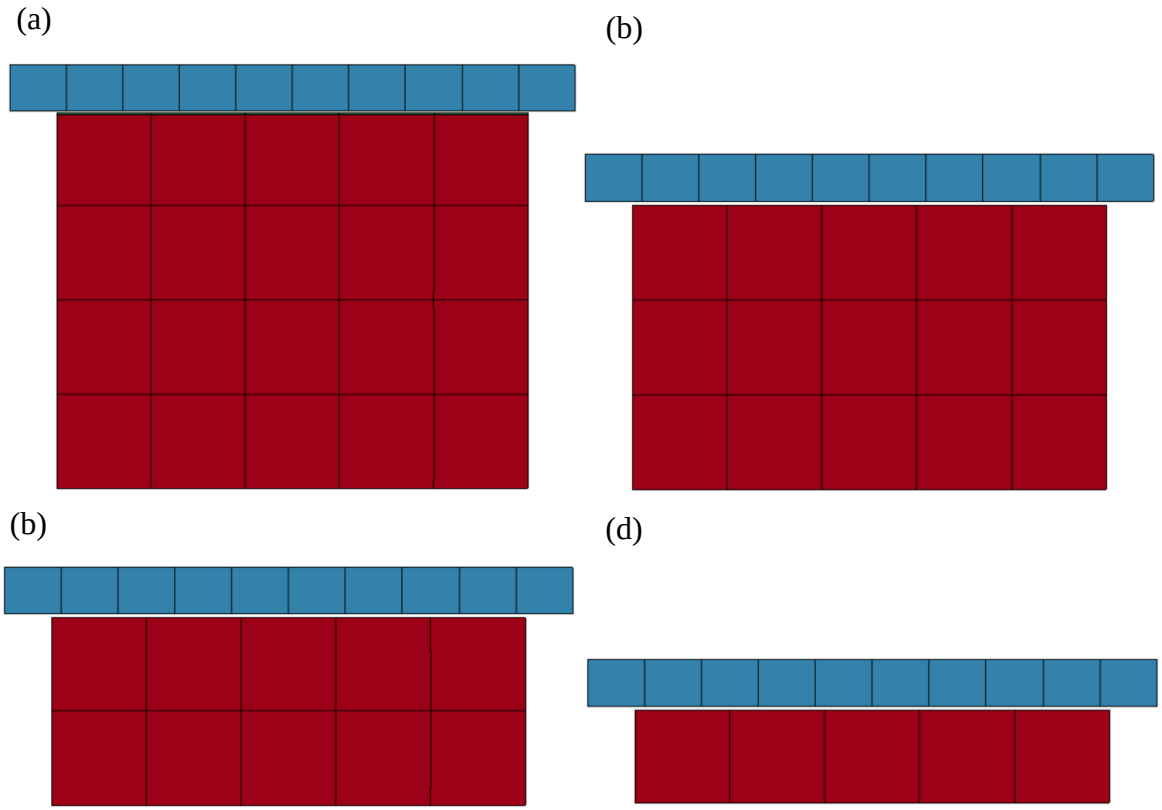

Figure 4.5-3. Failure progression for configuration with $[0/90]_{2s}$ trigger at 20%, 40%,60% and 80% of crushing, respectively (a) – (d).

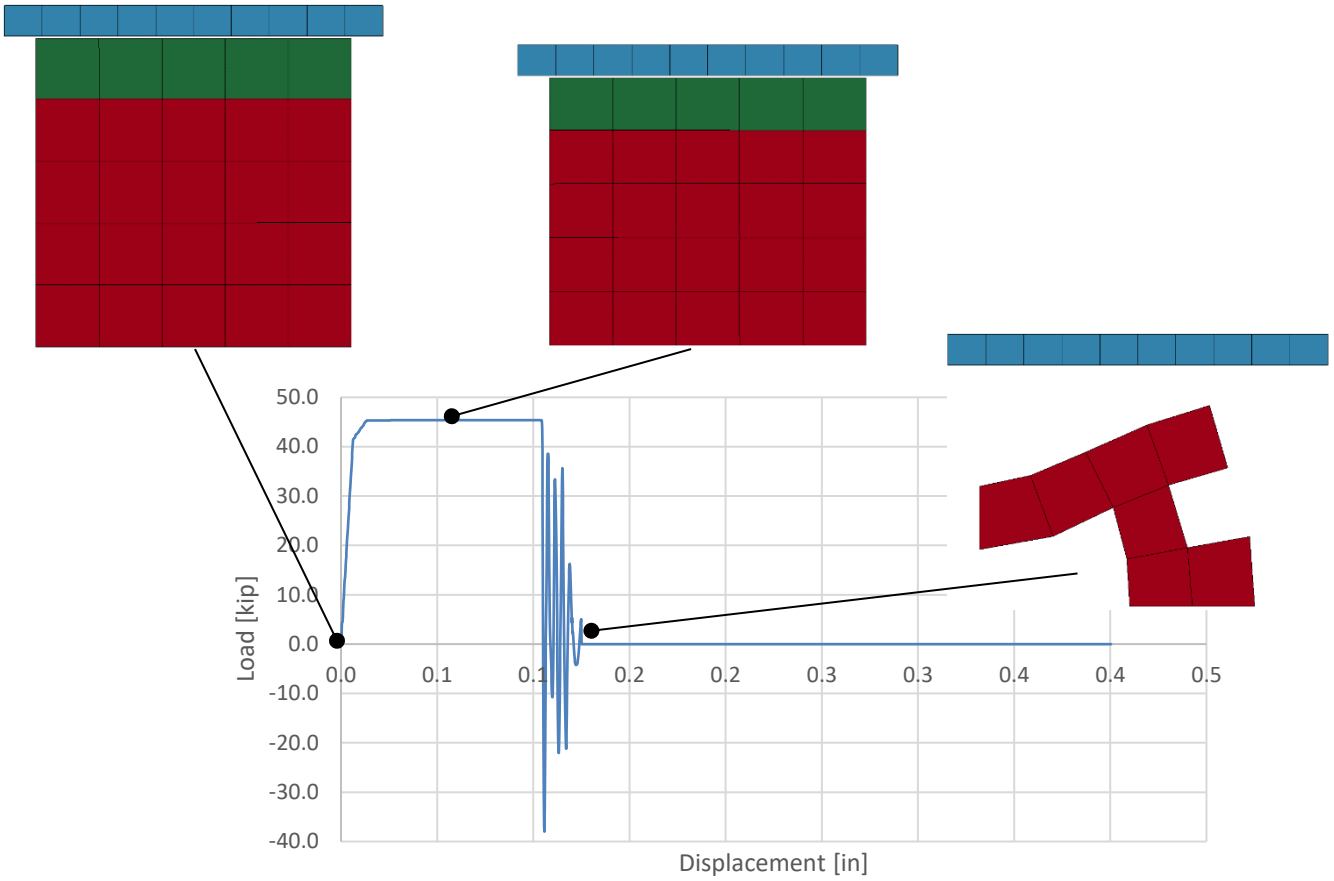

Figure 4.5-4. Load versus time results for configuration with trigger equal to the rest of the specimen.

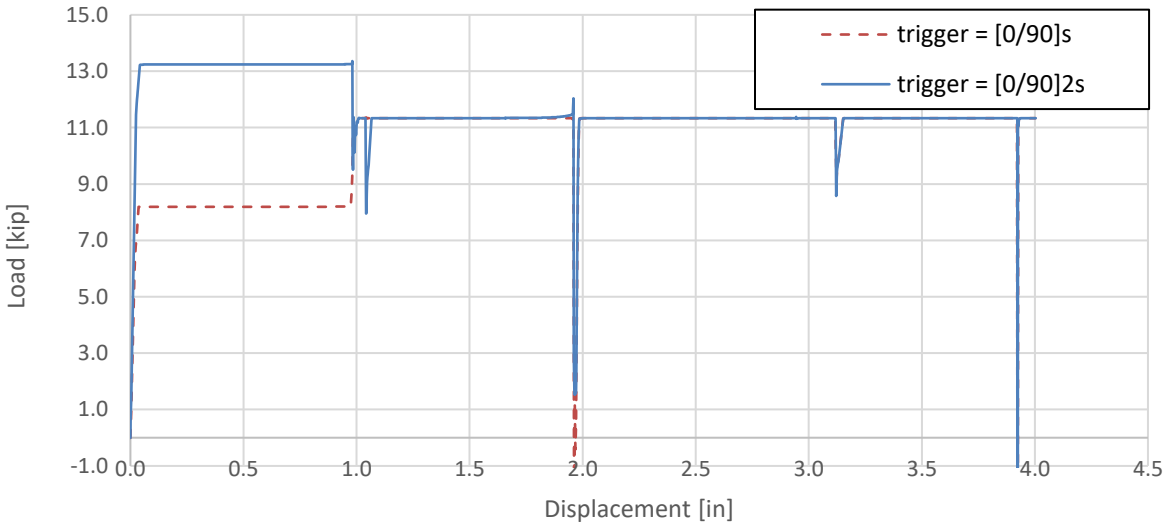

Figure 4.5-5. Load versus stroke results for crushing of plate with two different modelling strategies for the trigger. Loading speed: 15 in/s.

The results for the crushing speed at 15 in/s are shown in Figure 4.5-5. The waviness in the results present right after element deletion in Figure 4.5-2, for the 150 in/s solution, is significantly reduced when running at the lower speed.

Chapter 5. IMPLEMENTATION OF THEORY IN A LS-DYNA UMAT

The theory discussed in Chapter 4 is implemented into the commercially available Finite Elements package: LS-DYNA (Livermore Software Technology Corporation, 2014) via user-defined material models plus additional outside subroutines, which will be discussed in this Chapter. This was done for two reasons:

1. to take advantage of the existing solver capability, to assemble the FE equations (matrices) and solving the governing equations discussed in Section 3.2 through time,
2. to make use of the existing contact algorithms.

The version of LS-DYNA utilized is: *ls-dyna_smp_d_R711_win64*, which is version 7.11, symmetric multiprocessing (SMP), double precision (D) for Windows 64 bit. LSTC provides its users with a suite of files contained in the folder: ls-dyna_smp_d_R711_winx64_ifort131_lib. The main files of interest are the *dyn21.F* and *makefile*.

dyn21.F is a FORTRAN file which houses the user-defined material models according to the element type the subroutines are written for. The *makefile* file describes the relationships among the files in the program to be compiled and provides commands for updating each file. It specifies the list of targets and dependencies and defines commands which are executed to build the targets. LSTC also provides several include files and object file libraries, and the *nmake* application. *nmake* is a Windows based tool used to compile the code into an executable following the settings listed in the *makefile* file. The INTEL FORTRAN compiler: *Intel® Parallel Studio XE 2013* is utilized to build the executable. *Microsoft VISUAL STUDIO 2010 x64 tools* were also needed for proper functioning of the compiler. All materials models and additional subroutines are added in the following location within the *dyn21.F* file:

usrmat -> urmats -> umatXX

usrmat is the subroutine which calls the subroutines for user defined materials depending on the element type. *urmats* contains the user-defined material models for shell elements. LS-DYNA allows for up to 10 user-defined material models to be included in dyn21.F: UMAT41 – UMAT50. Even though it is not specified in the User Manual, it is recommended avoiding using UMAT42 for scalar implementations, and if writing a vectorized routine avoid using UMAT48V and UMAT49V.

Initially the material models created for this dissertation were written in vectorized form. Vectorized user-defined material models process elements in groups, whereas the non-vectorized routines process one element at a time. The number of elements processed each time a vectorized subroutine is called is the vector length, which is specified in the *nlqparm* include file. Initially the vectorized implementation was adopted as it is more computationally efficient, but the non-local implementation created for the crush analyses required a scalar user defined material implementation. Therefore, the subroutines described in this work are all scalar in nature.

One and two user-defined material models are added in the dyn21.F file respectively for the static and crush loading, as discussed in Sections 5.1 and 5.2. For a crush analysis the trigger row of elements is assigned a different material than the rest of specimen. While the two material models are very similar, the trigger elements do not need the non-local operations discussed in Section 4.2.6 and some of the cost reduction calls discussed in Section 5.3. Instead of generalizing the material model to be used for both trigger and rest of the specimen elements, it was deemed simpler to produce two independent material models, which also made the troubleshooting process easier.

Two ways are available for LS-DYNA user-defined material models users to save information from a timestep to the next:

1. Via history variables
2. Writing and reading data to external file

Method 1 above is the recommended way by LS-DYNA, but it has one fundamental limitation: it does not allow the access of data from different elements and integration point other than the one where the routine is running on. To obviate to this limitation and to implement the non-local damage progression method discussed in Section 4.2.6 Method 2 above is implemented, as discussed in Section 5.2 below. Method 2 is obviously not computationally efficient and therefore it requires the minimization of writing and reading operations via the methods discussed in Section 5.3. If the theory presented in this dissertation were to be implemented into a solver written by the author, or into a commercially available solver, not as a user-defined routine, but instead as a default material model, the limitation of method 1 above would not exist, and method 2 would not be needed.

As shown in Figure 3.3-1, LS-DYNA treats a user-defined material model as black box. At the beginning of each timestep the stresses from the end of the previous timestep are made available as inputs together with the strain increments, which LS-DYNA calculates from the stresses and stiffnesses. The required output from the material subroutine is the updated stress tensor. As discussed in Section 3.1 and Chapter 4, because a composite laminate is modelled at the lamina level, the orthotropic plane stress constitutive model is implemented in the shell element at each integration point. The out-of-plane shear stresses are however also needed to assure proper functioning of the material. Therefore, in addition to σ_1, σ_2, and τ_{12}, τ_{13} τ_{23} are also updated using the following relations:

$$\tau_{13} = G_{13}\varepsilon_{13}$$
$$\tau_{23} = G_{23}\varepsilon_{23} \quad (5.55)$$

All codes developed as part of this work were written in FORTRAN, using the 77, 90 and 95 conventions depending on convenience to the author. All code is not object-oriented.

5.1 UMAT FOR STATIC LOADING ANALYSES

The material model code for static failure analysis is added as UMAT45 in *dyn21.F* as discussed previously. The code is added in APPENDIX A of this dissertation. The code follows the logic summarized in Figure 3.3-1. Several history variables, as mentioned previously, are utilized to save information from a timestep to the other at each integration point of each element. As discussed previously in this Chapter, only the data pertinent to the same integration point are made available, and this is sufficient for the material model developed for static loading as no damage progression is necessary. Summarily, the code attached in APPENDIX A performs the following operations:

1. Initialize variables for the first cycle only or download data from the history variables for all subsequent cycles.
2. Download data from the material card with user inputted material properties..
3. Update strains from provided strain increments.
4. Calculate strain to failure values and linear strain softening according to mesh size and crack bend theory, discussed in Section 4.3.
5. Assess whether failure has initiated via modified Hashin's stress criteria as discussed in Section 4.1.
6. If damage has initiated, calculate damage variables discussed in Section 4.2.3.

7. Assess whether the integration point if fully damaged: if a damage variable has reached the unitary value activate element deletion flag. Outside the code shown in APPENDIX A, it is assessed whether all integration points within an element have been flagged for deletion and if that is the case the element is removed from the mesh, as discussed in Section 4.2.5.
8. Update plane stress stiffness matrix including the out-of-plane shear stresses of Equation 5.55 and calculate new stresses.
9. Updated history variable values.

5.2 UMATs FOR CRUSH LOADING ANALYSES

The implementation of the theory into material models for crush loading analyses is similar to what is discussed in Section 5.1, with some exceptions. All code developed as part of this dissertation is attached in APPENDIX B. In addition to the two user defined material models: one for the trigger and one for the rest of the specimen, four auxiliary subroutines were written which operate on three support files. The list of auxiliary subroutines and a summary of their function is provided in Table 5.2-1. Each support file contains a matrix. The list of support files with their functions and size is provided in Table 5.2-2. The differences in implementation for crush with respect to static loading analyses are summarized below:

- Trigger elements are assigned a separate UMAT from the rest of the specimen which has less outside calls to the auxiliary subroutines, as shown in Table 5.2-1 and Figure 5.2-1.
- In addition to the auxiliary subroutines, the UMATs make use of support files, listed in Table 5.2-2. Each file contains a matrix.
- The damage variables used to quantify damage from initiation until final failure are replaced with the ones discussed in Section 4.2.4.

- The number of history variables is greater as additional information is needed, such as the variable: *checkFail* which is saved as history variable number 36 and is used to minimize the number of calls to the subroutines: *writeOnElementState* and *checkElementState* as discussed in Section 5.3.

Figure 5.2-1 shows the analyses flow for the two UMATs developed for crush analyses. The four calls to the auxiliary subroutines are shown. In blue: findRow() and checkElementDamage() are not invoked at the trigger, while in green: writeOnElementState() and checkElementState() are called for all elements.

Table 5.2-1. List of auxiliary subroutines external to the user defined material models for crushing events.

Subroutine name	**Used in:**	**Function:**	**Reads from files:**	**Writes on file:**
findRow()	Rest of Specimen	It determines which row the element is in.	Element_Connectivity	-
checkElementDamage()	Rest of Specimen	It determines if the element has been flagged for strength reduction.	Element_Damages	-
writeOnElementState()	Both	It flags a failed integration point.	Element_State	Element_State
checkElementState()	Both	If all integration points of an element have been flagged for deletion, it flags the current element and the next in the crushing progression for strength reduction.	Element_State, Element_Connectivity, Element_Damages	Element_Damages

Table 5.2-2. List of support files used for crash loading analyses.

Support File	**Function:**	**Matrix Size**
Element_Connectivity	To determine position of element within the mesh.	rows of elements by cols of elements.
Element_Damages	To keep track of elements flagged for strength reduction.	# of elements by 1.
Element_State	To keep track of state of each intergration point in the mesh.	Total # of integration points in mesh by 1.

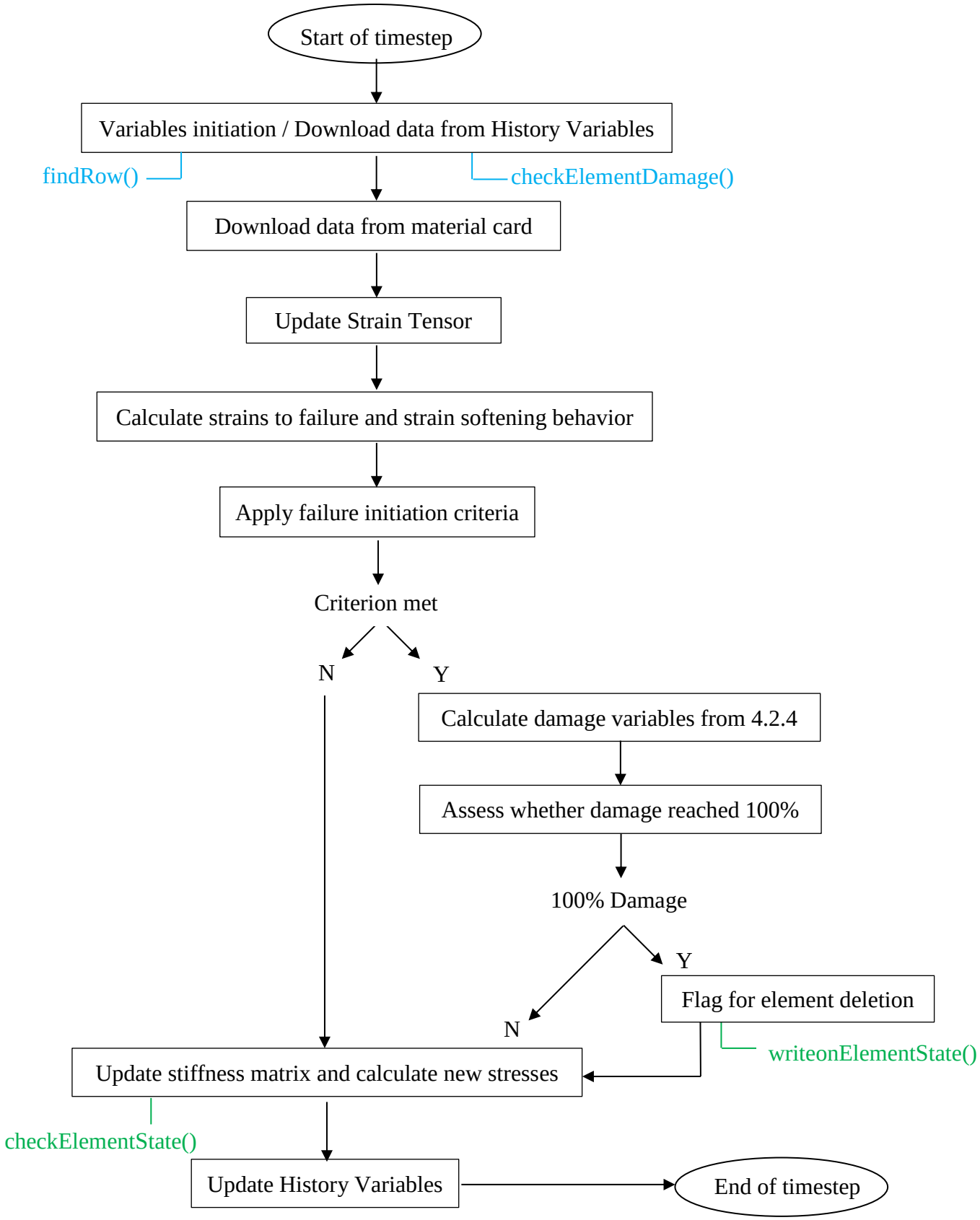

Figure 5.2-1. UMATs analysis flow for crash analyses with calls to auxiliary subroutines.

5.3 METHODS TO REDUCE THE COMPUTATIONAL COST

The amount of resources and/or time to run an explicit dynamic simulation is often a problem when conducting work, especially when modeling crush events. A fine difference is present between the definitions of crush and crash. A crush experiment is run at a slow speed and will last from a second to a few seconds. On the contrary its crash counterpart is run at higher velocity and will last few milliseconds [81]. In addition to the stringent timestep size limitation dictated by the Courant condition (Equation 3.24), which is in place in order to avoid instability of the results, and the cost associated with an increasing number of degrees of freedom, additional cost was due to the reading and writing operations performed by the auxiliary subroutines, as discussed in 5.2.
In this work typical techniques to reduce the computational cost are used:

- performing the analysis at higher speeds,
- mass scaling and,
- element deletion.

Increasing the speed of the simulation, by performing the same task at a reduced simulation time is a common way to lower the computational cost. Reducing the simulation time linearly reduces the total number of timesteps for explicit FEAs. Special caution needs to be taken however, to ensure that the analysis conditions are unchanged. For instance, if the problem being analysis is quasi-static the loading rate can be increased as long as dynamic effects are avoided. In this study, the experimental crushing speed is such that it qualifies it as a quasi-static problem due to its low speed, as discussed in Chapter 7. Increasing the speed has the risk of introducing dynamic behavior and increasing the effects of inertial forces. Therefore, to ensure that the problem retains quasi-static crushing behavior, the ratio of kinetic energy to internal energy should be less than five percent, and the force-displacement curve is independent on the speed (El-Hage, et al., 2010). If

this is the case, the simulation performed at higher loading speed is still considered quasi-static and it is equivalent to solving the original problem.

The mass scaling technique revolves around the idea of maximizing the minimum timestep Courant condition of Equation 3.24 by artificially increasing the density of the material. This, of course, comports the addition of nonphysical mass to the structure. When adding mass to the system, the results are affected, by Newton's second law of motion. The idea of mass scaling is to add as much mass to maximize the minimum time step, while resulting in insignificant effects on the solution. If this is case, the added nonphysical mass is justifiable. Certain advanced explicit dynamic finite element packages, like LS-DYNA (Livermore Software Technology Corporation, 2014) and ABAQUS/Explicit (Simulia, 2017) allow for a smart use of mass scaling: mass is added only to those elements which would otherwise dictate the timestep to be less than a specified value. This technique is referred to variable mass scaling. As the Courant condition states that the mesh size is linearly related to the resulting minimum timestep, usually the critical elements are the ones with the smaller side length, if the material is kept constant (Young's modulus). As shown in Equation 3.24, the minimum timestep is related to the inverse of the square root of the density. Similar to the technique of increasing the simulation speed, energy levels can be used to monitor the correct solution of the problem when using mass scaling. Most commercially available solvers calculate the energy associated with the increased mass. For instance, ABAQUS/Explicit calculates and makes it available as ALLMW. If the energy resulting from the added mass is less than five percent of the internal energy it can be inferred that solving the problem with mass scaling is equivalent to solving the original problem.

Element deletion has the opposite effect of mass scaling, as mass is being removed from the system. Deleting failed elements has the advantage of removing from the mesh elements which

have undergone a high amount of strain and therefore most likely dictate the minimum timestep size per the Courant condition. While removing mass is as nonphysical as mass scaling, during crush analyses, some pieces of crushed material physically dis-attach from the specimen. Among the material which remains attached, a lot of it is displaced from the line of loading and therefore does not contribute to the progressive solution of the problem and its removal is justifiable. As part of this work it was noticed that when failed elements are not removed from the mesh they become highly susceptible to numerical problems, such as hourglass due to vibrations, high accumulated strains and low modulus of elasticity. Hourglass can be avoided or delayed with added viscosity, by the adoption of hourglass control algorithms, and using fully integrated elements. However, it is the recommendation of the author to activate element deletion.

Another source of computational cost is caused by the reading and writing to files operations performed by the auxiliary functions needed to apply the non-local damage progression for crushing analyses discussed in Section 5.2. As shown in code documented in APPENDIX B mechanisms were put in place to reduce the number of calls to the very minimum.

Chapter 6. THEORY DEMONSTRATION: STATIC FAILURE

The theory developed for this dissertation, presented in Chapter 4 and implemented as a LS-DYNA user defined material model as discussed in Chapter 5 is applied to solve a static failure test. The specimen geometry chosen is the open-hole tensile strength specimen as specified in the ASTM standard D5766 (American Society for Testing Materials, 2011). The unnotched tensile test was simulated in Section 4.3. The notched tensile test is chosen herein in order to introduce a stress concentration and evaluate the related failure mechanism. The notched test method was developed in the early 1980s with the purpose of comparing toughness increases as new composite material systems were introduced. The machined circular hole is meant to represent an idealized impact damage or a manufacturing defect, enabling meaningful toughness comparisons between different materials. The notched test methods that emerged and later were standardized by ASTM for Open Hole Tension (OHT): (American Society for Testing Materials, 2011), Open Hole Compression (OHC): (American Society for Testing Materials, 2014), and Filled Hole Tension (FHT) and Compression (FHC): (American Society for Testing Materials, 2012). The OHT test method is selected in this dissertation because it does not require a fixture, which can sometimes affect the load path and therefore the results.

When performing material characterization for composite material systems, as opposed to metals, coupons geometries which include damage are performed in addition to the undamaged specimens. Materials A- and B- basis allowables are generated for specimens that have been degraded in a representative manner in order to be used in structural designs (Composite Materials Handbook-17, 2012) (Composite Materials Handbook-17, 2012). Open holes and filled holes test specimen, listed above, are used to simulate typical damage scenarios, as explained previously. Of particular importance to polymeric resin composites (PMCs), unlike metallic materials, is the static

notch sensitivity, which makes the open and filled holes tests of fundamental importance towards fully characterizing a PMC material system.

6.1 EMPIRICAL EXPERIMENTS

Test coupons were built with dimensions according to the ASTM standard D5766 (American Society for Testing Materials, 2011) as shown in Figure 6.1-1. Two layups are investigated: $[0]_8$ and $[0/90]_{2s}$, for a total of 8 plies. The material used is: T800/3900-2 unidirectional 12k tow tape prepreg which cures at 350ºF (177ºC), kindly donated by Toray Composites (America) Inc. Material strength characterization was performed. The material properties are listed in Table 6.1-1. The mode I and mode II specific fracture energies are taken from (Pineda, et al., 2011) and (Pineda, et al., 2013). As explained in Sections 2.2.1 and 4.2.2 the mode I and II specific fracture energies needs to be converted into the 1-2 directions fracture energy density values to be used in the methodology discussed in Sections 2.2.1, 4.2.2 and 6.2.

The specimens are applied a speckle pattern in order to utilize the Digital Image Correlation (DIC) technique. DIC is a 3D or 2D full-field non-contact optical technique to measure contour deformation. Pictures were taken during the tensile tests in an automated fashion. The open source 2D-DIC MATLAB program: Ncorr v1.2 is utilized for this work (Blaber, et al., 2015). A notched tensile test specimen with the speckle pattern prior to testing is shown in Figure 6.1-2.

Testing was conducted in the Aeronautics and Astronautics department at the University of Washington (UWAA) using an 8801 servo-hydraulic Intron system and BlueHill software. Two repetitions per laminate stacking sequence were performed. The $[0]_8$ and $[0/90]_{2s}$ results are respectively shown in Figure 6.1-3 and Figure 6.1-4.

The scatter both in ultimate laminate failure load and stiffness is much greater for the unidirectional laminates as the sensibility to the fiber angle is higher. The specimens were manufactured by hand.

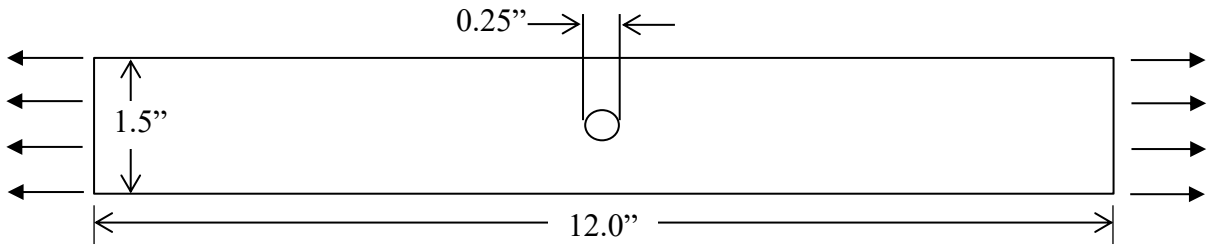

Figure 6.1-1. Schematic of Open-Hole Tension Test Specimen according to (American Society for Testing Materials, 2011) as used in this work.

Table 6.1-1. Material properties for T800/3900-2 as used in this study. From (Pineda, et al., 2011) and (Pineda, et al., 2013).

Material Property	**Value**
ρ [lb/in^3]	0.055
E_{11} [Msi]	23.2
E_{22} [Msi]	1.30
G_{12} [Msi	0.90
ν_{12}	0.28
X_T [ksi]	412
X_C [ksi]	225
Y_T [ksi]	8.72
Y_C [ksi]	24.3
S_C [ksi]	13.76
G^f_{IC} [lbf/in]	1026
G^m_{IC} [lbf/in]	2.39
G^m_{IIC} [lbf/in]	6.78

Figure 6.1-2. Notched tensile test specimen prior to testing with applied speckle pattern for digital image correlation (DIC).

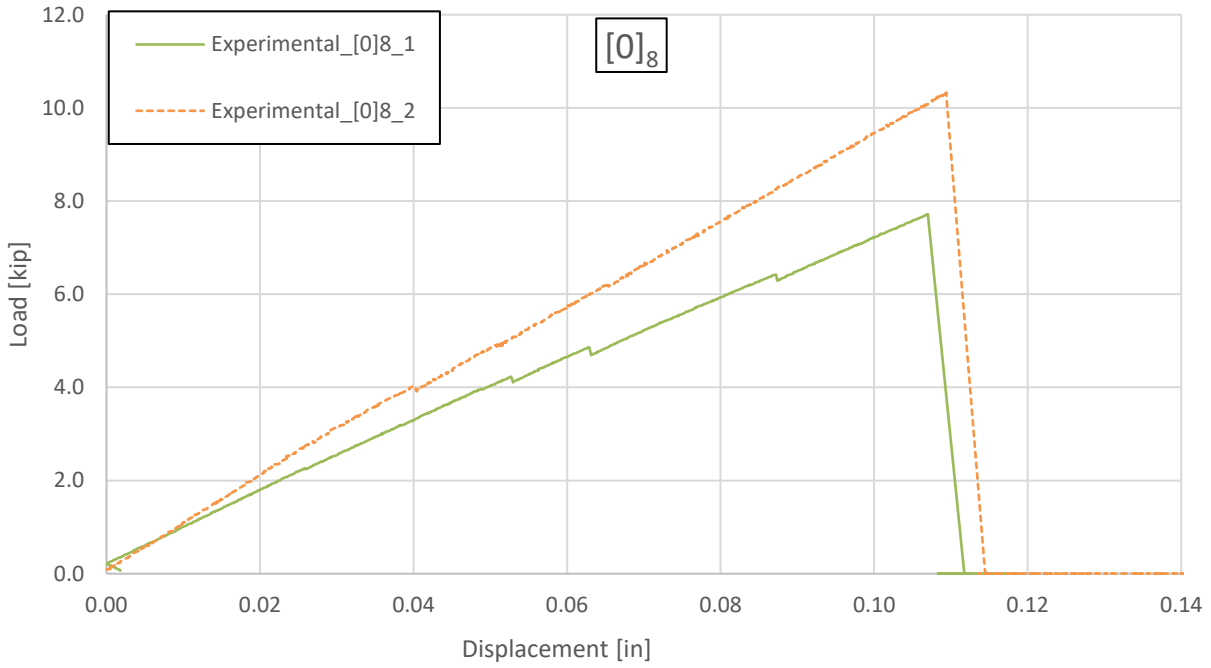

Figure 6.1-3. Experimental recorded load versus displacement for tensile tests of $[0]_8$ notched coupons.

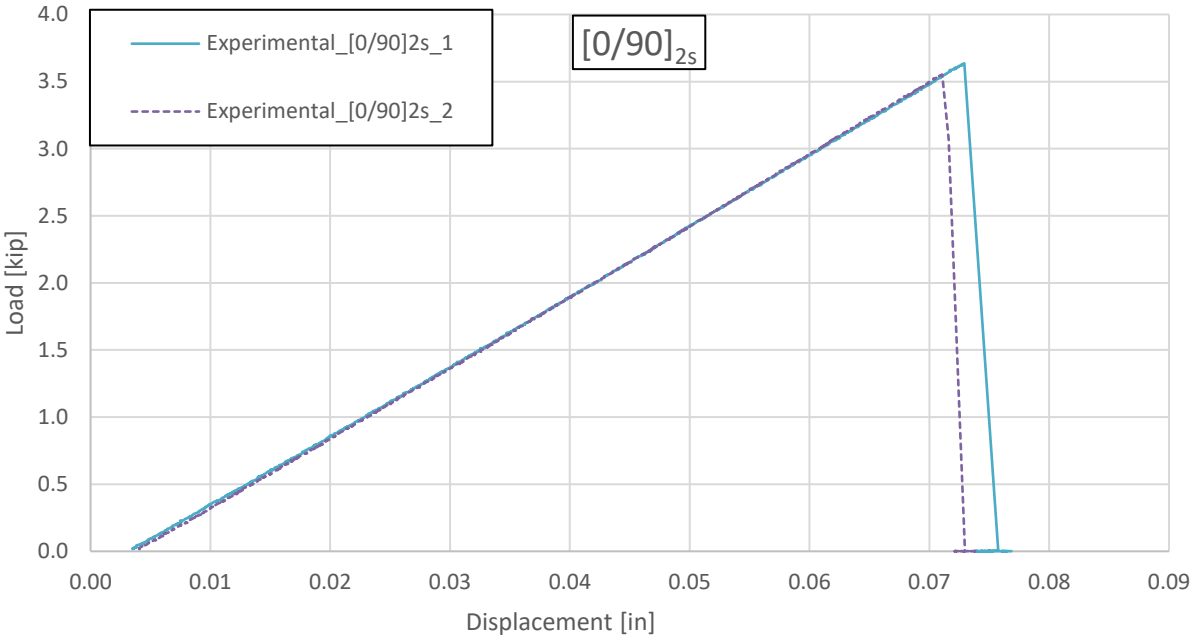

Figure 6.1-4. Experimental recorded load versus displacement for tensile tests of $[0/90]_{2s}$ notched coupons.

One failed specimen per stacking sequence is shown after being tested in Figure 6.1-5. For both layups failure initiates at the notch. For the $[0]_8$ laminate failure propagates in the direction of the fibers. When catastrophic failure finally occurs, the resulting shape for the laminate is composed of sub-strips as shown in (a). Damage for the $[0/90]_{2s}$ laminate, on the other hand, travels normal to the direction of loading and the resulting failure is a clean fracture, as shown in (b).

(a)

(b)

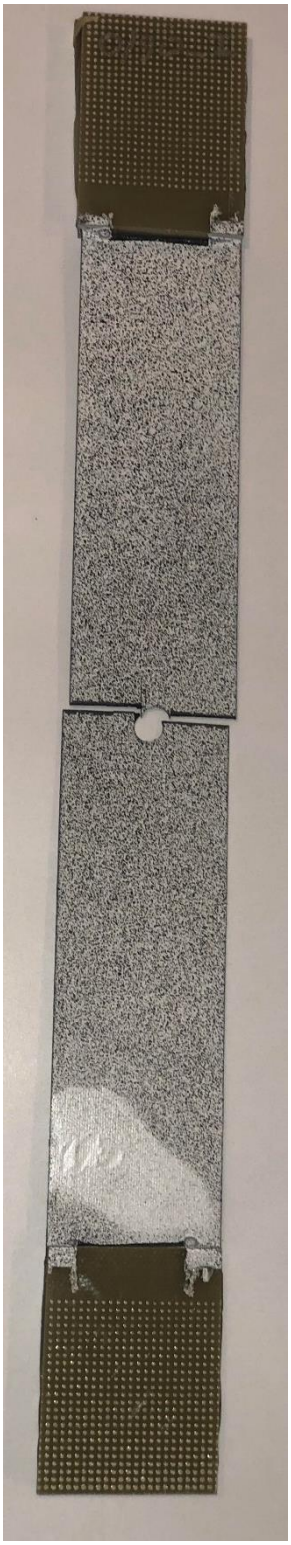

Figure 6.1-5. Selected failed test coupons for (a) $[0]_8$, and (b) $[0/90]_{2s}$ layups.

6.2 NUMERICAL MODELS AND COMPARISON

As discussed in Sections 2.2.1 and 4.2.2, the specific fracture energies provided in (Pineda, et al., 2011) - (Pineda, et al., 2013), and summarized in Table 6.1-1 are converted into fracture energy densities to be used in the methodology discussed in this work. The width of the crack band, h_c, as discussed in Section 2.2.2 is not possible to be measured as discussed in (Bazant, et al., 1983) but it is typically estimated to be in the order of millimeters for polymeric matrix composites. In this work h_c has been assumed to be: 6.0mm (0.24”). From Equation 2.8:

$$\gamma_{IT} = \frac{G^f_{IC}}{h_C} = 4343 \text{ psi} \tag{6.56}$$

The fracture energies used in this part of the work are listed in Table 6.2-1. Testing for the fracture energy density values is beyond the scope of this work. The values utilized in this study are a mix of data available in the literature and typical values from industry experience.

Table 6.2-1. Fracture energy density values as used in this study for T800/3900-2.

Material Property	**Value**
γ_{IT} [psi]	4343
γ_{IC} [psi]	1306
γ_{2T} [psi]	47.4
γ_{2C} [psi]	368

Table 6.2-2. LS-DYNA Material Card for the User-Defined Material Model.

```
$---+----1----+----2----+----3----+----4----+----5----+----6----+----7----+----8
*MAT_USER_DEFINED_MATERIAL_MODELS
$#     mid        ro        mt       lmc       nhv    iortho     ibulk        ig
         1 1.5000E-4        45        32        36         1         1         1
$#   ivect     ifail    itherm    ihyper      ieos      lmca    unused    unused
         0        -3         0         0         0         0         0         0
$#    aopt      mafc        xp        yp        zp        a1        a2        a3
     2.000  1.000000     0.000     0.000     0.000     0.000     1.000     0.000
$#      v1        v2        v3        d1        d2        d3      beta
     0.000     0.000     0.000     0.000     0.000     1.000     0.000
$#     cm1       cm2       cm3       cm4       cm5       cm6       cm7       cm8
    23.2e6    13.0e5         8     0.280      0.03       0.1    9.01e5    9.01e5
$#     cm9      cm10      cm11      cm12      cm13      cm14      cm15      cm16
    9.01e5    23.2e6   1.376e4    4.12e5    8.72e3    24.3e3       0.1   1.15e-9
$#    cm17      cm18      cm19      cm20      cm21      cm22      cm23      cm24
     0.025   -0.0232   -0.0472    0.0116      0.03       100      0.57    2.25e5
$#    cm25      cm26      cm27      cm28      cm29      cm30      cm31      cm32
      0.5     2.8e6    3.75e6  0.004594      4343      1306      47.4       368
$---+----1----+----2----+----3----+----4----+----5----+----6----+----7----+----8
```

Table 6.2-3. Material card and material parameters correlation for tensile notched simulations.

Material card variable	Material model parameter	Material card variable	Material model parameter
cm1	E_{11} [psi]	**cm17**	*Not used*
cm2	E_{22} [psi]	**cm18**	*Not used*
cm3	# of integration points / element	**cm19**	*Not used*
cm4	ν_{12}	**cm20**	*Not used*
cm5	β_{2T} from Equation 4.27	**cm21**	*Not used*
cm6	element size	**cm22**	*Not used*
cm7	G_{12} [psi]	**cm23**	*Not used*
cm8	*Not used*	**cm24**	X_C [psi]
cm9	*Not used*	**cm25**	β_{1T} from Equation 4.25
cm10	*Not used*	**cm26**	*Not used*
cm11	S_C [psi]	**cm27**	*Not used*
cm12	X_T [psi]	**cm28**	lamina thickness [mm]
cm13	Y_T [psi]	**cm29**	γ_{1T}
cm14	Y_C [psi]	**cm30**	γ_{1C}
cm15	*Not used*	**cm31**	γ_{2T}
cm16	*Not used*	**cm32**	γ_{2C}

The material properties are assembled in the material card which is shown in Table 6.2-2. The various entries are explained in the LS-DYNA User Manual (Livermore Software Technology

Corporation, 2014). The material card values cm1 – cm32 are the inputs utilized as material parameters in the UMAT. Among these are the elastic properties, strengths, and fracture energy densities. The full correlation is provided in Table 6.2-3.

Finite element models are built with the dimensions, and boundary and loading conditions as shown in Figure 6.1-1. Coarse, medium and fine mesh are generated, as shown in Figure 6.2-1. The finer the mesh and the better the numerical model was found able to replicate the failure morphology. The comparison between numerical calculated and experimentally measured load versus displacement results are shown in Figure 6.2-2 and Figure 6.2-3 respectively for the $[0]_8$ and $[0/90]_{2s}$ laminates.

Closeups of failure initiation for the $[0]_8$ and $[0/90]_{2s}$ laminates are shown respectively in Figure 6.2-4 and Figure 6.2-6. For both laminates failure initiates at the location of maximum stress concentration and initially grows in the direction normal to the loading direction. For the $[0]_8$ laminate the tendency for failure to propagate in the direction of the fibers is also observed, which is not present for the $[0/90]_{2s}$ laminate. The failure propagation morphology resembled what is experimentally observed during testing, as shown in Figure 6.1-5.

Final simulated failure the $[0]_8$ and $[0/90]_{2s}$ laminates are shown respectively in Figure 6.2-5 and Figure 6.2-7. For the $[0]_8$ laminate final failure is particularly destructive while a clean failure is obtained for the $[0/90]_{2s}$ laminate. The final failure morphology is consistent with the experimental evidence, as shown in Figure 6.1-5.

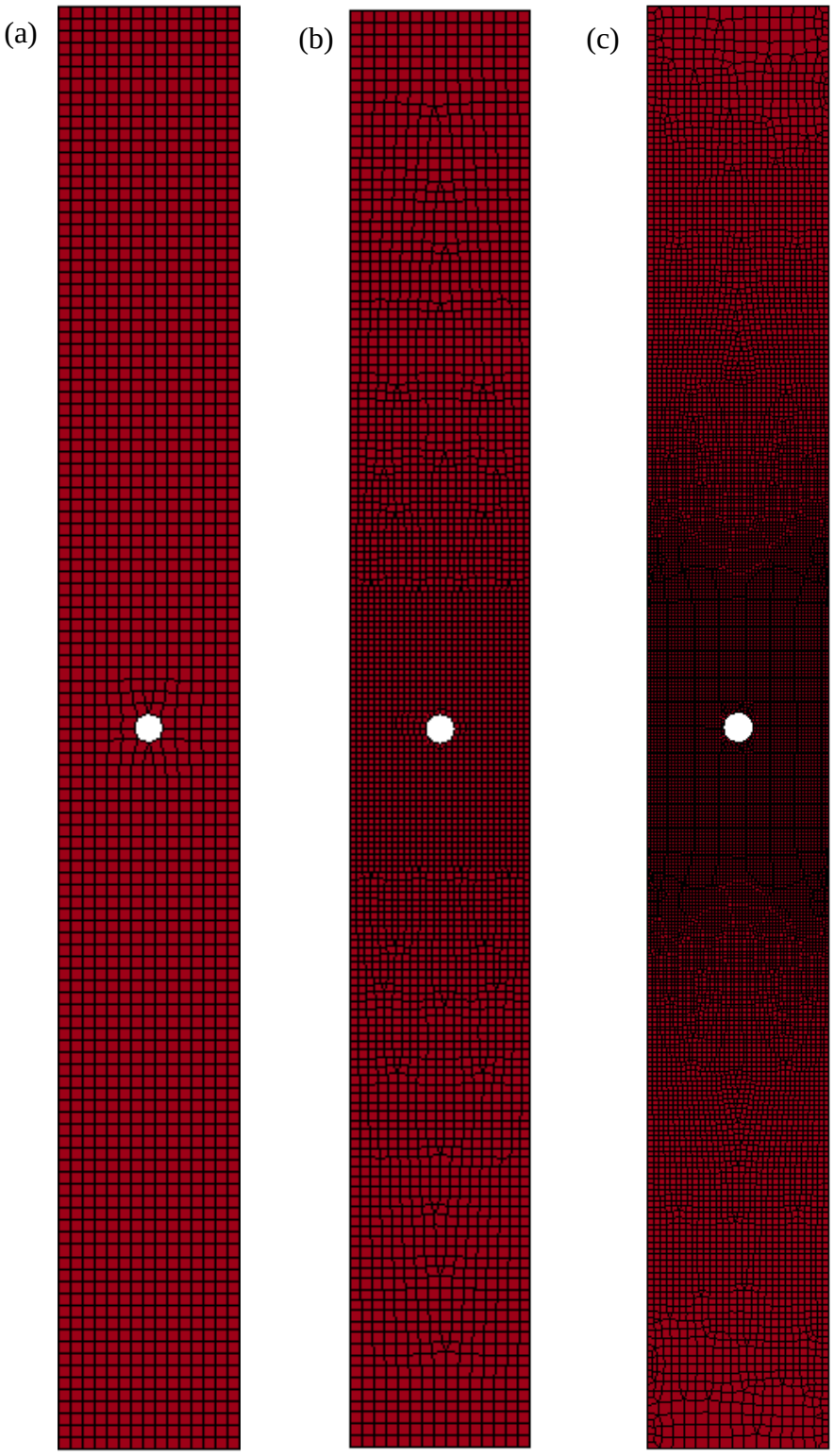

Figure 6.2-1. Finite element meshes for notched tensile test, a) coarse, b) medium, and c) fine.

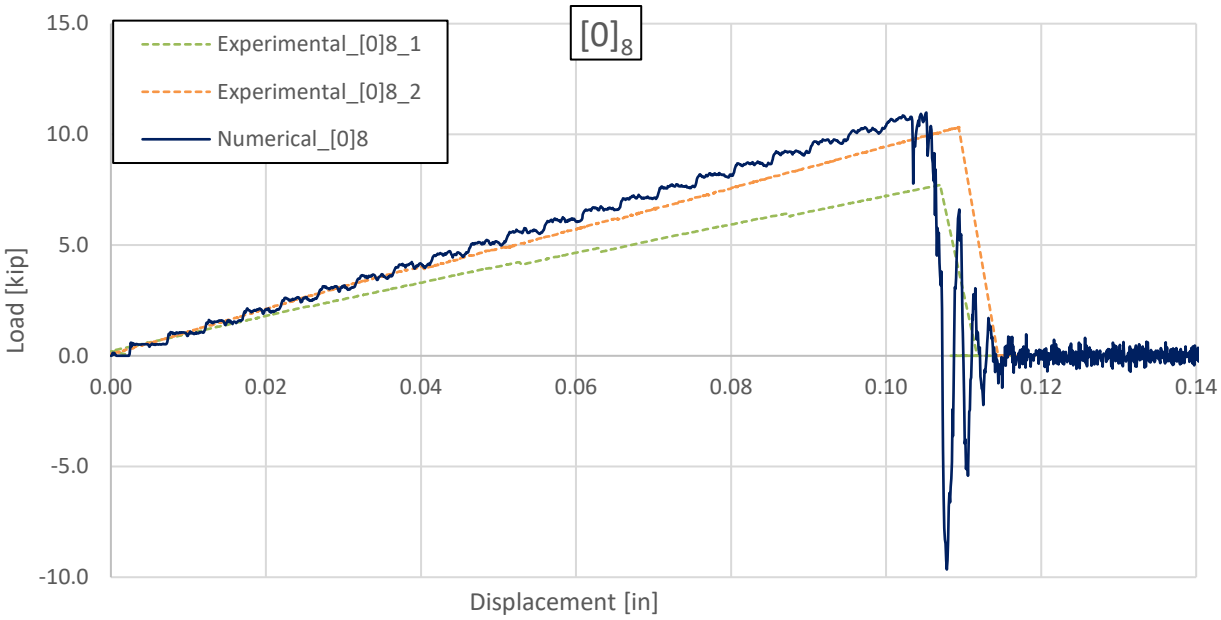

Figure 6.2-2. Load versus displacement results comparison between finite element results and experiments for the $[0]_8$ laminate.

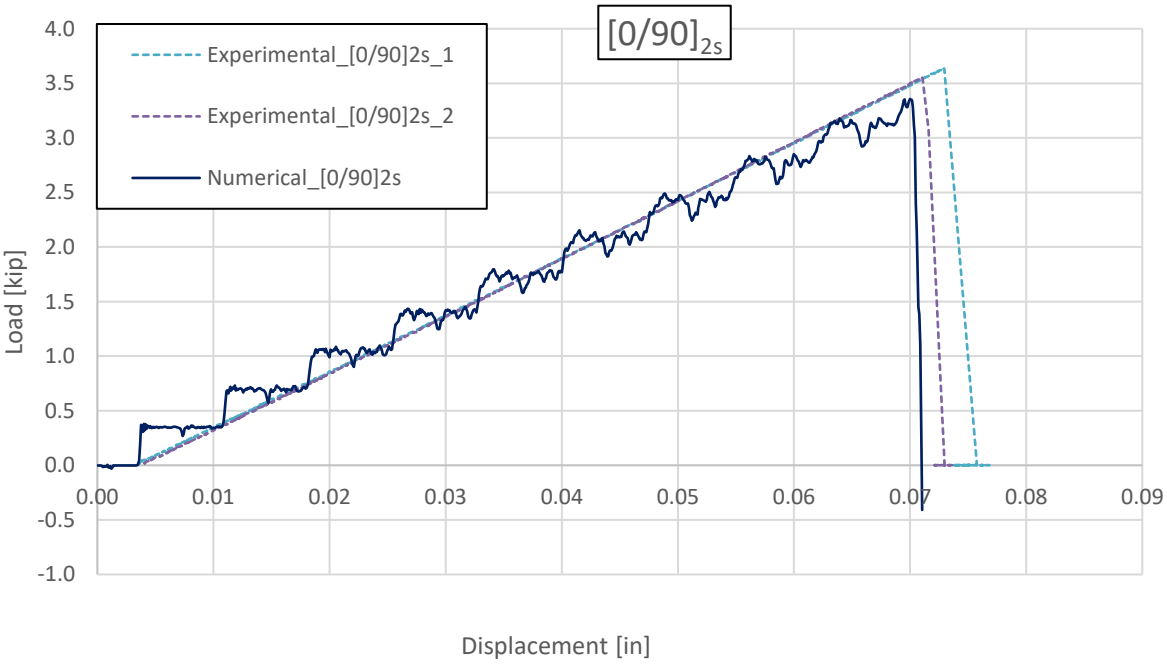

Figure 6.2-3. Load versus displacement results comparison between finite element results and experiments for the $[0/90]_{2s}$ laminate.

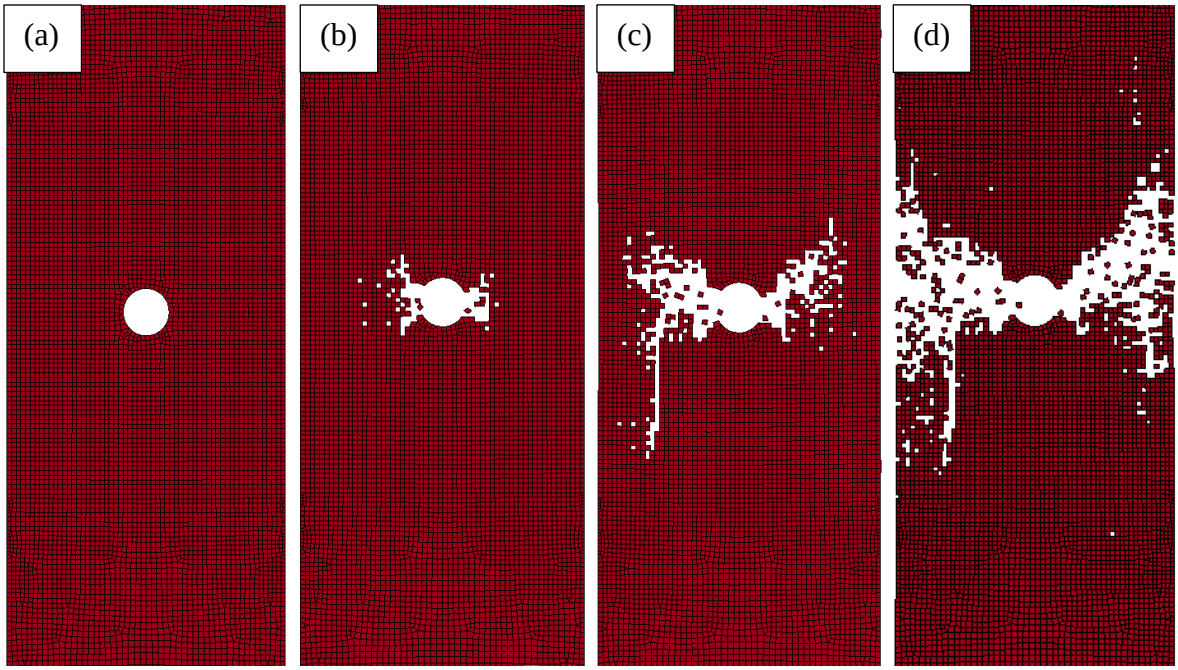

Figure 6.2-4. Failure progression around the stress concentration for the $[0]_8$ laminate, (a) before failure initiation, (b) failure initiating from stress concentration, (c) failure propagating with tendency of following fibers direction, (d) damage through entire width of the specimen.

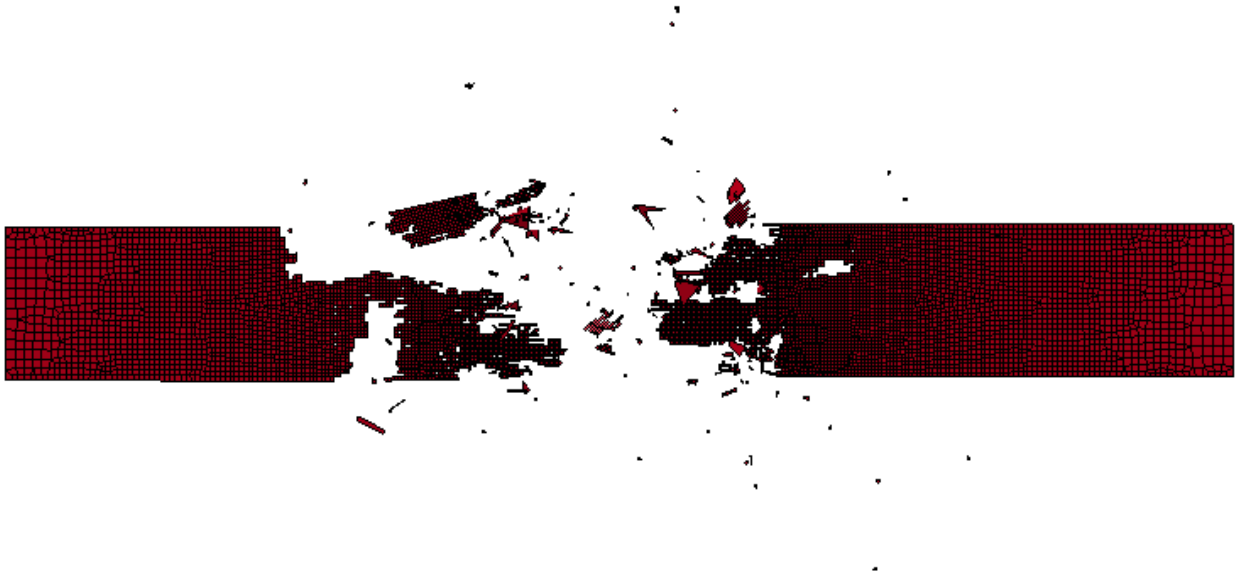

Figure 6.2-5. Final failure morphology for the simulation of the $[0]_8$ laminate.

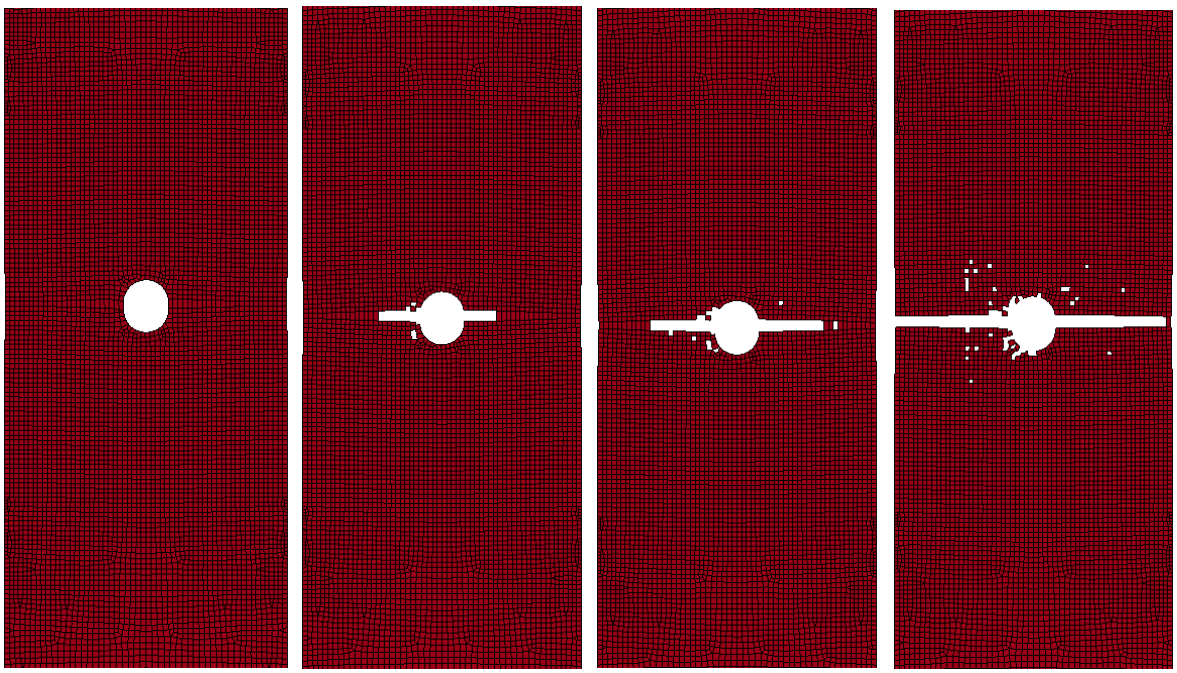

Figure 6.2-6. Failure initiation progression around the stress concentration for the $[0/90]_{2s}$ laminate.

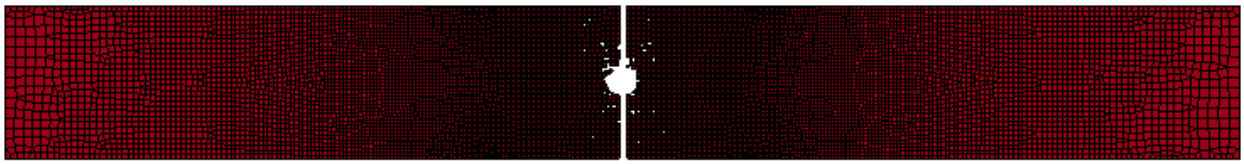

Figure 6.2-7. Final failure morphology for the simulation of the $[0/90]_{2s}$ laminate.

Chapter 7. THEORY DEMONSTRATION: CRASH LOADING

A fine difference is present between the definitions of crash and cush. A crash experiment is run at high speeds and will last a few milliseconds. On the contrary its crush counterpart is run at slower speeds and will last from a second to a few seconds (Bathe, et al., 1999). In this study, the experimental crushing speed is such that it qualifies it as a quasi-static problem due to its low speed. The theory developed for this dissertation, presented in Chapter 4 and implemented as a LS-DYNA user defined material model as discussed in Chapter 5 is applied to solve a crushing problem. The problem chosen is the quasi-static crush of a corrugated, also commonly referred to as sinusoidal specimen, which has been vastly investigated by the authors, from an experimental standpoint before (Deleo, 2011).

As discussed in (Carruthers, et al., 1998), (Deleo, 2011) and (Composite Materials Handbook-17, 2012) specific energy absorption, SEA, treated in Section 2.3 is not a material property for composites, as opposed to metals. SEA for a given composite material system (fiber and resin types, and ratio) is found to vary with stacking sequence, which is intuitive, and cross-sectional geometry, which is less intuitive. Varying the stacking sequence varies the strength and stiffness of the material and therefore it is expected that SEA depends on the lamina orientations. For a given stacking sequence, the cross-sectional geometry is found to have a strong impact on the ability of the composite material to dissipate energy while crushing. As discussed in (Deleo, 2011), which is the author Master thesis, flat segments of material when crushing fail in splaying, which is primarily driven by propagations of delaminations. The local bending stiffness of curved sections prevent splaying to occur and results in fragmention being the primary failure mode.

One of the primary reasons preventing the widespread adoption of composite materials for primary crash/crush structures is the absence of a standardize test method for characterizing the

specific energy absorption. Previous work by the author focused on the development of a standardized test method (Feraboli, et al., 2007) (Wade, et al., 2009). A flat-plate test specimen and fixture was developed (Feraboli, 2009) to measure the SEA for composites by modifying an existing NASA concept (Lavoie, et al., July 1993) (Jackson, et al., 1994) and (Lavoie, et al., 1996). It was found that there are four failure mechanisms: fragmentation, frond formation, local, and global buckling, which compete as the dominating mode according to the chosen unsupported distance. From the study it was also concluded that the specimen and fixture combination presented several limitations, which are due to the influence of the fixture. In order to address this problem a self-standing specimen type was proposed: the corrugated geometry (Feraboli, 2008).

A comprehensive experimental study was conducted on the AGATE material system: T700/2510 where several cross-sectional geometries were investigated (Deleo, et al., 2009) (Deleo, et al., 2011). The corrugated specimen is found to exhibit the highest value of SEA because, as mentioned previously, the predominant failure more is fragmentation. Because of the favorable energy absorption characteristic of the corrugated geometry and the simplicity due to its self-standing nature, this specimen type is chosen as crushing example in this work. In addition, a comprehensive numerical study was performed previously by the author on the crushing of the sinusoidal composite tape specimen using the state of the art commercially available MAT54: "Enhanced Composite Damage" material model built into LS-DYNA (Feraboli, et al., 2011). It was concluded that the existing material model can produce SEA results which can match experiment evidence but with extensive calibration of non-physical parameters. However, this requires artificially high stress-strain behavior at the element level which is not realistic. The same problem is encountered in (Wade, 2014). As shown in this chapter, the damage model developed

in this dissertation solves this issue and provides a predictive tool for both SEA, and element level stresses.

7.1 EMPIRICAL EXPERIMENTS

The sinusoidal crush specimen is manufactured by press-molding through a set of aluminum matching tools, shown in Figure 7.1-1. The mold was designed to manufacture three types of sinusoidal specimens: half-circular, high sine and low sine profiles, as discussed in (Deleo, et al., 2011). In the current study only the half-circular geometry is considered. The cross-sectional dimensions are shown in Figure 7.1-2. After curing a 45º chamfer is machined at one of the specimen as shown in Figure 7.1-3. The chamfer, also referred to as the trigger, serves the function of locally weakening the material and therebefore initiates failure which then develops in a progressive fashion. Without a trigger the specimen is found to fail in global buckling, which is undesirable from a crashworthiness standpoint as the SEA is much lower and the energy is not dissipated in a controlled fashion. The trigger is discussed in Section 4.2.6 and it is the first step of the damage progression model developed as part of this dissertation. No other types of trigger mechanisms are employed in this study, but several configurations were considered in the numerical investigation developed to support this study. Another feasible option to manufacture the trigger would be the use of internal ply-drops.

The coupon is tested in vertical configuration, resting on a polished hardened steel surface as shown in Figure 7.1-4. The crushing plate is free to slide along four vertical posts, which use roller bearings for alignment and reduced friction. A self-aligning sphere is used to introduce the load from the test frame onto the crushing plate. The material system is the AGATE, T700 carbon fiber/ 2510 epoxy prepreg, supplied by Toray Composites of America, comprising of a 270º F cure resin (132 ºC) designated for autoclave or oven-only cure. It is a low toughness resin and intermediate

strength fiber material system. The stacking sequence utilized in this study is $[0/90]_{3s}$ cross-ply. The testing speed was 51 mm/min (2.0 in/min).

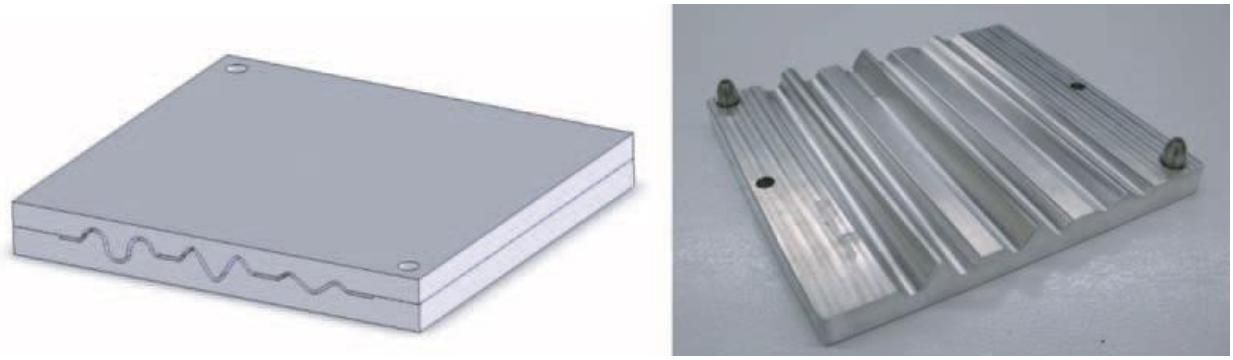

Figure 7.1-1. Molding tool as discussed in (Feraboli, 2008).

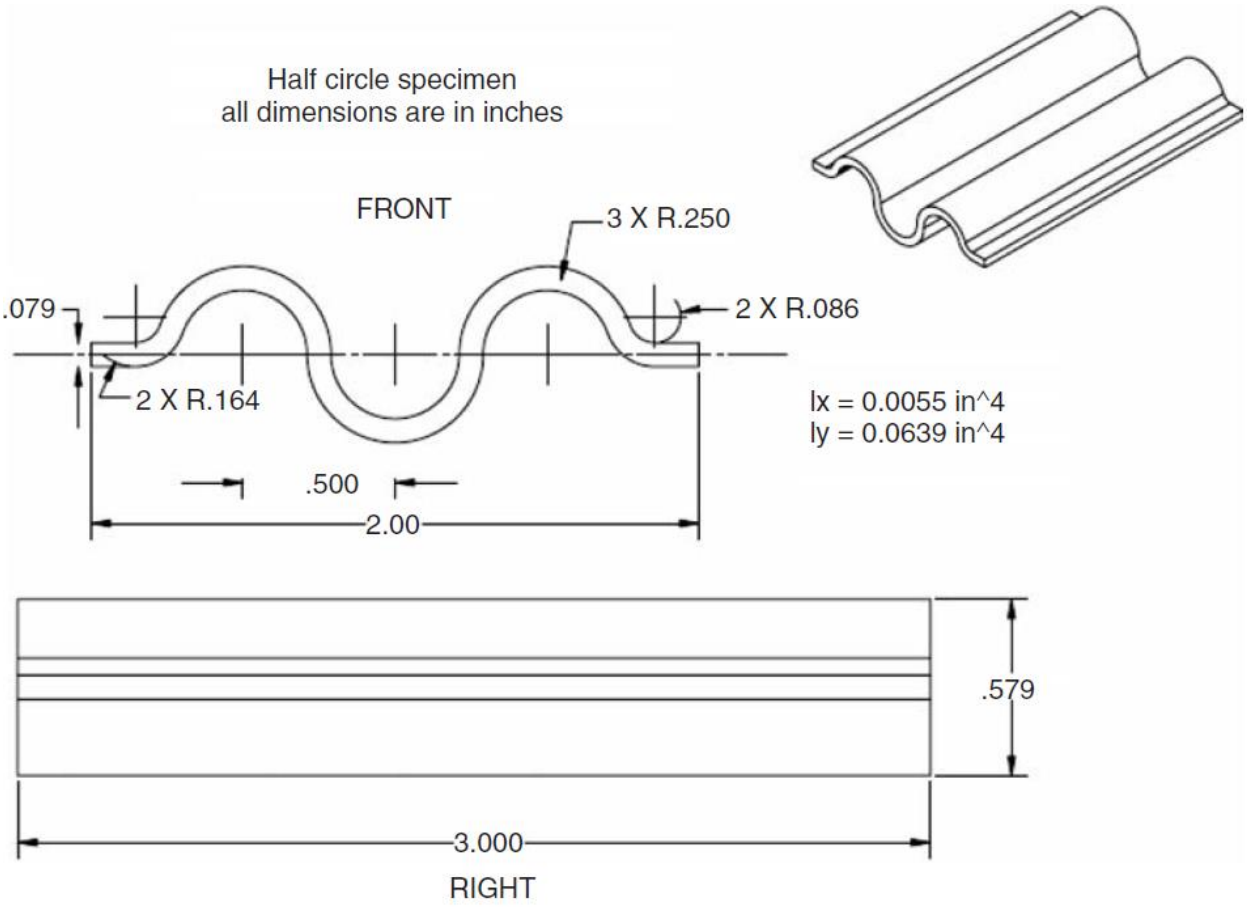

Figure 7.1-2. Cross-sectional shape of sinusoidal specimen for crushing experiments with dimensions in inches from (Deleo, 2011) and (Feraboli, 2008).

(a)

(b)

Figure 7.1-3. Prepreg tape sinusoidal specimen (a) with detail of the chamfered trigger (b).

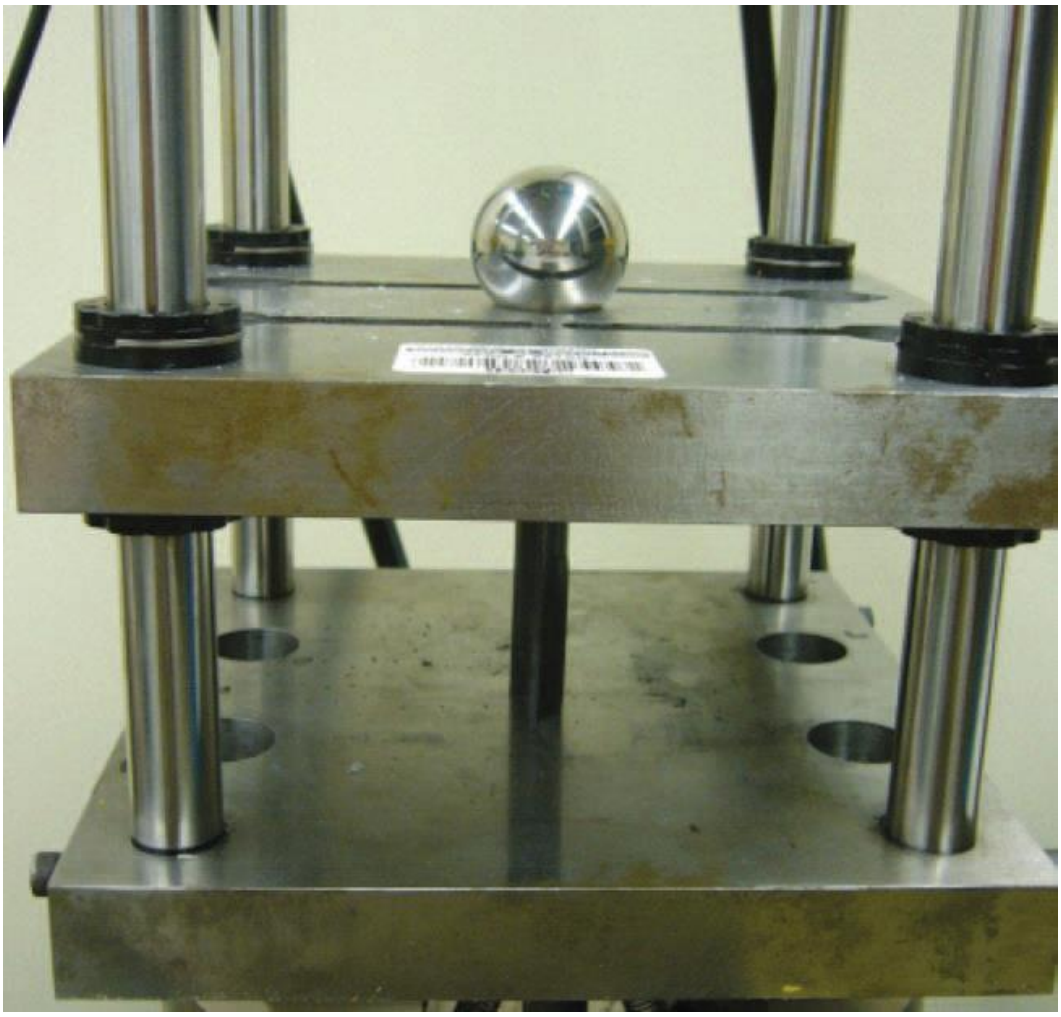

Figure 7.1-4. Sinusoidal specimen in crushing fixture prior to testing from (Feraboli, 2008).

Figure 7.1-5. Final crush morphology after testing for prepreg tape sinusoidal specimen.

Testing was conducted in the Aeronautics and Astronautics department at the University of Washington (UWAA) using an 8801 servo-hydraulic Intron system and BlueHill software. The crushed specimen is shown in Figure 7.1-5. The load is measured with a load cell installed in the Intron loading machine. The specimen is crushed 1.75 inches and the load versus stroke plot is shown in Figure 7.1-6 (a). The total energy absorption, EA, and the SEA versus stroke plots are shown in Figure 7.1-6 (b) and (c). The SEA is calculated as:

$$\mathrm{SEA} = \frac{\mathrm{W}}{\rho \cdot \mathrm{A} \cdot \partial} = \frac{\int_0^{\partial} \mathrm{F} \cdot \mathrm{d}\, \partial}{\rho \cdot \mathrm{t} \cdot \mathrm{S} \cdot \partial} = 67.1 \ \frac{\mathrm{J}}{\mathrm{g}} \tag{7.57}$$

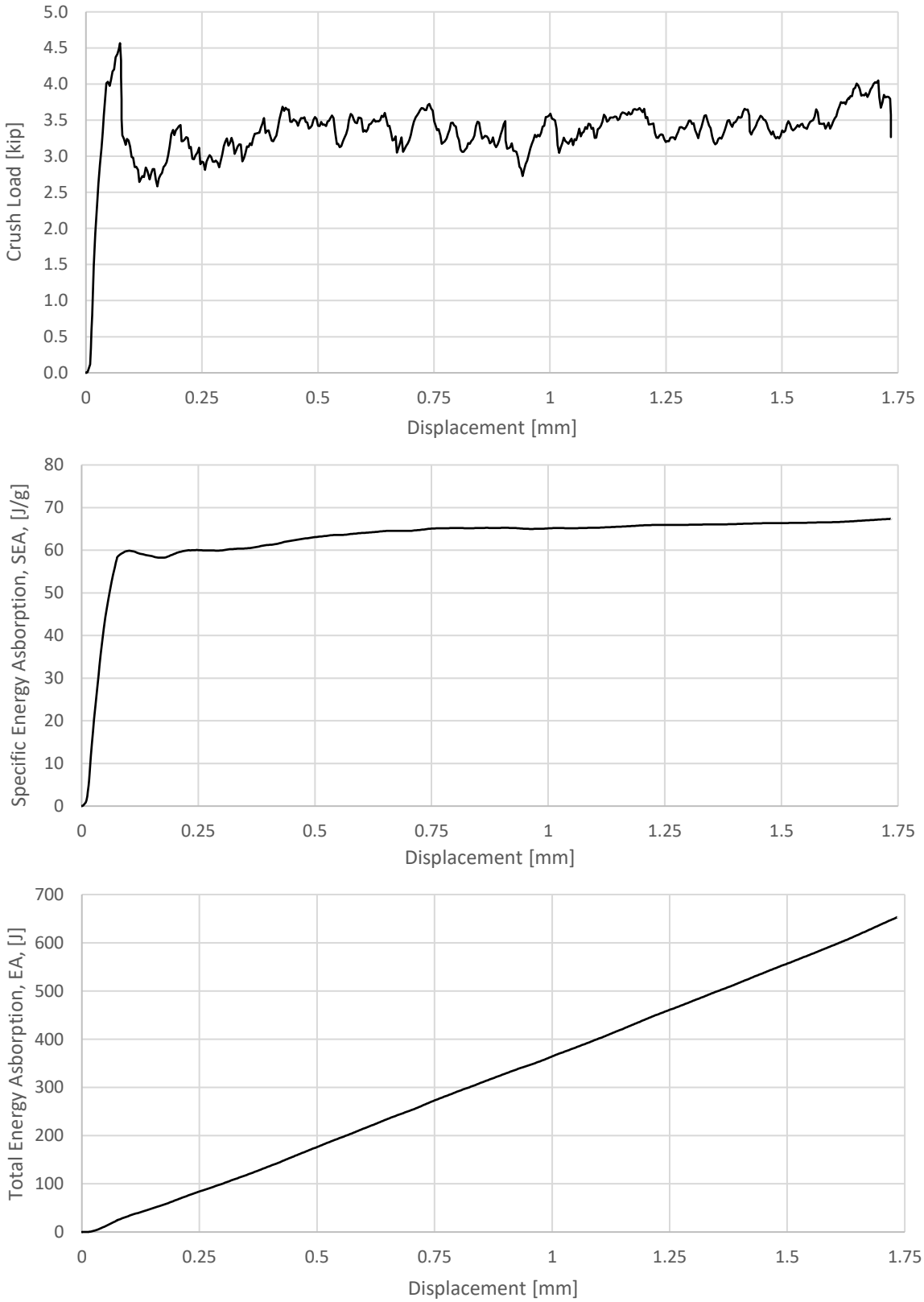

Figure 7.1-6. Experimental load-displacement curve (a), Specific Energy Absorption (b), as a function of displacement for the unidirectional tape corrugated specimen.

7.2 NUMERICAL MODELS AND COMPARISON

Material elastic and strength values are obtained from the Advanced General Aviation Transport Experiments program (AGATE) (Tomblin, et al., October 2002) and summarized in Table 7.2-1. The material properties were confirmed via several mechanical coupon tests performed according to the appropriate ASTM standards at the Aeronautics and Astronautics department at the University of Washington (UWAA).

Table 7.2-1. Material properties for AGATE T700/2510 as used in this study. From (Tomblin, et al., October 2002).

Material Property	**Value**
ρ [lb/in^3]	0.055
E11 [Msi]	18.4
E22 [Msi]	1.22
G12 [Msi]	0.61
v12	0.309
XT [ksi]	319
XC [ksi]	213
YT [ksi]	7.09
YC [ksi]	28.8
SC [ksi]	22.4

Table 7.2-2. Fracture energy density values as used in this study for T700/25150.

Material Property	**Value**
γ_{IT} [psi]	3043
γ_{IC} [psi]	1356
γ_{2T} [psi]	41.0
γ_{2C} [psi]	680

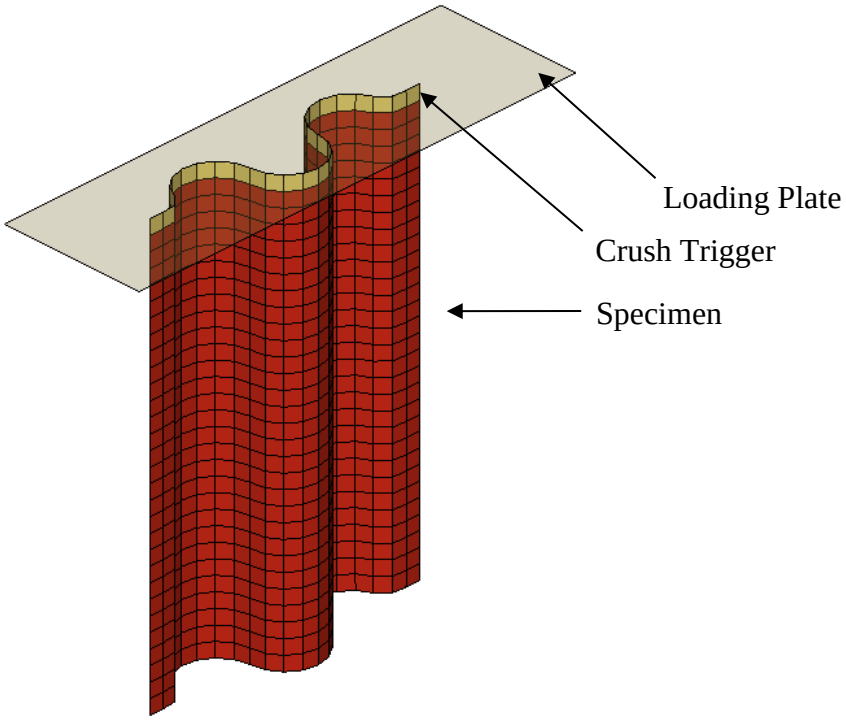

Figure 7.2-1. Finite element mesh for crushing simulation.

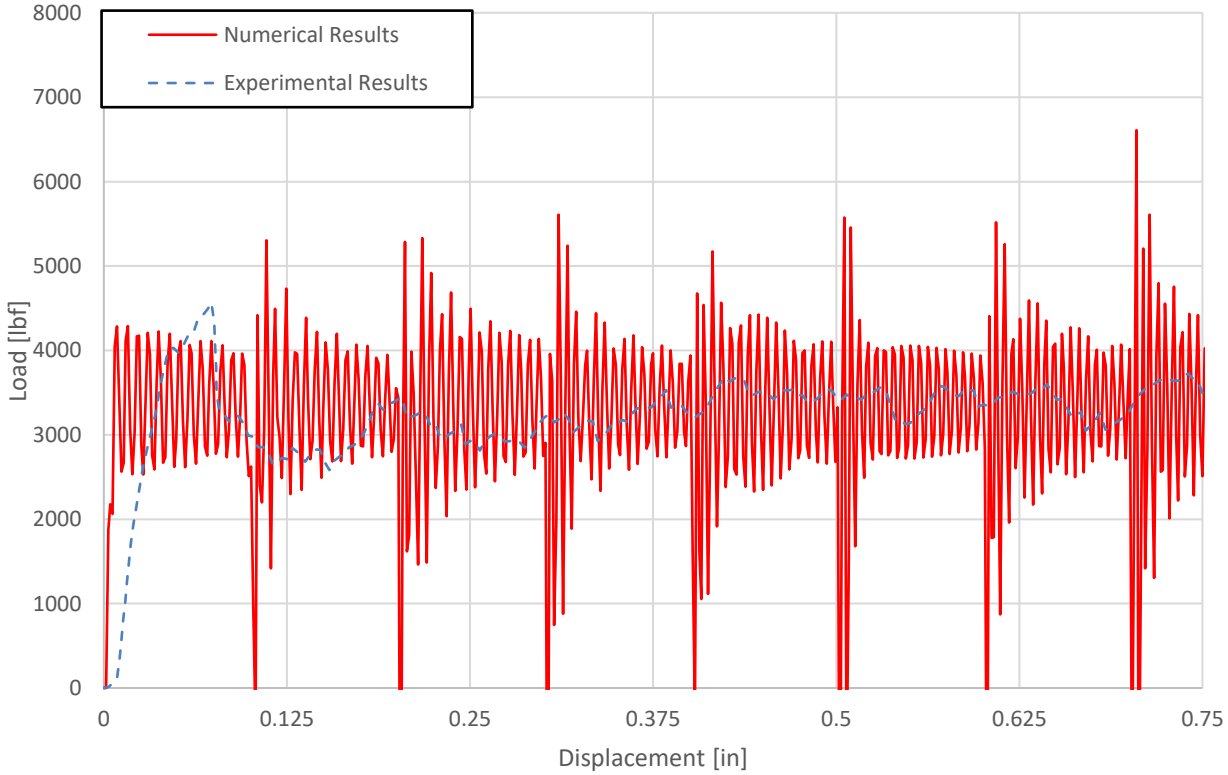

Figure 7.2-2. Load versus displacement results comparison between finite element results and experiment.

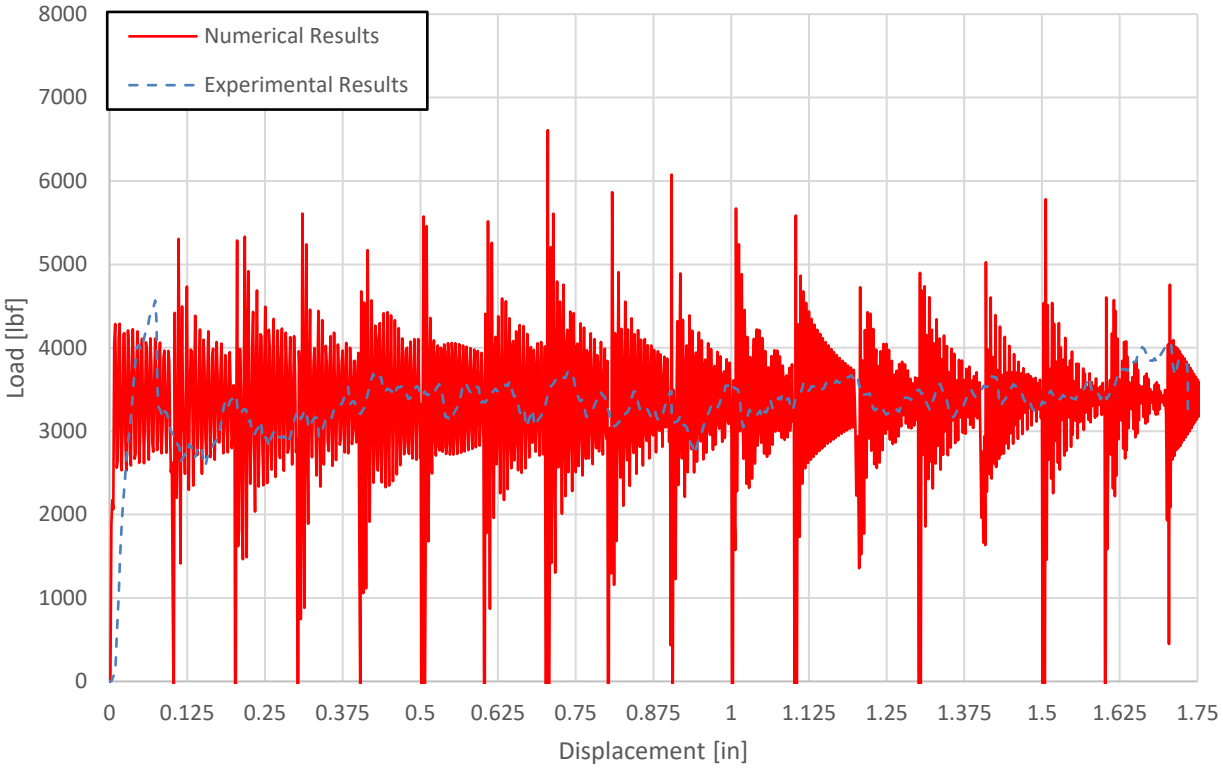

Figure 7.2-3. Load versus displacement results comparison between finite element results and experiment. Numerical model with anticipated element deletion to reduce computational cost.

The fracture energy density values used for T700/2510 are listed in Table 7.2-2 and they are typical values for an intermediate strength and low toughness composite material system. The finite element model mesh is shown in Figure 7.2-1. Three parts are modelled: the loading plate, trigger and the rest of the specimen. The loading plate is modelled with 1.0" x 3.0" x 0.1" volume meshed with 200 solid elements which are assigned a rigid material model. The first row of elements in the sinusoidal geometry is grouped into the trigger part. The remaining elements are grouped into a part called: the specimen. The trigger and the specimen are meshed with respectively 28 and 814 shell elements. Several shell formulations were found to work and did not produce a visible difference in the results. These are the Hughes-Liu (ELFORM = 1), Belytschko-Leviathan shell (ELFORM = 8) and fully integrated shell element (ELFORM = 16). The theoretical background

information on the various formulations is provided in (Livermore Software Technology Corporation (LSTC), 2016). The ELFORM = 16 option, because it is fully integrated, resulted being computationally prohibitive to solve without parallelization of the computing. The distribute damage model described in Section 4.2.6 requires single processor solution when utilized in the framework of a LS-DYNA UMAT due to the non-local nature of the solution approach. If the method presented in this dissertation is applied to larger crush models, it is recommended to adopt parallel computing which may require the development of a dedicated solver, or the implementation into a solver whose source code is available. The trigger and specimen are assigned the user-defined material models shown in APPENDIX B, respectively *umat43* and *umat45*. As described in Section 5.3, a separate model for the trigger is developed which has a reduced number of calls to the supporting subroutines of the distribute damage model needed for crush analyses. The bottom nodes of the specimen are constrained in the vertical direction plus a single node is also constrained in the in-plane directions. This is done in order to allow Poisson's effect and not overly constrain the base of the specimen. The loading plate is assigned a prescribed downward displacement of 150 inches/second. The loading is carried out an increased velocity, as explained in Section 5.3, in order to reduce the computational cost. It was made sure that the stress waves propagating through the material travel at a slower speed than that of sound and that the kinetic energy is small compared to the internal energy, therefore assuring that quasi-static conditions are maintained.

Two crush models are presented in this section were solved with a 64-bit Windows 10 laptop with 16.0 GB of RAM and Intel® Core ™ i7-6700HQ CPU operating at 2.60 GHz. The first model utilized the theory exactly as discussed in Chapter 4 resulted being very computationally expensive. The model ran for 129 hours and 27 mins until it was interrupted. The

model simulated the first 0.8” of crushing, while the experimental crushing was conducted to a maximum stroke of 1.75”, as shown in Figure 7.1-6 (a). The load versus stroke comparison between the experiment and numerical solution is shown in Figure 7.2-2. An additional element deletion criterion was added to the ones discussed in Section 4.2.4. A time deletion criterion was implemented. As shown in the code of Appendix B, the subroutine determines on which element row the integration point in question resides. A criterion is added which deletes an element if the simulation time exceeds a predetermined time value. The value of the predetermined time, which is a function of the row the element is on, can be adjusted. The earlier an element is deleted and the fastest the simulation run, and vice-versa. The reason for this is that the when a row of element is crushed to a reduced height, the minimum timestep requirement dictated by the Courant condition of Equation 3.27 also reduces in a linearly proportional fashion. For instance, the elements with reduced height due to crushing shown in Figure 7.2-5 drive the timestep to be one order of magnitude less than it is at the beginning of the simulation. When an element is fully crushed, and therefore removed, the time step returned to its original value and the simulation speeds us. The earlier and element is deleted and the fastest the simulation run as less iterations at reduced minimum timestep are needed. If the time element deletion criterion is set the time required to crush 95% of the element height the solution shown in Figure 7.2-3 is obtained. the analysis ran until 2.10” of stroke and then was interrupted. The model took 50 hours and 2 mins to solve in its entirety. The crush progression occurs in a controlled and stable manner as shown in Figure 7.2-4. The disadvantage of adding the time deletion criteria is that when elements are deleted prematurely and a gap is suddenly introduced between the specimen and the loading plate vibrations due to the unloading of the elastic stresses results.

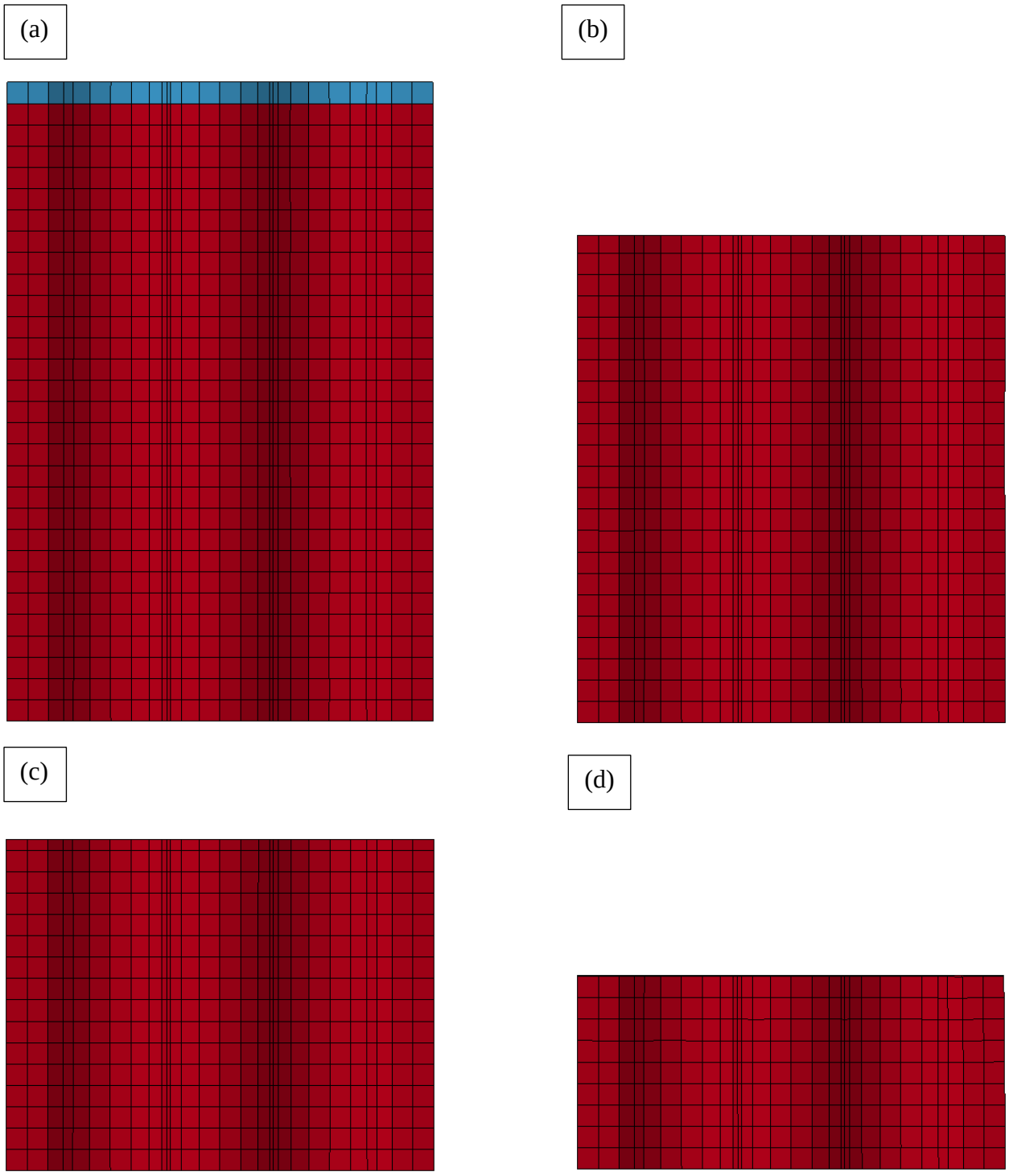

Figure 7.2-4. Crush progression with loading plate hidden for clarity. (a): initial conditions, (b): t = 0.00484s, d = 0.726”, (c): t = 0.00969s, d = 1.45”, (d): t = 0.0140s, d = 2.10”.

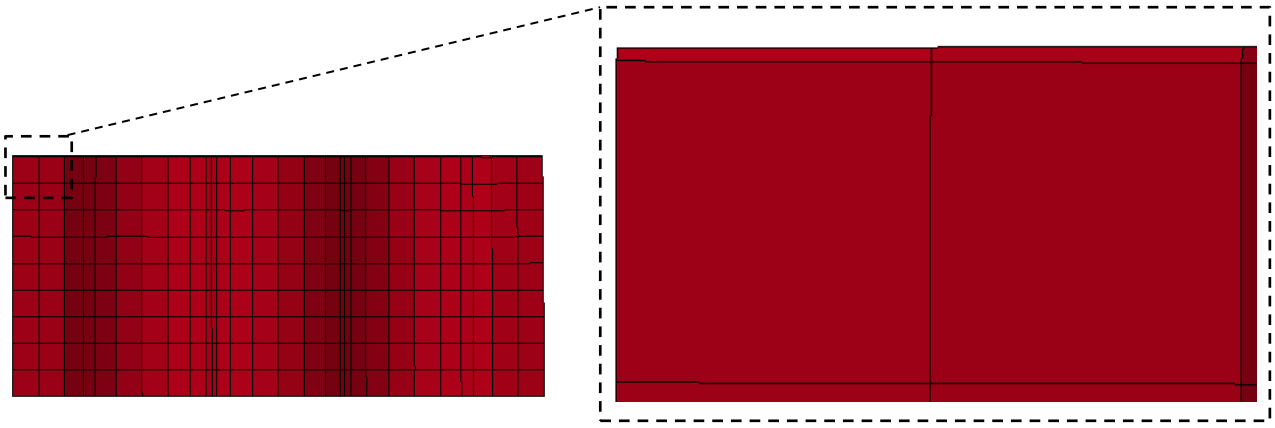

Figure 7.2-5. Crush progression at end of simulation, (d) from Figure above, which shows last row of elements being reduced to minimum height.

The resulting stress waves sum and subtract at the constraints and create more waviness in the load - displacement results as shown in the numerical results of Figure 7.2-3, as compared to those of Figure 7.2-2. The technique of adding a time related deletion criteria is commonly used in crash and crush analyses and for instance it is default option in LS-DYNA MAT54 material model (Livermore Software Technology Corporation (LSTC), 2016).

Both crush models discussed in this section utilize a hard contact algorithm: the *CONTACT_AUTOMATIC_NODES_TO_SURFACE LS_DYNA default contact. A quick introduction on contact algorithms within the finite elements framework is presented in Section 3.3.2. As discussed in Section 7.3, the possibility of using a ‘hard’ contact is a significant improvement over the existing techniques which require the use of a penalty-based contact algorithm, and the calibration of the load – penetration curve well outside the physical realm.

As discussed in Sections 4.2.6 and 7.1 a crushing initiator, also referred as trigger, is necessary both experimentally and numerically to avoid the global buckling failure mode and initiate the progressive crushing mode. The trigger is usually implemented as a local weakening at the beginning of the composite specimen. The same concept is present for metallic dedicated energy

absorption structures, which include a local weakness, such as a dimple, to promote the initiation of the progressive folding crushing mode, typical of ductile metals.

Several methods to model the trigger were experimented in the supporting work which led to the material presented in this dissertation. Two of the approaches are shown in an idealized fashion in Figure 7.2-7. An alternative way is to keep the layup of the trigger the same as the specimen and reduce the material strength. Ultimately all methods are found to be equivalent as long as the objective of initiating progressive crushing is achieved: the trigger row of elements are the first to fail and damage is propagated to the next row, which then become the weakest of the remaining mesh. By varying the modelled thickness of the trigger it is possible to adjust the initial load-displacement peak of the numerical results. This value can be obtained by trial and error. In this study, as shown in Figure 7.2-2, it could have been possible to obtain better matching for the initial peak by increasing the trigger thickness, however re-running the model was not deemed a value added to the theory and methodology described in this dissertation.

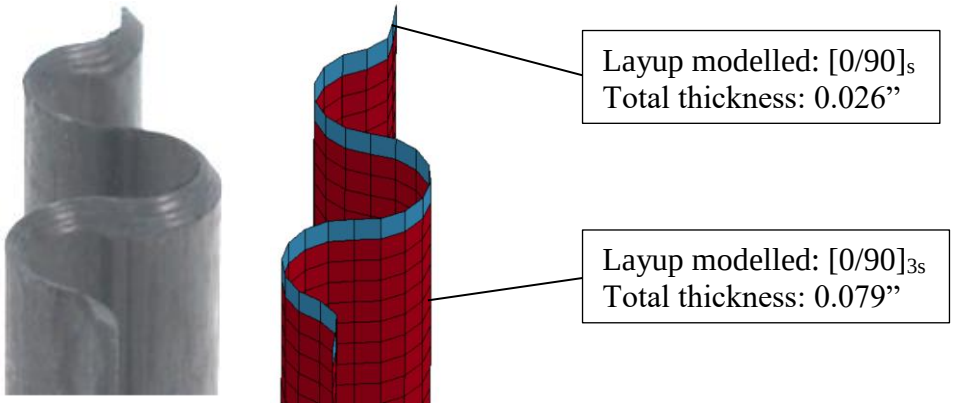

Figure 7.2-6. Crush initiator: trigger (a) as manufactured, (b) as modeled.

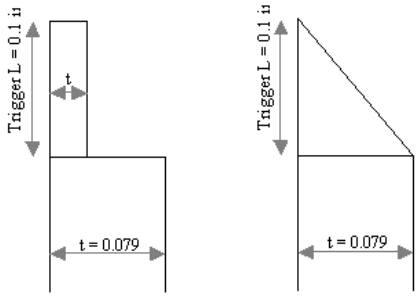

Figure 7.2-7. Different trigger modelling approaches.

7.3 ADVANTAGES OVER EXISTING CRUSH MODELLING TECHNIQUES

As discussed in 7.2, several advantages are introduced over existing state of the art crush techniques. Two of the most important advantages are the fact that no solution filtering contact stiffness calibration is required. First and foremost, current modelling techniques for crashworthiness analysis of composite structures require the use of filtering of the calculated load – displacement results. For instance the models described in (Deleo, et al., 2009), (Feraboli, et al., 2011) and (Wade, 2014), which is the same model for all references, simulate crushing of the sinusoidal specimen described in this dissertation and obtain the results shown in Figure 7.3-1 marked as: Raw data. The raw data is what is actually calculated by the model. The load calculated by the model oscillates from 0 to double the experimentally observed crushing value, meaning that if the energy absorbing member were part of the larger structure (i.e. stanchion in aircraft floor), the rest of the structure would see impulse loading of twice the real magnitude which have the potential of causing numerical instabilities or premature failure at other locations. The methods of (Deleo, et al., 2009), (Feraboli, et al., 2011) and (Wade, 2014) propose that the raw data is filtered with a low-pass digital filter with a channel frequency (CFC) of 600 Hz during post-processing, which results in the filtered load – displacement curve of Figure 7.3-1. Both the filtering method and frequency are not physical and simply serve as an averaging numerical scheme. This

unphysical modelling strategy has also been recommended in (U.S. Department of Transportation, Federal Aviation Administration, 2016). One of the intent of this dissertation work is to improve on the current physically-ill methods which are recommended to use in certification of general public transportation vehicles.

The current crashworthiness methods for composite structures, (Deleo, et al., 2009), (Feraboli, et al., 2011), (Wade, 2014) and (U.S. Department of Transportation, Federal Aviation Administration, 2016), require trial and error calibration of a penalty-based contact algorithm, via the implementation of a non-physical load-penetration curve. The methods mentioned above are not found to work if a 'hard' contact is utilized and the resulting outcome is the global buckling failure mode.

Figure 7.3-2 shows a sensitivity study on the load-penetration curve for the contact algorithm utilized in those studies. In (a) several load – penetration curves are shown and in (b) their effect is compared for the filtered results. For the sinusoidal specimen the red curve from (a) is found to produce a filtered resulting load – displacement curve which match the experimental SEA value. However the stiffness of the load – penetration curve does not have any physical significance as modeled and it is most likely geometry dependent, meaning that a new trial and error calibration would be needed if the cross-sectional shape were to be changed.

The theory and methodology developed for this dissertation does not require any filtering of the results and it is demonstrated to work with a 'hard' contact, therefore eliminating the need to calibrate the load – penetration curve.

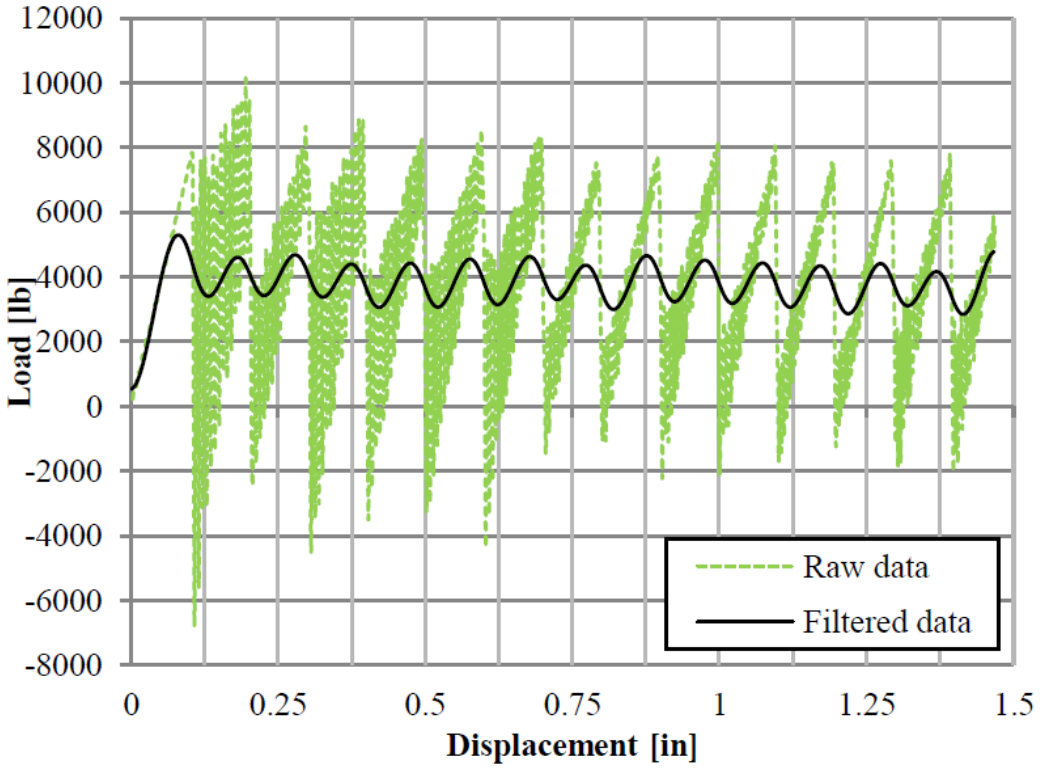

Figure 7.3-1. Actual (raw) and filtered load versus displacement numerical results from one the current crashworthiness techniques (Wade, 2014).

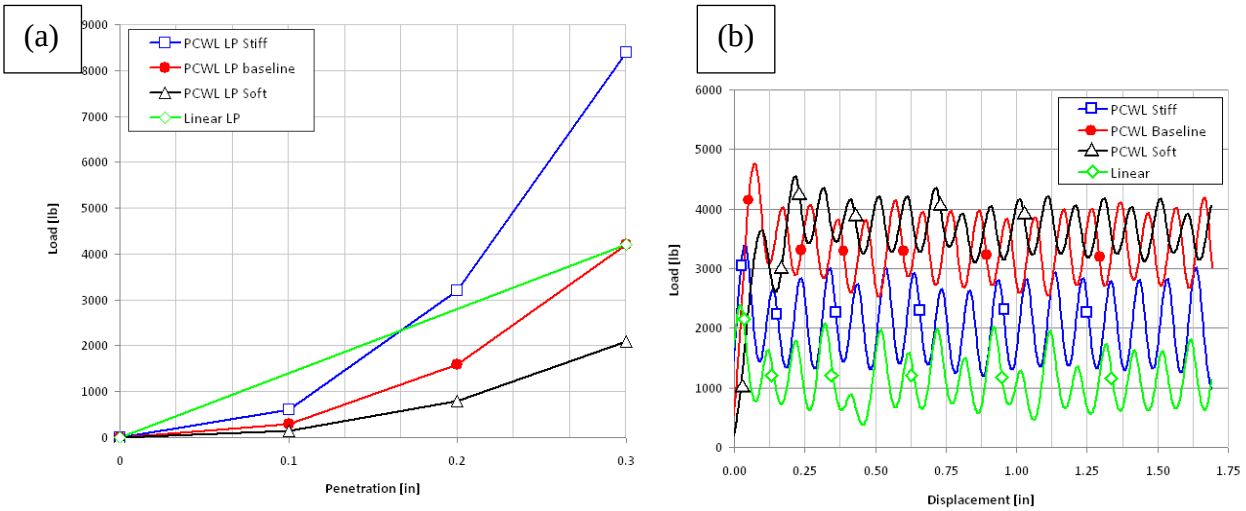

Figure 7.3-2. (a) Various load-penetration curves for a penalty-based contact algorithm, and (b) the resulting effect of the filtered load-displacement results of a sinusoidal specimen crushing solved with the theory from (Deleo, et al., 2009), (Feraboli, et al., 2011) and (Wade, 2014).

Chapter 8. CONCLUSIONS

A novel energy based composite continuum damage model is presented in this dissertation. The composite laminate is modelled at the meso-scale using the finite element method. Shell elements are utilized in this study. Each composite lamina is modelled with one or four integration points through the thickness as explained in Section 3.3, depending if reduced or full integration elements are chosen to carry out an analysis. Each lamina is modelled as a 2D plane stress orthotropic material and damage is included by degrading the stiffness matrix. Element deletion is added when all integration points have failed.

The theory is developed to predict failure initiation using a modified version of the Hashin's failure criteria and failure growth is modelled using damage variables which are developed as part of this work. The theory has been written to be used for both static failure and crush analyses, which build upon the significant author's experience on the matter. The theory was presented in Chapter 4. When applied to model a static failure problem, the damage variables derived in Section 4.2.3 are utilized. When modelling a crush event, the damage variables from Section 4.2.4 are utilized. In addition, when modelling crush, the distribute damage model discussed in Section 4.2.6 needs to be included in order to correctly simulate the progressive failure crush mode. The continuum damage model is energy based as the fracture energies densities of the four failure directions: fiber and matrix directions, tension and compression, are adopted.

Mesh size objectivity of the results is assured via the adoption of the Crack Band Theory explained in Section 2.2.3. Mesh objectivity is demonstrated by refining the mesh of the model shown in Section 4.3 and obtaining the same results.

The theory presented herein is implemented into an LS-DYNA user defined material model (UMAT) in order to take advantage of the pre-built contact algorithms needed for crush analyses

and solving the governing equation of motion shown in Equation 3.25. The implementation is discussed in Chapter 5.

The theory is applied to a static and crush problem with excellent agreement between the experimental evidence and numerical results for both cases. In Chapter 6 a tensile notched specimen is tested and simulated. Both the failure morphology and resulting load-displacement results at the constraint are found to match very well. In Chapter 7 a crush experiment carried out by the author as part of his Master's research is simulated.

In addition to matching the experimental results with a high degree of accuracy, the theory discussed herein offers significant advantages over alternative damage models present in the literature, as discussed in Section 7.3. One of the main advantages is the elimination for the need of filtering the load – displacement results using a non-physical numerical scheme and the elimination of the high impulse loads which make the models presented in (Deleo, et al., 2009), (Feraboli, et al., 2011), (Wade, 2014) and (U.S. Department of Transportation, Federal Aviation Administration, 2016) not suitable for use crush analyses of large structures. In addition, the theory presented in this dissertation offers a level of robustness and stability which allows it to be used with any contact type, including 'hard' contact and therefore eliminates the need to calibrate the penalty-based contact algorithm's load penetration curve with non-physical stiffnesses.

It is the hope of the author that many industries will find the work produced and shared with this dissertation useful towards producing innovative products and therefore advancing technologies which will benefit generations to come.

Chapter 9. PROPOSED AREAS FOR FURTHER RESEARCH

While developing the work described in this dissertation a few areas were highlighted to further the research and are quickly mentioned in this Chapter.

9.1 NONLINEAR STRAIN SOFTENING BEHAVIOR

As discussed in Section 4.2.3 and shown in Section 5.1, the post-failure initiation region of the lamina's material behavior is simulated with linear strain softening. This was not always the case. Initially a non-linear strain softening behavior was investigated with both successful and unsuccessful results. In order to keep this dissertation concise, the work with non-linear softening is not documented herein and might be published at a later date in a dedicated study. One reason for this choice is that additional work would like to be conducted by the author. Linear softening was eventually adopted in order to address a series of numerical problems which occurred in the explicit dynamic simulations of crush events. It has not yet been proved that the non-linear strain softening model was the sole, nor a, reason for the instabilities. While a non-linear strain softening behavior is more realistic of the actual material behavior, which is to be expected by empirical evidence, furthermore, of importance is the fact that the model be energy consistent using the fracture energies densities, discussed in Section 4.2.2.

9.2 NONLOCAL MODEL IMPLEMENTATION

It is the opinion of the author of this dissertation that an alternative way to solve the mesh sensitivity problem which results from strain localization due to the softening behavior of composites undergoing damage is via the utilization of a non-local continuum modeling approach. Non-localization in the work presented in this dissertation is used in the distribute damage model

used for crush analysis discussed in Section 4.2.6. In a local continuum damage model, the stress at a point depends only of the strain at that point. In a nonlocal continuum on the other hand, the stress at a point depends also on the strains in the neighborhood of that point or some sort of average strain in the vicinity (Bazant, et al., 1998). The proposed physical reason why a nonlocal approach is deemed promising is that micro-cracks at the location of damage are thought to interact and the formation of damage at one point either promotes of inhibits the formation of damage in adjacent areas. A few examples are present in the literature. For instance, in (Tvergaard, et al., 1995) a nonlocal constitutive formulation was developed and investigated for a porous ductile material and it was demonstrated that inherent mesh sensitivity issues were removed.

Chapter 10. BIBLIOGRAPHY

American Society for Testing Materials Open-Hole Compressive Strength of Polymer Matrix Composite Laminates, ASTM D 6484-14 [Report]. - W. Conshohocken, PA, US : ASTM International, 2014.
American Society for Testing Materials Standard Practice for Filled-Hole Tension and Compression Testing of Polymer Matrix Composite Laminates, ASTM D 6742-12 [Report]. - W. Conshohocken, PA, US : ASTM International, 2012.
American Society for Testing Materials Standard Test Method for Linear-Elastic Plane-Strain Fracture Toughness KIc of Metallic Materials, ASTM E399 - 17 [Journal] // ASTM International. - 2017.
American Society for Testing Materials Standard Test Method for Mode I Interlaminar Fracture Toughness of Unidirectional Fiber-Reinforced Polymer Matrix Composites, ASTM D5528-13 [Report]. - W. Conshohocken, PA, US : ASTM, 2013.
American Society for Testing Materials Standard Test Method for Open-Hole Tensile Strength of Polymer Matrix Composite Laminates, D5766-11 [Report]. - W. Conshohocken, PA, US : ASTM International, 2011.
ASTM International ASTM D 7085-05. V-Notched rail shear test [Book]. - West Conshohocken, Pa : ASTM International, 2005.
ASTM International D 3039/D 3039M - 08. Standard test method for tensile properties of polymer matrix composite materials. [Book]. - West Conshohocken, Pa : ASTM International, 2008.
ASTM International D 695 - 96. Standard Test Method for Compressive Properties of Rigid Plastics [Book]. - West Conshohocken, Pa : ASTM International, 1996.
Barbero E. J and Lonetti P. An Inelastic Damage Model for Fiber Reinforced Laminates [Journal] // Journal of Composite Materials. - 2002. - 8 : Vol. 36. - pp. 941-962.
Bathe K. J. [et al.] Advances in crash analysis [Journal] // Computers & Structures. - 1999. - Vol. 72. - pp. 31-47.
Bathe K. J. Numerical Methods in Finite Element Analysis [Book]. - Englewood Cliffs, NJ : Prentice-Hall, 1976.
Bazant Z. and Chang T. Nonlocal finite element analysis of strain-softening solids [Journal] // Journal of Engineering Mechanics. - 1987. - 1 : Vol. 113. - pp. 89-105.
Bazant Z. and Planas J. Fracture and Size Effect in Concrete and Other Quasibrittle Materials [Book]. - Boca Raton, FL : CRC Press LLC, 1998.
Bazant Z. P. and Oh B. Crack Band Theory for Fracture of Concrete [Journal] // Materials and Structures. - 1983. - Vol. 16. - pp. 155-177.
Bazant Z.P. Size effect on compression strength of fiber composites failing by kink band propagation [Journal] // International Journal of Fracture. - 1999. - Vol. 95. - pp. 103-141.
Blaber J, Adair B. and Antoniou A. Ncorr: Open-Source 2D Digital Image Correlation Matlab Software [Journal] // Experimental Mechanics. - Atlanta, GA : Georgia Institute of Technology, 2015. - 6 : Vol. 55. - pp. 1105-1122.
Blanco N. [et al.] Intralaminar fracture toughness characterization of woven composite lamintes. Part I: Design and analysis of a compact tension (CT) specimen [Journal] // Engineering Fracture Mechanics. - 2014. - Vol. 131. - pp. 349-360.

Campbell F. C. Manufacturing Processes for Advanced Composites [Book]. - New York, NY : Elsevier, 2004.
Carruthers J.J., Kettle A.P. and Robinson A.M. Applied mechanics reviews.Applied mechanics reviews.: Energy Absorption Capability and Crashworthiness of Composite Material Structures: A Review [Journal] // Applied Mechanics Reviews. - 1998. - 10 : Vol. 51. - pp. 635-649.
Chamis C. C. Failure criteria for filamentary composites [Journal] // Testing and Designm ASTM STP 460. - 1969. - pp. 336-460.
Chang Fu-Kuo and Chang Kuo-Yen A progressive damage model for laminated composites cointaning stress concentrations [Journal] // Journal of Composite Materials. - 1987. - pp. 834 - 855.
Cheboche J.L Continuous damage mechanics - a tool to describe phenomena before crack initiation [Journal] // Nuclear Engineering and Design. - 1981. - Vol. 64. - pp. 233-247.
Claunch E.C. Forecasting on Composites - Markets, Products, and Demands [Journal] // Journal of Textile and Apparel, Technology and Management. - 2015. - 2 : Vol. 9.
Composite Materials Handbook-17 Volume 3 Chapter 12 Damage resistance, durability, and damage tolerance [Book Section] // Composite Materials Handbook. - [s.l.] : SAE International on behalf of CMH-17, a division of Wichita State University, 2012.
Composite Materials Handbook-17 Volume 3 Chapter 16 Crashworthiness and Energy Management [Book Section] // Composite Materials Handbook. - [s.l.] : SAE International on behalf on CMH-17, a division of Wichita State University, 2012.
Composite Materials Handbook-17 Volume 3 Chapter 2 Introduction to Composite Structure Development [Book Section] // Composite Materials Handbook. - [s.l.] : SAE International on behalf of CMH-17, a division of Wichita State University, 2012.
Composite Materials Handbook-17 Volume 3 Chapter 3 Aircraft Structure Certification and Compliance [Book Section] // Composite Materials Handbook. - [s.l.] : SAE International on behalf on CMH-17, a division of Wichita State University, 2012.
Courant R. Variational Methods for the Solution of Problems of Equilibrium and Vibrations [Journal] // Bulletin of the American Mathematical Society. - 1943. - pp. 1-23.
Courant R., Friedrichs K. and Lewy H. On the Partial Difference Equations [Journal] // IBM Journal of Research and Development. - 1967. - pp. 11 (2): 215-234.
Cuntze R. G. and Freund A. The predictive capability of failure mode concept-based strength criteria for multidirectional laminates [Journal] // Composites Science and Technology. - 2004. - Vol. 64. - pp. 343-377.
Curiel Sosa J.L. Finite Element Analysis of Progressive Degradation versus Failure Stress Criteria on Composite Damage Mechanics. [Book Section] // Advances in Composite Materials - Ecodesign and Analysis. - 2011.
Deleo F. [et al.] Crushing of composite structures: Experiment and simulation [Conference] // Collection of Technical Papers - AIAA/ASME/ASCE/AHS/ASC Structures, Structural Dynamics and Materials Conference. - Palm Springs, CA : [s.n.], 2009.
Deleo F. and Feraboli P. Crashworthiness energy absorption of carbon fiber composites: Experiment and simulation [Conference] // Society of Plastics Engineers - 11th-Annual Automotive Composites Conference and Exhibition, ACCE. - Troy, MI : [s.n.], 2011.
Deleo F. Crashworthiness Energy Absorption of Carbon Fiber Composites: Experiment and Simulation [Report]. - Seattle, WA. : Master of Science in Aeronautics and Astronautics, University of Washington, 2011.

Dickson R. [et al.] The environmental fatigue behaviour of carbon fibre reinforced polyether ether ketone [Journal] // Journal of Materials Science. - 1985. - 1 : Vol. 20. - pp. 60-70.
El-Hage H., Mallick P. K. and Zamani N. A numerical study on the quasi-static axial crush characteristics of square aluminum tubes with chamfering and other triggering mechanisms [Journal] // International Journal of Crashworthiness. - 2010. - 2 : Vol. 10. - pp. 183-196.
Evans R. H. and Marathe M. S. Microcracking and stress-strain curves for concrete in tension [Journal] // Materials and Structures. - 1968. - 1 : Vol. 1. - pp. 61-64.
Farley G. L. and Jones R. M. Prediction of the energy-absorption capability of composite tubes [Journal] // Journal of Composite Materials. - 1992. - 3 : Vol. 26. - pp. 388-404.
Feraboli P. [et al.] Predictive modeling of an energy absorption sandwich structural concept using the building block approach [Journal] // Composites: Part A. - 2010. - Vol. 41. - pp. 774-786.
Feraboli P. and Wade B. Crushing Behavior of Laminated, DOT/FAA/TC-15/25 [Report]. - Springfield, Virginia : National Technical Information (NTIS), 2016.
Feraboli P. Development of a Corrugated Test Specimen for Composite Materials Energy Absorption [Journal] // Journal of Composite Materials. - 2008. - 3 : Vol. 42. - pp. 229-256.
Feraboli P. Development of a Modified Flat-plate Test Specimen and Fixture for Composite Materials Crush Energy Absorption [Journal] // Journal of Composite Materials. - 2009. - Vol. 43. - pp. 1967-1990.
Feraboli P., Deleo F. and Garattoni F. Efforts in the standardization of composite materials crashworthiness energy absorption [Conference] // American Society for Composites - 22nd Technical Conference of the American Society for Composites 2007 - Composites: Enabling a New Era in Civil Aviation, Vol.1, pp.741-759. - Seattle, WA : [s.n.], 2007.
Feraboli P., Wade B. and Deleo F. LS-DYNA MAT54 modeling of the axial crushing of a composite tape sinusoidal specimen [Journal] // Composites Part A. - 2011. - 11 : Vol. 42. - pp. 1809-1825.
Fleming D.C. Delamination Modeling of Composites for Improved Crash Analysis [Journal] // Journal of Composite Materials. - 2001. - 19 : Vol. 35. - pp. 1777-1792.
Garikipati K. and Hughes T.J.R. A variational multiscale approach to strain localization - formulation for multidimensional problems [Journal] // Computer methods in applied mechanics and engineering. - 2000. - Vol. 188. - pp. 39-60.
Gibson R. F. Principles of Composite Material Mechanics, fourth edition [Book]. - Boca Raton, FL : Taylor & Francis, 2016.
Gol'denblat I. and Kopnov V. Strength of glass-reinforced plates in the complex stress state, English translation [Journal] // Polymeric Mechanics. - 1966. - Vol. 1.
Hamada H., and Ramakrishna S. A FEM Method for Prediction of Energy Absorption Capability of Crashworthy Polymer Composite Materials [Journal] // Journal of Reinforced Plastics and Composites. - 1997. - 3 : Vol. 16. - pp. 226-242.
Hashin Z. Failure Criteria for Unidirectional Fiber Composites [Journal] // Journal of Applied Mechanics. - 1980. - pp. 329-334.
Hillerborg A. The theoretical basis of a method to determine the fracture energy GF of concrete [Journal] // Materials and Structure. - 1985. - Vol. 18. - pp. 291-296.
Hinton M. J. and Kaddour A. S. The background of the second world-wide failure exercise (WWFE-II) [Journal] // Journal of Composite Materials. - 2012. - Vol. 46. - pp. 2283-2294.
Hinton M. J., Kaddour A. S. and Soden P. D. Failure criteria in fibre reinforced polymer composites: The world-wide failure exercise [Book]. - Oxford, UK : Elsevier Science Ltd, 2004.

Hoffman O The brittle strength of orthotropic materials [Journal] // Journal of Composites Materials. - 1967. - Vol. 1. - pp. 200-206.
Houbolt J. C. A Recurrence Matrix Solution for the Dynamic Response of Elastic Aircraft [Journal] // Journal of Aeronautical Science. - 1950. - pp. Vol. 17, 540-550..
Hrennikoff A. Solution of Problems in Elasticity by the Frame Work Method [Journal] // Journal of Applied Mechanics. - 1941. - pp. 169-175.
Hufenbach W. [et al.] Theoretical and experimental investigation of anisotropic damage in textile-reinforced composite structures [Journal] // Mechanics of Composite Materials. - 2004. - 6 : Vol. 40. - pp. 519-532.
Hughes B. P. and Chapman G. P. The complete stress-strain for concrete in direct tension [Journal] // RILEM Bulletin. - 1966. - Vol. 30. - pp. 95-97.
Hull D. A unified approach to progressive crushing of fibre-reinforced composite tubes [Journal] // Composites Science and Technology. - 1991. - Vol. 40. - pp. 377-421.
Jackson K. [et al.] Scaling of Energy Absorbing [Journal] // Journal of the AHS. - 1994. - 1 : Vol. 39. - pp. 17-23.
Jirásek M. and Bauer M. Numerical aspects of the crack band approach [Journal] // Computers and Structures. - 2012. - pp. 60-78.
Jones R. M. Mechanics of Composite Materials, 2nd edition [Book]. - Philadelphia, PA : Taylor & Francis, 1999.
Jose S. [et al.] Intralaminar fracture toughness of a cross-ply laminate and its constituent sub-laminates [Journal] // Composites Science and Technology. - 2011. - Vol. 61. - pp. 1115-1122.
Kachanov L.M. Time of the rupture process under creep conditions [Journal] // Izvestiya Akademii Nauk SSR. - 1958. - 8 : Vol. 8. - pp. 26-31.
Kaddour A. S. [et al.] A comparison between the predictive capability of current matrix cracking, continuum damage and fracture criteria for fibre reinforced composite laminates: Part A of the WWFE-III. [Journal] // Journal of Composite Materials. - 2013. - pp. 2749-2779.
Kaddour A. S. [et al.] Damage, matrix cracking criteria for fibre reinforced polymeric composites: part A of the third world-wide failure exercise [Journal] // Journal of Composite Materials. - 2013. - pp. 20-21.
Kaddour A. S. [et al.] Mechanical properties and details of composite laminates for the test cases used in the third world-wide failure exercise. [Journal] // Journal of Composite Materials. - 2013. - pp. 2427-2442.
Kaddour A. S. [et al.] The background to the third world-wide failure exercise [Journal] // Journal of Composite Materials. - 2013. - pp. 2417-2426.
Kaddour A. S. [et al.] The world-wide failure exercises: how can composites design and manufacture communities build their strength [Conference] // ECCM16-16th European Conference on Composites Materials. - Seville, Spain : [s.n.], 2014.
Kaddour A. S. and Hinton M. J. Evaluation of theories for predicting failure in polymeric composites laminates under 3-D states of stress: Part A of the second World-Wide Failure Exercise (WWFE-II) [Journal] // Journal of Composite Material. - 2012. - Special Issue. - pp. 19-20.
Kaddour A.S. and Hinton M.J. 1.23 Failure criteria for composites [Book Section] // Comprehensive Composite Materials II. - [s.l.] : Elsevier, 2017.
Kaddour A.S. and Hinton M.J. Evaluation of theories for predicting failure in polymeric composite laminates under 3-D states of stress: Part B of the second World-Wide Failure

Exercise (WWFE-II) [Journal] // Journal of Composite Materials. - 2013. - Special Issue. - pp. 6-7.
Kaw A. K. Mechanics of Composite Materials, 2nd edition [Book]. - Boca Raton, FL : Taylor & Francis, 2006.
King S. and Richards T. Solving Contact Problems with Abaqus [Conference] // DS UK Ltd. - Coventry : [s.n.], 2013.
Kollar L.P. and Springler G.S. Mechanics of Composite Structure [Book]. - Cambridge, UK : Cambridge University Press, 2003.
Konter A. Undertake a Contact and Friction Analysis [Book]. - [s.l.] : NAFEMS Ltd, 2000.
Kress G. Examination of Hashin's failure criteria for Part B of the second world-wide failure exercise: comparison with test data. [Journal] // Journal of Composite Materials. - 2013. - pp. 867-891.
Kress G. Examination of Hashin's failure criteria for the second world-wide failure exercise [Journal] // Journal of Composite Materials. - 2012. - pp. 2539-2561.
Laffan M.J. [et al.] Translaminar fracture toughness testing of composites: A review [Journal] // Polymer Testing. - 2012. - Vol. 31. - pp. 481-489.
Lapczyk I. and Hurtado J. A. Progressive damage modeling in fiber-reinforced materials [Journal] // Composites: Part A. - 2007. - Vol. 37. - pp. 2333-2341.
Lavoie J.A. and Kellas S. Dynamic Crush Tests of Energy-absorbing Laminated [Journal] // Composites Part A. - 1996. - 6 : Vol. 27.
Lavoie J.A. and Morton J. Design and Application of a Quasistatic Crush Test [Report]. - [s.l.] : NASA CR 4526, July 1993.
Lemaitre J. A Course on Damage Mechanics [Book]. - [s.l.] : Springer-Verlag Berlin Heidelberg, 1992.
Lin K. Y. Composite Materials: Materials, Manufacturing, Analysis, Design and Repair [Book]. - Charleston, SC : [s.n.], 2015.
Lisle Teddy [et al.] Measure of fracture toughness of compressive fiber failure in composite structures using infrared thermography [Journal] // Composites Science and Technology. - 2015. - Vol. 112. - pp. 22-33.
Livermore Software Technology Corporation (LSTC) LS-DYNA Theory Manual [Report]. - Livermore, CA : LSTC, 2016.
Livermore Software Technology Corporation LS-DYNA R7. - Livermore, CA : LSTC, 2014.
Logan D. L. A first course in the Finite Element Method [Book]. - [s.l.] : Cengage, 2017.
Madhusadana C.V. and Fletcher L.S. Contact Heat Transfer - The Last Decade [Journal] // AIAA Journal. - 2014 : [s.n.], 1986. - 3 : Vol. 24. - pp. 510-523.
Maimi P. [et al.] A continuum damage model for composite laminates: Part II – Computational implementation and validation [Journal] // Mechanics of Materials. - 2007. - Vol. 39. - pp. 909-919.
Maimi P. [et al.] A thermodynamically consistent damage model for advanced composites [Report]. - [s.l.] : NASA/TM-2006-214282, 2006.
Matzenmiller A. and Schweizerhof K. Crashworthiness Simulations of Composite Structures - a first Step with Explicit Time Integration [Journal] // Nonlinear computational mechanics. - 1991. - pp. 642-670.
Matzenmiller A., Lubliner J. and Taylor R.L. A constitutive model for anisotropic damage in fiber-composites [Journal] // Mechanics of Materials. - 1995. - 2 : Vol. 20. - pp. 125-152.

McHenry D. A Lattice Analogy for the Solution of Plane Stress Problems [Journal] // Journal of Institurion of Civl Engineers. - 1943. - pp. 59-82.
Moore D. R. and Seferis J. C. Intrinsic characterization of continous fibre reinforced thermoplastic composites - I. Toughness chracterization of carbon fibre/polyether ether ketone (CF/PEEK) Laminates [Journal] // Pure and Applied Chemistry. - 1991. - 11 : Vol. 63. - pp. 1609-1625.
Morthorst M. and Horst P. Failure model for composite materials under quasi-static crushing conditions [Journal] // Journal of Strain Analysis for Engineering Design. - 2004. - 5 : Vol. 39. - pp. 411-421.
Newmark N. W. A Method of Computation for Structural Dynamics [Journal] // Journal of Engineering Mechanics Division. - 1959. - pp. Vol. 85, No. EM3, 67-94.
Pineda E. J. and Waas A. M. Numerical implementation of a multiple-ISV thermodynamically-based work potential theory for modeling progressive damage and failure in fiber-reinforced lamiantes, NASA/TM-2011-217401 [Report]. - Cleveland, OH : National Aeronautics and Space Administration, 2011.
Pineda E. J. and Waas A. M. Numerical implementation of a multiple-ISV thermodynamically-based work potential theory for modeling progressive damage and failure in fiber-reinforced laminates [Journal] // Internal Journal of Fracture. - 2013. - Vol. 182. - pp. 93-122.
Pinho S.T. Modelling failure of laminated composites using physically-based failure models. Doctoral Dissertation. [Report]. - London, UK : Department of Aeronautics, Imperial College, 2005.
Pinho S.T., Iannucci L. and Robinson P. Physically based failure models and criteria for laminated fibre-reinforced composites with emphasis on fibre kinking. Part II: FE implementation [Journal] // Composites: Part A. - 2006. - Vol. 37. - pp. 766-777.
Ratcliffe J., Jackson W. and Schaff J. Compression strength predictions of impact-damaged composite sandwich panels [Conference] // American Helicopter Society 60th Annual Forum. - Baltimore, MD : [s.n.], 2004.
Sandhu R. S. A survey of failure theories of isotropic and anisotropic materials. AFFDL-TR-72-71, AD756889 [Report]. - Wright-Patterson Air Force Base, Ohio : Air Force Flight Dynamics Laboratory, 1972.
Schijve J. Fatigue of Structures and Materials [Book]. - [s.l.] : Springer Netherlands, 2009.
Shi D. A robust crash simulation model for composite structures [Report]. - Mechanical Engineering Dept, Michigan State University. : Doctor of Philosophy Dissertation, 2016.
Simulia ABAQUS/Explicit. - 2017.
Society of Automotive Engineers.;National Institute for Aviation Research (U.S.) Composite materials handbook. Volume 3, Polymer matrix composites materials usage, design, and analysis [Book]. - Warrendale, Pa : SAE International, 2012.
Sokolinsky V.S., Indermuehle K.C. and Hurtado J.A. Numerical simulation of the crushing process of a corrugated composite plate [Journal] // Composites: Part A. - 2011. - Vol. 42. - pp. 1119-1126.
Soni S. R. A comparative study of failure envelopes in composite laminates [Journal] // Journal of Reinforced Plastic Composites. - 1983. - Vol. 2. - pp. 34-42.
Soutis C. and Curtis P.T. A method for predicting the fracture toughness of CFRP laminates failing by fibre microbuckling. [Journal] // Composites: Part A. - 2000. - Vol. 31. - pp. 733-740.

Tabiei A. and Chen Q. Micromechanics Based Composite Material Model for Crashworthiness Explicit Finite Element Solution [Journal] // Journal of Thermoplastic Composite Materials. - 2001. - Vol. 14. - pp. 264-289.
Tomblin J. [et al.] A – Basis and B – Basis Design Allowables for Epoxy – Based Prepreg TORAY T700GC-12K-31E/#2510 Unidirectional Tape, AGATE-WP3.3-033051-135 [Report]. - Wichita, KS : National Institute for Aviation Research, Wichita State University, October 2002.
Tsai S. and Wu E. A general theory of strength for anisotropic materials [Journal] // Journal of Composite Materials. - 1971. - Vol. 5. - pp. 58-80.
Tsai S.W. Strength Theories of Filamentary Structures Fundamental Aspects of Fiber Reinforced Plastic Composites [Book]. - New York : Wiley-Interscience, 1968.
Turner M. J. [et al.] Stiffness and Deflections Analysis of Complex Structures [Journal] // Journal of Aeronautical Sciences. - 1956. - pp. 805-823.
Tuttle M. E. Structural Analysis of Polymeric Composite Materials [Book]. - Boca Raton, FL : CRC Press, 2013.
Tvergaard V. and Needleman A. Effects of Nonlocal Damage in Porous Plastic Solids [Journal] // International Journal of Solids and Structures. - 1995. - 8-9 : Vol. 32. - pp. 1063-1077.
U.S. Department of Transportation, Federal Aviation Administration Crushing Behavior of Laminated Composite Structural Elements: Experiment and LS-DYNA Simulation, DOT/FAA/TC-12/25 [Report]. - Atlantic City International Airport, NJ : U.S. Department of Transportation, Federal Aviation Administration, 2016.
Van Der Meer F. P. and Sluys L. J. Continuum Models for the Analysis of Progressive Failure in Composite Laminates [Journal] // Journal of COMPOSITE MATERIALS. - 2009. - Vol. 43. - pp. 2131-2156.
Wade B. [et al.] Toward the development of a standard for characterizing the energy absorption of composite materials [Conference] // ICCM International Conferences on Composite Materials. - Edinburgh, UK : [s.n.], 2009.
Wade B. Capturing the Energy [Report]. - Seattle, WA : Doctoral Dissertation, University of Washington, 2014.
Xu W. and Waas A. M. Modeling damage growth using the crack band model; effect of different strain measures [Journal] // Engineering Fracture Mechanics. - 2016. - Vol. 152. - pp. 126-138.
Zienkiewicz O.C., Taylor R.L. and Zhu J.Z. The Finite Element Method Its Basis & Fundamentals, 7th edition [Book]. - Waltham, MA : Elsevier, 2013.

APPENDIX A: MATERIAL MODEL FOR STATIC LOADING

```
      subroutine umat45(cm,capa,eps,nip,sig,hsv,ncycle,failel,i,ipt)
c
      include 'nlqparm'
      include 'bk13.inc'
      include 'memaia.inc'
c Material array constants, history variables, stresses
      dimension cm(*),hsv(*),sig(*),eps(*)
c Failure initiation flags
      real sf2,sfc2,sm2,smd2
      real iflagc,iflagf,iflagd,iflagm
c Stiffness matrix constants
      real c11,c12,c21,c22,c44
c Not sure about these:
      real ix1,ix2,ix3,ix4
c Damage variables
      real D1T,D2T,D3S,D1C,D2C,D12TC
c Post elastic strain components
      real eps1elultp,eps1elultn,eps2elultp,eps2elultn,eps12elult
c Element failure initiation flags
      real count1tel,count1cel,count2tel,count2cel,count12el
c Nonlocal stiffness matrix damage componen
      real d1tnli,d2tnli,d1cnli,d2cnli
c Constants utilized
      real nux,nuy,ymx,ymy,beta,sxy,syz,szx,beta2t,dfail1t,dfail1c
      real dfail2t,dfail2c,dfails,sc,xt,xc,yt,yc,ycd
      real m1t,m1c,m2t,m2c,denom,top1t,bot1t,top1c,bot1c
      real top2t,bot2t,top2c,bot2,elLength
c laminas orientations
c     dimension theta(4)
      integer i,iext
      integer failipt
      logical failel
c
c Matrix with elements for 5x5 crash to enforce element strength degradation.
c     INITIALIZATION
      if (ncycle.eq.1.) then
        D1T=0.
        D2T=0.
        D3S=0.
        D1C=0.
        D2C=0.
        D12TC=1.
        eps1elultp=0.
        eps1elultn=0.
        eps2elultp=0.
        eps2elultn=0.
        eps12elult=0.
```

```
        count1tel=0.
        count1cel=0.
        count2tel=0.
        count2cel=0.
        count12el=0.
        failipt=1.
        iflagd=0.
        iflagm=0.
        iflagf=0.
        iflagc=0.
        d1tnli=0.
        d2tnli=0.
        d1cnli=0.
        d2cnli=0.
c           call failipts(nip,ipt,ncycle,fail,i,lft,llt)
c           call dxx(nip,ipt,ncycle,i,lft,llt,ipt_thk,D1T(i),D1C(i),
c     * D2T(i),D2C(i),theta)
c           call elconnect(lft,llt,ix1,ix2,ix3,ix4)
c           print*, 'Element: ',i, 'has nodes:'
c           print*, els(i,1),els(i,2),els(i,3),els(i,4)
c       call usermsg('umat45')
        iext = lqfinvf(i,4)
c         print*, 'Internal and external element#:', i, iext
c       print*, 'Integration point #:', ipt
      else
        iext = lqfinvf(i,4)
        D1T=hsv(4)
        D2T=hsv(5)
        D3S=hsv(6)     !Only one parameter for shear damage.
        D1C=hsv(7)
        D2C=hsv(8)
        eps1elultp=hsv(9)
        eps1elultn=hsv(10)
        eps2elultp=hsv(11)
        eps2elultn=hsv(12)
        eps12elult=hsv(13)
        count1tel=hsv(14)
        count1cel=hsv(15)
        count2tel=hsv(16)
        count2cel=hsv(17)
        count12el=hsv(18)
        failipt=hsv(19)
        iflagd=hsv(20)
        iflagm=hsv(21)
        iflagf=hsv(22)
        iflagc=hsv(23)
        d1tnli=hsv(24)
        d2tnli=hsv(25)
        d1cnli=hsv(26)
        d2cnli=hsv(27)
        D12TC=hsv(28)
```

```
      endif
c
c     call checkElementDamage(iext,redFac)
c     if (redFac.lt.1.) then
c       print*, 'Element: ',iext,' has a reduced strength'
c     endif
c UPDATING STRAIN VECTOR
      hsv(1)=hsv(1)+eps(1)
      hsv(2)=hsv(2)+eps(2)
      hsv(3)=hsv(3)+eps(4)
      hsv(34)=hsv(34)+eps(5)
      hsv(35)=hsv(35)+eps(6)
c
c     material constants
      ymx =cm(1)
      ymy =cm(2)
      nux =cm(4)
      nuy = nux*ymy/ymx
      sxy =cm(7)
      syz =capa*cm(8)
      szx =capa*cm(9)
c
c     more material constants
      beta  = cm(25)
      beta2t = cm(5)
      elLength = cm(6)
      sc = cm(11)
      xt = cm(12)
      xc = -cm(24)
      yt = cm(13)
      yc = -cm(14)
c     dfail1t = cm(17) ! -xt/ymx
c     dfail1c = cm(18) ! +xc/ymx
c     dfail2c = cm(19) ! +yc/ymy
c     dfail2t = cm(20) ! -yt/ymy
      dfail1s = cm(21)
      thickness = cm(28)
      G1t = cm(29)
      G1c = cm(30)
      G2t = cm(31)
      G2c = cm(32)
c
c CALCULATING ultimate strains for linear softnening
      dfail1t = 2*G1t/(thickness*xt*elLength)
      dfail1c = 2*G1c/(thickness*xc*elLength)
      dfail2t = 2*G2t/(thickness*yt*elLength)
      dfail2c = 2*G2c/(thickness*yc*elLength)
c CALCULATING LINEAR SOFTENING SLOPES
      m1t = -xt/(dfail1t-xt/ymx)
      m1c = -xc/(dfail1c-xc/ymx)
      m2t = -yt/(dfail2t-yt/ymy)
```

```
      m2c = -yc/(dfail2c-yc/ymy)
      denom = 1-nux**2*ymy/ymx
c
c
c -- begin Chang/Chang SOFTENING criteria --------------------------------
c
C_VECTOR
      if ((sig(1).ge.0.)) then   !for tensile fiber mode
c
c       sf2(i)=(sig1(i)/((1-D1T(i))*xt))**2+beta*(sig4(i)/sc)
        sf2=(sig(1)/xt)**2+beta*(sig(4)/sc)**2
        sfc2=-1.
      else                       !for compressive fiber mode
c
        sf2=-1.
        sfc2=(sig(1)/xc)**2
      endif
c
      if ((sig(2).ge.0.)) then    !for tensile matrix mode
c
        sm2=(sig(2)/yt)**2+beta2t*(sig(4)/sc)**2
        smd2=-1.
      else                        !for compressive matrix mode
c
        sm2=-1.
        ycd=abs(yc)*(1-D2C)
        smd2=(sig(2)/(2*sc))**2+((ycd/(2*sc))**2-1.0)*(sig(2)/ycd)+
     1        (sig(4)/sc)**2
      endif
c
c     mode failure flags
      if (smd2.gt.(1-D2T-D2C)**2) iflagd=1      ! Compressive Matrix Failure Initiation
      if (sm2.gt.(1-D2T-D2C)**2) iflagm=1       ! Tensile Matrix Failure Initiation
      if (sf2.gt.(1-D1T-D1C)**2) iflagf=1       ! Tensile Fiber Failure Initiation
      if (sfc2.gt.(1-D1C-D1T)**2) iflagc=1      ! Compressive Fiber Failure Initiation
c
c -- end Chang/Chang SOFTENING criteria ----------------------------------
c
c
c -- DAMAGE TENSOR PARAMETERS CALCULATIONS
      if (iflagf.eq.1) then  ! Tensile Fiber Failure
         if (eps(1).ge.0) then
           top1t = m1t*(hsv(1)-xt/ymx)+xt
           bot1t = (ymx-nux**2*ymy)*hsv(1)/denom
           if ((1-top1t/bot1t).ge.D1T) then
              D1T = 1 - top1t / bot1t
              eps1elultp=hsv(1)-xt/ymx
           endif
         else
           if (sf2.gt.(1-D1T)**2) then
             iflagf=0
```

```
            endif
          endif
          if (D1T.lt.0.) then
            D1T = 0.
          endif
        endif
        if (iflagc.eq.1) then  ! Compressive Fiber Failure
          if (eps(1).le.0) then
            if (hsv(1).le.0) then
c               top1c = m1c*((hsv(1)+eps1elultp)-xc/ymx)+xc
c               bot1c = (ymx-nux**2*ymy)*(hsv(1)+eps1elultp)/denom
              top1c = m1c*(hsv(1)-xc/ymx)+xc
              bot1c = (ymx-nux**2*ymy)*hsv(1)/denom
              if ((1-top1c/bot1c).ge.D1C) then
                D1C = 1 - top1c / bot1c
                eps1elultn=-hsv(1)-xc/ymx
                print*, 'D1C: ', D1C
                print*, 'hsv(1): ', hsv(1)
                print*, 'eps1elultp: ', eps1elultp
              endif
            endif
          else
            if (sfc2.gt.(1-D1C)**2) then
              iflagc=0
            endif
          endif
          if (D1C.lt.0.) then
            D1C = 0.
          endif
        endif
        if (iflagm.eq.1) then  ! Tensile Matrix Failure
          if (eps(2).ge.0) then
            top2t = m2t*(hsv(2)-yt/ymy)+yt
            bot2t = (1-nux*nuy)*ymy*hsv(2)/denom
            if ((1-top2t/bot2t).ge.D2C) then
              D2T = 1 - top2t / bot2t
              eps2elultp=hsv(2)-yt/ymy
            endif
          else
            if (sm2.gt.(1-D2T)**2) then
              iflagm=0
            endif
          endif
        endif
        if (iflagd.eq.1) then  ! Compressive Matrix Failure
          if (eps(2).le.0) then
            top2c = m2c*(hsv(2)-yc/ymy)+yc
            bot2c = (1-nux*nuy)*ymy*hsv(2)/denom
            if ((1-top2c/bot2c).ge.D2C) then
              D2C = 1 - top2c / bot2c
              eps2elultn=hsv(2)-yc/ymy
```

```
          endif
        else
          if (smd2.gt.1) then
            iflagd=0
          endif
        endif
      endif
c
c ELEMENT DELETION
c       fiber tensile rupture
      if (D1T.ge.1) then
        D1T=1.
c         print*, 'Deletion because of D1T critical is reached'
c         print*, 'Element and IPT:', iext, ipt,' to be deleted'
c         print*, sig1(i), ' sig1(i)'
        sig(1)=0.000001*ymx
        failel=.true.
c         print*, '------------------------------'
c         print*, 'Element failed'
c         failipt(i)=0.
c         call failipts(nip,ipt,ncycle,fail,i,lft,llt)
      endif
c
c       fiber compressive rupture
      if (D1C.ge.1) then
        D1C=1.
c         print*, 'Deletion because of D1C critical is reached'
c         print*, 'Element and IPT:', iext, ipt,' to be deleted'
c         sig(1)=0.000001*ymx
        failel=.true.
c         print*, '------------------------------'
c         print*, 'Element failed'
c         failipt(i)=0.
c         call failipts(nip,ipt,ncycle,fail,i,lft,llt)
      endif
C
c      matrix tensile rupture
      if (D2T.ge.1) then
        D2T=1.
c         print*, 'Deletion because of D2T critical is reached'
c         print*, 'Element and IPT:', iext, ipt,' to be deleted'
        sig(2)=0.000001*ymx
        failel=.true.
c         print*, '------------------------------'
c         print*, 'Element failed'
c         failipt(i)=0.
c         call failipts(nip,ipt,ncycle,fail,i,lft,llt)t)
      endif
c
c     matrix compressive rupture
      if (D2C.ge.1) then
```

```
          D2C=1.
c         print*, 'Deletion because of D2C critical is reached'
c         print*, 'Element and IPT:', iext, ipt,' to be deleted'
c         sig(2)=0.000001*ymx
          failel=.true.
c         print*, '------------------------------'
c         print*, 'Element failed'
c         failipt(i)=0.
c         call failipts(nip,ipt,ncycle,fail,i,lft,llt)
        endif
c
c
c CALCULATE STIFFNESS MATRIX COEFFICIENTS
      D12TC=(1-D1T)*(1-D1C)*(1-D2T)*(1-D2C)
      c11=(1-D1T)*(1-D1C)*ymx/(1.-nux**2*ymy/ymx)
      c12=D12TC*nux*ymy/(1.-nux**2*ymy/ymx)
      c21=c12
      c22=(1-D2T)*(1-D2C)*ymy/(1.-nux**2*ymy/ymx)
      c44=sxy
      c55=syz
      c66=szx
c
c     UPDATE STRESS TENSOR
      if ((D1T.gt.1).or.(D1C.gt.1)) then
         c11=0.
         c12=0.
         c21=0.
      endif
      if ((D2T.gt.1).or.(D2C.gt.1)) then
         c12=0.
         c21=0.
         c22=0.
      endif
      sig(1)=c11*hsv(1)+c12*hsv(2)
      sig(2)=c21*hsv(1)+c22*hsv(2)
      sig(3)=0.0
      sig(4)=c44*hsv(3)
      sig(5)=c55*hsv(34)
      sig(6)=c66*hsv(35)
c
c  SAVING INFO INTO THE HISTORY VARIABLES
      hsv(4)=D1T
      hsv(5)=D2T
      hsv(6)=D3S
      hsv(7)=D1C
      hsv(8)=D2C
      hsv(9)=eps1elultp
      hsv(10)=eps1elultn
      hsv(11)=eps2elultp
      hsv(12)=eps2elultn
      hsv(13)=eps12elult
```

```
      hsv(14)=count1tel
      hsv(15)=count1cel
      hsv(16)=count2tel
      hsv(17)=count2cel
      hsv(18)=count12el
      hsv(19)=failipt
      hsv(20)=iflagd
      hsv(21)=iflagm
      hsv(22)=iflagf
      hsv(23)=iflagc
      hsv(24)=d1tnli
      hsv(25)=d2tnli
      hsv(26)=d1cnli
      hsv(27)=d2cnli
      hsv(28)=D12TC
      hsv(29)=c11
      hsv(30)=c12
      hsv(31)=c22
      hsv(32)=c44
      hsv(33)=denom
c
      return
      end
c
```

APPENDIX B: MATERIAL MODEL FOR CRUSH LOADING

```
c TRIGGER
      subroutine umat43(cm,capa,eps,nip,sig,hsv,ncycle,failel,i,ipt,tt,
     1 nnm1)
c
      include 'nlqparm'
      include 'bk13.inc'
      include 'memaia.inc'
c
c Material array constants, history variables, stresses
      dimension cm(*),hsv(*),sig(*),eps(*)
c Failure initiation flags
      real sf2,sfc2,sm2,smd2
      real iflagc,iflagf,iflagd,iflagm
c Stiffness matrix constants
      real c11,c12,c21,c22,c44
c Not sure about these:
      real ix1,ix2,ix3,ix4
c Damage variables
      real D1T,D2T,D3S,D1C,D2C,D12TC
c Post elastic strain components
      real eps1elultp,eps1elultn,eps2elultp,eps2elultn,eps12elult
c Element failure initiation flags
      real count1tel,count1cel,count2tel,count2cel,count12el
c Nonlocal stiffness matrix damage components
      real d1tnli,d2tnli,d1cnli,d2cnli,capa,tfail,tt
c Constants utilized
      real nux,nuy,ymx,ymy,beta,sxy,syz,szx,beta2t,dfail1t,dfail1c
      real dfail2t,dfail2c,dfails,sc,xt,xc,yt,yc,ycd
      real m1t,m1c,m2t,m2c,denom,top1t,bot1t,top1c,bot1c,top2t,bot2t
      real top2c,bot2,elLength,m1ch,m2ch,top1ch,bot1ch,top2ch,bot2ch
      integer i,iext,checkFail
c Not used anymore but kept
      integer failipt
      logical failel
c
      dimension ElementDamages(840)
      real, dimension(30,28) :: elements
      real, dimension(840,12) :: ElementsState
c
c      INITIALIZATION
      if (ncycle.eq.1.) then
        D1T=0.
        D2T=0.
        D3S=0.
        D1C=0.
        D2C=0.
        D12TC=1.
        eps1elultp=0.
```

```
      eps1elultn=0.
      eps2elultp=0.
      eps2elultn=0.
      eps12elult=0.
      count1tel=0.
      count1cel=0.
      count2tel=0.
      count2cel=0.
      count12el=0.
      failipt=1.
      iflagd=0.
      iflagm=0.
      iflagf=0.
      iflagc=0.
      d1tnli=0.
      d2tnli=0.
      d1cnli=0.
      d2cnli=0.
      checkFail=0
      iext = lqfinvf(i+nnm1,4)
      tfail = 0.00068
    else
      iext = lqfinvf(i+nnm1,4)
      D1T=hsv(4)
      D2T=hsv(5)
      D3S=hsv(6)
      D1C=hsv(7)
      D2C=hsv(8)
      eps1elultp=hsv(9)
      eps1elultn=hsv(10)
      eps2elultp=hsv(11)
      eps2elultn=hsv(12)
      eps12elult=hsv(13)
      count1tel=hsv(14)
      count1cel=hsv(15)
      count2tel=hsv(16)
      count2cel=hsv(17)
      count12el=hsv(18)
      failipt=hsv(19)
      iflagd=hsv(20)
      iflagm=hsv(21)
      iflagf=hsv(22)
      iflagc=hsv(23)
      d1tnli=hsv(24)
      d2tnli=hsv(25)
      tfail=hsv(26)
      d2cnli=hsv(27)
      D12TC=hsv(28)
      checkFail=hsv(36)
    endif
c
```

```
c UPDATING STRAIN VECTOR
      hsv(1)=hsv(1)+eps(1)
      hsv(2)=hsv(2)+eps(2)
      hsv(3)=hsv(3)+eps(4)
      hsv(34)=hsv(34)+eps(5)
      hsv(35)=hsv(35)+eps(6)
c
c     material constants
      ymx =cm(1)
      ymy =cm(2)
      nux =cm(4)
      nuy = nux*ymy/ymx
      sxy =cm(7)
      syz =capa*cm(8)
      szx =capa*cm(9)
c
c     more material constants
      beta  = cm(25)
      beta2t = cm(5)
      elLength = cm(6)
      sc = cm(11)
      xt = cm(12)
      xc = -cm(24)
      yt = cm(13)
      yc = -cm(14)
      dfail1s = cm(21)
      thickness = cm(28)
      G1t = cm(29)
      G1c = cm(30)
      G2t = cm(31)
      G2c = cm(32)
c
c CALCULATING ultimate strains for linear softnening
      dfail1t = 2*G1t/(thickness*xt*elLength)
      dfail1c = 2*G1c/(thickness*xc*elLength)
      dfail2t = 2*G2t/(thickness*yt*elLength)
      dfail2c = 2*G2c/(thickness*yc*elLength)
c CALCULATING LINEAR SOFTENING SLOPES
      m1t = -xt/(dfail1t-xt/ymx)
      m1c = -xc/(dfail1c-xc/ymx)
      m2t = -yt/(dfail2t-yt/ymy)
      m2c = -yc/(dfail2c-yc/ymy)
      m1ch = 3*ymx
      m2ch = 3*ymy
      denom = 1-nux**2*ymy/ymx
c
c
c -- begin Chang/Chang SOFTENING criteria --------------------------------
c
C_VECTOR
      if ((sig(1).ge.0.)) then   !for tensile fiber mode
```

```
c
c       sf2(i)=(sig1(i)/((1-D1T(i))*xt))**2+beta*(sig4(i)/sc)
        sf2=(sig(1)/xt)**2+beta*(sig(4)/sc)**2
        sfc2=-1.
      else                      !for compressive fiber mode
c
        sf2=-1.
        sfc2=(sig(1)/xc)**2
      endif
c
      if ((sig(2).ge.0.)) then    !for tensile matrix mode
c
        sm2=(sig(2)/yt)**2+beta2t*(sig(4)/sc)**2
        smd2=-1.
      else                       !for compressive matrix mode
c
        sm2=-1.
        ycd=abs(yc)*(1-D2C)
        smd2=(sig(2)/(2*sc))**2+((ycd/(2*sc))**2-1.0)*(sig(2)/ycd)+
     1        (sig(4)/sc)**2
      endif
c
c     mode failure flags
      if (smd2.gt.1) iflagd=1              ! Compressive Matrix Failure Initiation
      if (sm2.gt.(1-D2T)**2) iflagm=1       ! Tensile Matrix Failure Initiation
      if (sf2.gt.(1-D1T)**2) iflagf=1       ! Tensile Fiber Failure Initiation
      if (sfc2.gt.(1-D1C)**2) iflagc=1      ! Compressive Fiber Failure Initiation
c
c -- end Chang/Chang SOFTENING criteria --------------------------------
c
c -- DAMAGE TENSOR PARAMETERS CALCULATIONS
      if (iflagf.eq.1) then  ! Tensile Fiber Failure
         if (eps(1).ge.0) then
           top1t = m1t*(hsv(1)-xt/ymx)+xt
           bot1t = (ymx-nux**2*ymy)*hsv(1)/denom
           if ((1-top1t/bot1t).ge.D1T) then
              D1T = 1 - top1t / bot1t
              eps1elultp=hsv(1)-xt/ymx
           endif
         else
           if (sf2.gt.(1-D1T)**2) then
             iflagf=0
           endif
         endif
         if (D1T.lt.0.) then
           D1T = 0.
         endif
      endif
       if (iflagc.eq.1) then  ! Compressive Fiber Failure
          if (eps(1).le.0) then
            if (hsv(1).gt.-4.0) then
```

```
          top1c = xc*denom
          bot1c = (ymx-nux**2*ymy)*hsv(1)
          if ((1-top1c/bot1c).ge.D1C) then
            D1C = 1 - top1c / bot1c
          endif
        elseif (hsv(1).le.-4.0) then
          if (checkFail.eq.0) then
            call writeOnElementsState(ElementsState,iext,ipt)
            checkFail=1
          endif
          failel=.true.
        endif
      else
        if (sfc2.gt.(1-D1C)**2) then
          iflagc=0
        endif
      endif
      if (D1C.lt.0.) then
        D1C = 0.
      endif
    endif
    if (iflagm.eq.1) then  ! Tensile Matrix Failure
      if (eps(2).ge.0) then
        top2t = m2t*(hsv(2)-yt/ymy)+yt
        bot2t = (1-nux*nuy)*ymy*hsv(2)/denom
        if ((1-top2t/bot2t).ge.D2C) then
          D2T = 1 - top2t / bot2t
          eps2elultp=hsv(2)-yt/ymy
        endif
      else
        if (sm2.gt.(1-D2T)**2) then
          iflagm=0
        endif
      endif
    endif
    if (iflagd.eq.1) then  ! Compressive Matrix Failure
      if (eps(2).le.0) then
        if (hsv(2).gt.-4.0) then
          top2c = yc*denom
          bot2c = (1-nux**2)*ymy*hsv(2)
          if ((1-top2c/bot2c).ge.D2C) then
            D2C = 1 - top2c / bot2c
          endif
        elseif (hsv(2).le.-4.0) then
          if (checkFail.eq.0) then
            call writeOnElementsState(ElementsState,iext,ipt)
            checkFail=1
          endif
          failel=.true.
        endif
      else
```

```
            if (smd2.gt.1) then
              iflagd=0
            endif
          endif
        endif
c
c ELEMENT DELETION
c       fiber tensile rupture
      if (D1T.ge.1) then
        D1T=1.
        sig(1)=0.000001*ymx
        failel=.true.
        if (checkFail.eq.0) then
          call writeOnElementsState(ElementsState,iext,ipt)
          checkFail=1
        endif
      endif
c
c       fiber compressive rupture
      if (D1C.ge.1) then
        D1C=1.
      endif
C
c       matrix tensile rupture
      if (D2T.ge.1) then
        D2T=1.
        sig(2)=0.000001*ymx
        failel=.true.
        if (checkFail.eq.0) then
          call writeOnElementsState(ElementsState,iext,ipt)
          checkFail=1
        endif
      endif
c
c     matrix compressive rupture
      if (D2C.ge.1) then
        D2C=1.
      endif
      if (tt.gt.tfail) then
        if (ipt.eq.1) then
          print*, 'Time deletion occured on element: ', iext
        endif
        failel=.true.
        if (checkFail.eq.0) then
          call writeOnElementsState(ElementsState,iext,ipt)
          checkFail=1
        endif
      endif
c
c
c
```

```
c CALCULATE STIFFNESS MATRIX COEFFICIENTS
      D12TC=(1-D1T)*(1-D1C)*(1-D2T)*(1-D2C)
      c11=(1-D1T)*(1-D1C)*ymx/(1.-nux**2*ymy/ymx)
      c12=D12TC*nux*ymy/(1.-nux**2*ymy/ymx)
      c21=c12
      c22=(1-D2T)*(1-D2C)*ymy/(1.-nux**2*ymy/ymx)
      c44=sxy
      c55=syz
      c66=szx
c
c     UPDATE STRESS TENSOR
      if ((D1T.gt.1).or.(D1C.gt.1)) then
         c11=0.
         c12=0.
         c21=0.
      endif
      if ((D2T.gt.1).or.(D2C.gt.1)) then
         c12=0.
         c21=0.
         c22=0.
      endif
      sig(1)=c11*hsv(1)+c12*hsv(2)
      sig(2)=c21*hsv(1)+c22*hsv(2)
      sig(3)=0.0
      sig(4)=c44*hsv(3)
      sig(5)=c55*hsv(34)
      sig(6)=c66*hsv(35)
c
      if (checkFail.eq.1) then
c Routine to check if all ipts of the elements are failed. If that's the case, then the element number
c entry for the the element and the next in line are updated on Element_Damages
         call checkElementState(iext,ipt,ElementsState,ElementDamages,
     1    elements)
      endif
c
c  SAVING INFO INTO THE HISTORY VARIABLES
      hsv(4)=D1T
      hsv(5)=D2T
      hsv(6)=D3S
      hsv(7)=D1C
      hsv(8)=D2C
      hsv(9)=eps1elultp
      hsv(10)=eps1elultn
      hsv(11)=eps2elultp
      hsv(12)=eps2elultn
      hsv(13)=eps12elult
      hsv(14)=count1tel
      hsv(15)=count1cel
      hsv(16)=count2tel
      hsv(17)=count2cel
      hsv(18)=count12el
```

```
      hsv(19)=failipt
      hsv(20)=iflagd
      hsv(21)=iflagm
      hsv(22)=iflagf
      hsv(23)=iflagc
      hsv(24)=d1tnli
      hsv(25)=d2tnli
      hsv(26)=tfail
      hsv(27)=d2cnli
      hsv(28)=D12TC
      hsv(29)=c11
      hsv(30)=c12
      hsv(31)=c22
      hsv(32)=c44
      hsv(33)=denom
      hsv(36)=checkFail
c
      return
      end
c
c SPECIMEN
      subroutine umat45(cm,capa,eps,nip,sig,hsv,ncycle,failel,i,ipt,tt,
     1 nnm1)
c
c Material array constants, history variables, stresses
      dimension cm(*),hsv(*),sig(*),eps(*)
c Failure initiation flags
      real sf2,sfc2,sm2,smd2
      real iflagc,iflagf,iflagd,iflagm
c Stiffness matrix constants
      real c11,c12,c21,c22,c44
c Not sure about these:
      real ix1,ix2,ix3,ix4
c Damage variables
      real D1T,D2T,D3S,D1C,D2C,D12TC
c Post elastic strain components
      real eps1elultp,eps1elultn,eps2elultp,eps2elultn,eps12elult
c Element failure initiation flags
      real count1tel,count1cel,count2tel,count2cel,count12el
c Nonlocal stiffness matrix damage components
      real d1tnli,d2tnli,d1cnli,d2cnli
c Constants utilized
      real nux,nuy,ymx,ymy,beta,sxy,syz,szx,beta2t,dfail1t,dfail1c
      real dfail2t,dfail2c,dfails,sc,xt,xc,yt,yc,ycd
      real m1t,m1c,m2t,m2c,denom,top1t,bot1t,top1c,bot1c,top2t,bot2t
      real top2c,bot2,elLength,m1ch,m2ch,top1ch,bot1ch,top2ch,bot2ch
      real redFac,tt,capa,tfail
c laminas orientations
c     dimension theta(4)
      integer i,iext,checkFail,redFacFound,rowNum
c Not used anymore but kept
```

```
      integer failipt
      logical failel
c
      dimension ElementDamages(840)
      real, dimension(30,28) :: elements
      real, dimension(840,12) :: ElementsState
c
c Matrix with elements for 5x5 crash to enforce element strength degradation.
c      INITIALIZATION
      if (ncycle.eq.1.) then
        D1T=0.
        D2T=0.
        D3S=0.
        D1C=0.
        D2C=0.
        redFacFound=0
        eps1elultp=0.
        eps1elultn=0.
        eps2elultp=0.
        eps2elultn=0.
        eps12elult=0.
        count1tel=0.
        count1cel=0.
        count2tel=0.
        count2cel=0.
        count12el=0.
        failipt=1.
        iflagd=0.
        iflagm=0.
        iflagf=0.
        iflagc=0.
        d1tnli=0.
        d2tnli=0.
        d1cnli=0.
        redFac=1.
        checkFail=0
        iext = lqfinvf(i+nnm1,4)
        call findRow(rowNum,iext)
        tfail = 0.00068+(rowNum-1)*0.1/150
      else
        iext = lqfinvf(i+nnm1,4)
        D1T=hsv(4)
        D2T=hsv(5)
        D3S=hsv(6)
        D1C=hsv(7)
        D2C=hsv(8)
        eps1elultp=hsv(9)
        eps1elultn=hsv(10)
        eps2elultp=hsv(11)
        eps2elultn=hsv(12)
        eps12elult=hsv(13)
```

```
        count1tel=hsv(14)
        count1cel=hsv(15)
        count2tel=hsv(16)
        count2cel=hsv(17)
        count12el=hsv(18)
        failipt=hsv(19)
        iflagd=hsv(20)
        iflagm=hsv(21)
        iflagf=hsv(22)
        iflagc=hsv(23)
        d1tnli=hsv(24)
        d2tnli=hsv(25)
        tfail=hsv(26)
        redFac=hsv(27)
        redFacFound=hsv(28)
        checkFail=hsv(36)
        rowNum=hsv(33)
      endif
c
      elLength = cm(6)
c  check if the stregth needs reducing only if it is time to be crushed
      if (tt.gt.((rowNum-1)*elLength/150+0.000014)) then
c       For the element whose strenght is being reduced, only check this once
        if (redFacFound.eq.0) then
          call checkElementDamage(iext,redFac)
        endif
        if (redFac.lt.1.) then
          redFacFound = 1
        endif
      endif
c
c UPDATING STRAIN VECTOR
      hsv(1)=hsv(1)+eps(1)
      hsv(2)=hsv(2)+eps(2)
      hsv(3)=hsv(3)+eps(4)
      hsv(34)=hsv(34)+eps(5)
      hsv(35)=hsv(35)+eps(6)
c
c     material constants
      ymx =cm(1)
      ymy =cm(2)
      nux =cm(4)
      nuy = nux*ymy/ymx
      sxy =cm(7)
      syz =capa*cm(8)
      szx =capa*cm(9)
c
c     more material constants
      beta  = cm(25)
      beta2t = cm(5)
      sc = cm(11)*redFac
```

```
      xt = cm(12)*redFac
      xc = -cm(24)*redFac
      yt = cm(13)*redFac
      yc = -cm(14)*redFac
      dfail1s = cm(21)
      thickness = cm(28)
      G1t = cm(29)
      G1c = cm(30)
      G2t = cm(31)
      G2c = cm(32)
c
c CALCULATING ultimate strains for linear softnening
      dfail1t = 2*G1t/(thickness*xt*elLength)
      dfail1c = 2*G1c/(thickness*xc*elLength)
      dfail2t = 2*G2t/(thickness*yt*elLength)
      dfail2c = 2*G2c/(thickness*yc*elLength)
c CALCULATING LINEAR SOFTENING SLOPES
      m1t = -xt/(dfail1t-xt/ymx)
      m1c = -xc/(dfail1c-xc/ymx)
      m2t = -yt/(dfail2t-yt/ymy)
      m2c = -yc/(dfail2c-yc/ymy)
      m1ch = 3*ymx
      m2ch = 3*ymy
      denom = 1-nux**2*ymy/ymx
c
c
c -- begin Chang/Chang SOFTENING criteria --------------------------------
c
C_VECTOR
      if ((sig(1).ge.0.)) then   !for tensile fiber mode
c
        sf2=(sig(1)/xt)**2+beta*(sig(4)/sc)**2
        sfc2=-1.
      else                       !for compressive fiber mode
c
        sf2=-1.
        sfc2=(sig(1)/xc)**2
      endif
c
      if ((sig(2).ge.0.)) then    !for tensile matrix mode
c
        sm2=(sig(2)/yt)**2+beta2t*(sig(4)/sc)**2
        smd2=-1.
      else                        !for compressive matrix mode
c
        sm2=-1.
        ycd=abs(yc)*(1-D2C)
        smd2=(sig(2)/(2*sc))**2+((ycd/(2*sc))**2-1.0)*(sig(2)/ycd)+
     1        (sig(4)/sc)**2
      endif
c
```

```
c     mode failure flags
      if (smd2.gt.1) iflagd=1                ! Compressive Matrix Failure Initiation
      if (sm2.gt.(1-D2T)**2) iflagm=1        ! Tensile Matrix Failure Initiation
      if (sf2.gt.(1-D1T)**2) iflagf=1        ! Tensile Fiber Failure Initiation
      if (sfc2.gt.(1-D1C)**2) iflagc=1       ! Compressive Fiber Failure Initiation
c
c -- end Chang/Chang SOFTENING criteria --------------------------------
c
c -- DAMAGE TENSOR PARAMETERS CALCULATIONS
      if (iflagf.eq.1) then  ! Tensile Fiber Failure
         if (eps(1).ge.0) then
           top1t = m1t*(hsv(1)-xt/ymx)+xt
           bot1t = (ymx-nux**2*ymy)*hsv(1)/denom
           if ((1-top1t/bot1t).ge.D1T) then
              D1T = 1 - top1t / bot1t
              eps1elultp=hsv(1)-xt/ymx
           endif
         else
           if (sf2.gt.(1-D1T)**2) then
             iflagf=0
           endif
         endif
         if (D1T.lt.0.) then
           D1T = 0.
         endif
       endif
       if (iflagc.eq.1) then  ! Compressive Fiber Failure
          if (eps(1).le.0) then
            if (hsv(1).gt.-4.0) then
              top1c = xc*denom
              bot1c = (ymx-nux**2*ymy)*hsv(1)
              if ((1-top1c/bot1c).ge.D1C) then
                D1C = 1 - top1c / bot1c
              endif
            elseif (hsv(1).le.-4.0) then
              if (checkFail.eq.0) then
                call writeOnElementsState(ElementsState,iext,ipt)
                checkFail=1
              endif
              failel=.true.
            endif
          else
            if (sfc2.gt.(1-D1C)**2) then
              iflagc=0
            endif
          endif
          if (D1C.lt.0.) then
            D1C = 0.
          endif
       endif
       if (iflagm.eq.1) then  ! Tensile Matrix Failure
```

```
          if (eps(2).ge.0) then
            top2t = m2t*(hsv(2)-yt/ymy)+yt
            bot2t = (1-nux*nuy)*ymy*hsv(2)/denom
            if ((1-top2t/bot2t).ge.D2C) then
              D2T = 1 - top2t / bot2t
              eps2elultp=hsv(2)-yt/ymy
            endif
          else
            if (sm2.gt.(1-D2T)**2) then
              iflagm=0
            endif
          endif
        endif
        if (iflagd.eq.1) then  ! Compressive Matrix Failure
          if (eps(2).le.0) then
            if (hsv(2).gt.-4.0) then
              top2c = yc*denom
              bot2c = (1-nux**2)*ymy*hsv(2)
              if ((1-top2c/bot2c).ge.D2C) then
                D2C = 1 - top2c / bot2c
              endif
            elseif (hsv(2).le.-4.0) then
              if (checkFail.eq.0) then
                call writeOnElementsState(ElementsState,iext,ipt)
                checkFail=1
              endif
              failel=.true.
            endif
          else
            if (smd2.gt.1) then
              iflagd=0
            endif
          endif
        endif
c
c ELEMENT DELETION
c       fiber tensile rupture
      if (D1T.ge.1) then
          D1T=1.
          sig(1)=0.000001*ymx
          failel=.true.
          if (checkFail.eq.0) then
            call writeOnElementsState(ElementsState,iext,ipt)
            checkFail=1
          endif
        endif
c
c       fiber compressive rupture
        if (D1C.ge.1) then
          D1C=1.
        endif
```

```
C
c     matrix tensile rupture
      if (D2T.ge.1) then
        D2T=1.
        sig(2)=0.000001*ymx
        failel=.true.
        if (checkFail.eq.0) then
          call writeOnElementsState(ElementsState,iext,ipt)
          checkFail=1
        endif
      endif
c
c     matrix compressive rupture
      if (D2C.ge.1) then
        D2C=1.
      endif
      if (tt.gt.tfail) then
        if (ipt.eq.1) then
          print*, 'Time deletion occured on element: ', iext
        endif
        failel=.true.
        if (checkFail.eq.0) then
          call writeOnElementsState(ElementsState,iext,ipt)
          checkFail=1
        endif
      endif
c
c
c CALCULATE STIFFNESS MATRIX COEFFICIENTS
      D12TC=(1-D1T)*(1-D1C)*(1-D2T)*(1-D2C)
      c11=(1-D1T)*(1-D1C)*ymx/(1.-nux**2*ymy/ymx)
      c12=D12TC*nux*ymy/(1.-nux**2*ymy/ymx)
      c21=c12
      c22=(1-D2T)*(1-D2C)*ymy/(1.-nux**2*ymy/ymx)
      c44=sxy
      c55=syz
      c66=szx
c
c     UPDATE STRESS TENSOR
      if ((D1T.gt.1).or.(D1C.gt.1)) then
        c11=0.
        c12=0.
        c21=0.
      endif
      if ((D2T.gt.1).or.(D2C.gt.1)) then
        c12=0.
        c21=0.
        c22=0.
      endif
      sig(1)=c11*hsv(1)+c12*hsv(2)
      sig(2)=c21*hsv(1)+c22*hsv(2)
```

```
      sig(3)=0.0
      sig(4)=c44*hsv(3)
      sig(5)=c55*hsv(34)
      sig(6)=c66*hsv(35)
c
      if (checkFail.eq.1) then
c Routine to check if all ipts of the elements are failed. If that's the case, then the element number
c entry for the the element and the next in line are updated on Element_Damages
        call checkElementState(iext,ipt,ElementsState,ElementDamages,
     1    elements)
      endif
c
c  SAVING INFO INTO THE HISTORY VARIABLES
      hsv(4)=D1T
      hsv(5)=D2T
      hsv(6)=D3S
      hsv(7)=D1C
      hsv(8)=D2C
      hsv(9)=eps1elultp
      hsv(10)=eps1elultn
      hsv(11)=eps2elultp
      hsv(12)=eps2elultn
      hsv(13)=eps12elult
      hsv(14)=count1tel
      hsv(15)=count1cel
      hsv(16)=count2tel
      hsv(17)=count2cel
      hsv(18)=count12el
      hsv(19)=failipt
      hsv(20)=iflagd
      hsv(21)=iflagm
      hsv(22)=iflagf
      hsv(23)=iflagc
      hsv(24)=d1tnli
      hsv(25)=d2tnli
      hsv(26)=tfail
      hsv(27)=redFac
      hsv(28)=redFacFound
      hsv(29)=c11
      hsv(30)=c12
      hsv(31)=c22
      hsv(32)=c44
      hsv(33)=rowNum
      hsv(36)=checkFail
c
      return
      end
c
c
      subroutine findRow(rowNum,iext)
      real, dimension(30,28) :: elements
```

```
      integer iext,rowNum,k,j
c
      open(8, file='Element_Connectivity')
         do k=1,30
           read(8,*) elements(k,:)
         enddo
      close(8, status='KEEP')
c
      do k=1,30
        do j=1,28
          if (elements(k,j).eq.iext) then
            rowNum = k
          endif
        enddo
      enddo
c      print*, 'Element: ', iext, 'is in row:', rowNum
c
      return
      end
c
      subroutine writeOnElementsState(ElementsState,iext,ipt)
      real, dimension(840,12) :: ElementsState
      integer iext,ipt,k,j
c
      open(12, file='Element_State')
          do k=1,840
            do j=1,12
              read(12,*) ElementsState(k,j)
            enddo
          enddo
      close(12, status='KEEP')
c
c
      ElementsState(iext,ipt) = 0
      open(11, file='Element_State')
          do k=1,840
            do j=1,12
              write(11,*) ElementsState(k,j)
            enddo
          enddo
      close(11, status='KEEP')
c
c
      return
      end
c
      subroutine checkElementState(iext,ipt,ElementsState,
     1    ElementDamages,elements)
      real, dimension(840,12) :: ElementsState
      real, dimension(30,28) :: elements
      dimension ElementDamages(840)
```

```
      integer iext,ipt,k,summ,j,nextEl
c
c      print*, 'I am inside checkElementState'
      summ = 0
c
      open(12, file='Element_State')
          do k=1,840
            do j=1,12
              read(12,*) ElementsState(k,j)
            enddo
          enddo
      close(12, status='KEEP')
c Sum over columns (IPTS) for the element number in question (row) if sum is less than 1 then it means
that not even one ipt is
c in the unfailed state. Therefore the in ElementDamages the elements in the next row are flagged to have
damage added.
c
      do k=1,12
        summ = summ + ElementsState(iext,k)
      enddo
      if (summ.lt.1) then
c Find next element in line
        open(8, file='Element_Connectivity')
           do k=1,30
             read(8,*) elements(k,:)
           enddo
        close(8, status='KEEP')
c
         do k=1,30
           do j=1,28
             if (elements(k,j).eq.iext) then
                nextEl = elements(k+1,j)
             endif
           enddo
         enddo
c
         print*, 'Element failed:', iext
         print*, 'Element reduced', nextEl
c
        open(12, file='Element_Damages')
           do k=1,840
             read(12,*) ElementDamages(k)
           enddo
        close(12, status='KEEP')
c
        ElementDamages(iext) = 0
        ElementDamages(nextEl) = 0
c
        open(11, file='Element_Damages')
           do k=1,840
             write(11,*) ElementDamages(k)
```

```
          enddo
        close(11, status='KEEP')
c
      endif
c
      return
      end
c
      subroutine checkElementDamage(iext,redFac)
      dimension ElementDamages(840)
      real redFac
      integer k,iext
c
c Read Element_Damages and figure out if this element needs to be reduced in strength
      open(13, file='Element_Damages')
         do k=1,840
            read(13,*) ElementDamages(k)
         enddo
      close(13, status='KEEP')
c
      if (ElementDamages(iext).eq.0) then
        redFac = 0.15
      else
        redFac = 1.
      endif
      return
      end
```

VITA

Francesco Deleo was born in the city of Fano located on the Adriatic coast of central Italy. He moved to the United States for his senior year in high school with the intent of eventually attending the University of Washington (UW) and study aeronautical engineering, following his father's steps. Francesco received his Bachelor of Science, Master of Science, and PhD (with this work) from the Aeronautics and Astronautics department at the UW (UWAA). During the first years in graduate school Francesco worked at the Advanced Composites Structures Laboratory (ACSL) in UWAA where he eventually assumed the role of manager. He was the lead analyst of the group and responsible for supervising all dynamic simulations, including crush and ballistic analyses. He was also the focal for technical research between the lab at UWAA and Automobili Lamborghini. During the cooperation with Lamborghini, Francesco's work and research had a direct impact on the Aventador and Sesto Elemento vehicles.

After receiving his Master of Science degree and during his doctoral studies, Francesco worked at GreenPoint Technologies first and then TerraPower later. At GreenPoint technologies Francesco was a stress analyst and eventually was promoted to a lead position overseeing the stress work on the interior modification of a Boeing 747-8 aircraft to private jet. During his time at GreenPoint Technolgies, Francesco worked on cut-edge technology and the most advanced finite element modelling the company had ever done. On the last project he worked on before departing, Francesco introduced the use of comparative analysis via finite elements to justify loading on the floor of a Boeing 787-8, instead of relying of Boeing's expensive feedback and approval. Francesco developed the plan, got it approved and saved GreenPoint Technologies time and millions of dollars. Francesco also created a connection between UWAA and GreenPoint. A connection which was missing prior to Francesco's time at GreenPoint despite the close geographical proximity between the two entities. Francesco represented GreenPoint at the UW in several networking events and career fairs and recommended several people who were then hired. Francesco remains a friend of GreenPoint Technologies.

In 2014 Francesco joined TerraPower after being approached by a recruiter and decided to try a new exciting experience and change of career path. TerraPower is a nuclear reactor design company working on few advanced reactor concepts, including the flagship project called the

Traveling Wave Reactor (TWR). Francesco works on the TWR as a core design senior stress analysis engineer focusing on methods development for mechanical analyses. Francesco is the house fatigue and fracture mechanics expert and one of the finite elements and stress analysis expert. Francesco remains employed at TerraPower at this time and enjoys the work there very much.

One of Francesco's biggest passion is teaching. For a few years while in graduate school, in his free time, Francesco volunteered at Bryant Elementary School in Seattle and served as science fair mentor. He had an opportunity to introduce children to science, and plan and conduct experiments. Starting from his first year in graduate school Francesco served as Teaching Assistant in UWAA for several graduate and undergraduate courses. During his second year in graduate school, Prof. Safarian, now one of Francesco's dearest mentors and friends, asked him to assist him in teaching a metal fatigue and damage tolerance (F&DT) course at the university and privately. It was the beginning of a great relationship and to date Francesco and Prof. Patrick Safarian taught over 50 F&DT courses in the United States and abroad, and recently developed a finite element analysis (FEA) course tailored to the aerospace industry. The first FEA course was taught at Honda Aerospace in North Carolina and was very successful. The course is now offered twice a year. Dr. Safarian and Francesco are in the process of developing three more courses which benefit from Dr. Safarian's decades of industry's experience and knowledge and Francesco's theoretical expertise, which include the latest state of the art techniques. Francesco has also been teaching his own courses at UWAA starting in 2012. To date Francesco taught Aerospace Structures II, Finite Element Analysis, and Aerospace Composites, for a total of six times. In 2015 Francesco was voted instructor of the year in UWAA and nominated for the teaching excellence award for the UW college of engineering.

In his free time Francesco loves playing soccer and he's involved in the local soccer community. In 2015 Francesco was nominated president of Olympic Soccer Academy FC (OSA FC) which is the second most important soccer club in the State of Washington, after the Seattle Sounders FC, and competes in the National Premier Soccer League (NPSL).